GEOLOGICAL SURVEY OF DENMARK AND GREENLAND BULLETIN 17 • 2009

Review of Survey activities 2008

Edited by
Ole Bennike, Adam A. Garde and W. Stuart Watt

GEOLOGICAL SURVEY OF DENMARK AND GREENLAND
MINISTRY OF CLIMATE AND ENERGY

Geological Survey of Denmark and Greenland Bulletin 17

Keywords
Geological Survey of Denmark and Greenland, survey organisations, current research, Denmark, Greenland.

Cover photographs from left to right
1. Inspection of cores in Jameson Land, East Greenland. Photo: John Boserup.
2. Field work in West Greenland. Photo: Denis Schlatter.
3. Investigations and sampling of an outcrop at Conde, Bahia, Brazil. Photo: Peter Japsen.
4. Field experiments with remediation of contaminated soil in Vadsby, west of Copenhagen. Photo: Knud Erik S. Klint.

Frontispiece: facing page
Visit at the automatic weather station 'Lower Nuuk' on 30 July 2008 for data retrieval and maintenance. The station is located on the glacier Qamanaarsuup Sermia near the margin of the Greenland ice sheet, east of Godthåbsfjord (64°29′N, 49°31′W). It collects weather information and data about the local ablation and was established in 2007 as part of the *Promice* project (www.promice.org). Photo: Søren Nielsen.

Printers: Schultz Grafisk, Albertslund, Denmark
Manuscripts submitted: 23 January – 27 March 2009
Final versions approved: 25 May 2009
Printed: 8 July 2009

ISSN 1603-9769 (Review of Survey activities)
ISSN 1604-8156 (Geological Survey of Denmark and Greenland Bulletin)
ISBN 978-87-7871-250-9

Citation of the name of this series
It is recommended that the name of this series is cited in full, viz. *Geological Survey of Denmark and Greenland Bulletin*.
If abbreviation of this volume is necessary, the following form is suggested: *Geol. Surv. Den. Green. Bull.* 17, 84 pp.

Available from
Geological Survey of Denmark and Greenland (GEUS)
Øster Voldgade 10, DK-1350 Copenhagen K, Denmark
Phone: +45 38 14 20 00, fax: +45 38 14 20 50, e-mail: geus@geus.dk


OY-HGW

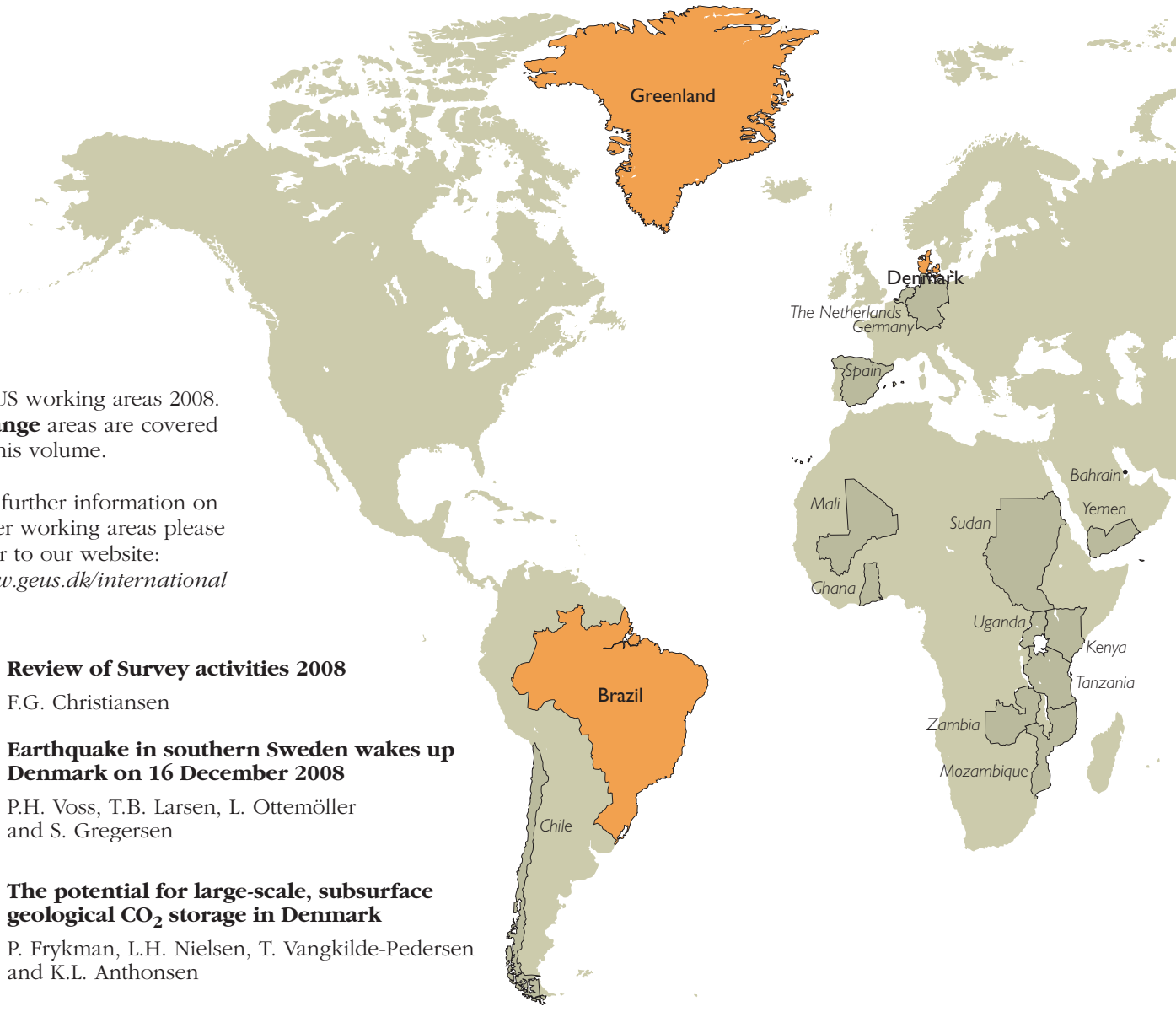

GEUS working areas 2008. **Orange** areas are covered in this volume.

For further information on other working areas please refer to our website: *www.geus.dk/international*

Review of Survey activities 2008

Flemming G. Christiansen
Deputy Director

Following a number of years with major changes of the scientific environment in Denmark and also within the management of the Geological Survey of Denmark and Greenland (GEUS), 2008 was a year of stability and consolidation, a situation that will hopefully continue. Many new projects have been initiated and many previous projects have been completed at a time with strong focus on GEUS' activities politically, commercially and from the media.

This sixth annual issue of Review of Survey activities describes selected projects that GEUS and its partners carry out in Denmark, Greenland and internationally. Together with the previous five published issues (also available at www.geus.dk), it provides a good overview of the Survey's many different types of research and advisory activities. It contains a total of 19 four-page papers: ten on Denmark, eight on Greenland and one on international work.

Geology was on the lips of most of the Danish population an early morning in December 2008 when one of the strongest earthquakes recorded in Scandinavia woke up hundreds of thousands of people in southern Sweden and on Sjælland. One paper in this issue describes the background and details of the earthquake, including input from the public that contacted GEUS through its website.

Reduction of the emission of CO_2 is high on the political agenda in Denmark and internationally. One of the possibilities to reduce CO_2 emission from large point sources is to use carbon capture and storage (CCS). The Danish subsurface has a high potential to store CO_2, and structures such as the Vedsted structure in northern Jylland could be among the first dozen storage facilities utilised in Europe, and thereby become a key area for detailed research and monitoring for many years to come. The background for CCS and geological possibilities in Denmark are described in one paper.

Oil and gas exploration and production are still very important for the economy of Denmark, and GEUS has a strong emphasis on research within this field. Two papers concentrate on petroleum geology. One of them is based on laboratory flooding experiments and describes the possibility of increasing oil recovery from reservoirs in chalk using injection of CO_2-enriched water; the other provides a detailed biostratigraphic correlation of the Late Triassic succession in the Norwegian–Danish Basin.

Most surface features in Denmark have been formed by glacial and coastal processes during the Quaternary. Several papers in this issue describe such processes; one of them demonstrates the use of sophisticated analytical techniques such as computer-controlled, scanning electron microscopy of heavy minerals and laser ablation, inductively coupled mass spectrometry of zircon grains to describe erosion and re-deposition of sand along the west coast of Jylland. The structural development of the famous Møns Klint geosite is dealt with in one paper, and the occurrence of neotectonic fracture valleys in central Jylland in another. A third paper describes soil erosion and land use change during the last six millennia as recorded in lake sediments from Gudme Sø on Fyn.

Groundwater mapping and management have a very high priority in Denmark. One paper describes the many different geophysical methods that are used in hydrogeological mapping, as well as the administration of the geophysical data that are archived in a major database hosted at GEUS. Another paper describes the exchange between lake water and groundwater of lake Skærsø in Jylland.

In 2008 there was a high level of field activities in Greenland. The two largest campaigns in southern West Greenland and eastern Greenland are described in individual papers. The West Greenland field work was a follow-up on earlier projects focused on updating previous maps and thereby creating a better understanding of the potential distribution of mineral occurrences. The field work in eastern Greenland is the start of a major oil industry sponsored programme that has been launched to support and promote petroleum exploration within the coming five-year period. It includes shallow core drilling.

One paper addresses a question often raised by scientists and explorers: what is the bedrock geology under the Inland Ice that covers 81% of the total area of Greenland? Available

geological and geophysical data are shortly reviewed and ideas for future studies presented. Another paper introduces a 3-D modelling of one of the best studied intrusions in the world, the Paleocene Skaergaard intrusion in East Greenland. Identification of significant platinum group and gold occurrences in this intrusion has lead to detailed investigations and exploration drilling over many years. The last decade of diamond exploration in West Greenland has provided a wealth of data on the dykes of kimberlite and ultramafic lamprophyres that may host diamonds. One paper summarises new data on petrology and age distribution of the dykes that have important implications for future diamond exploration. In a large country like Greenland, use of remote sensing data is important and cost-effective in mapping and exploration. One paper presents an analysis of hyperspectral data from the Sarfartoq carbonatite complex in West Greenland. The paper illustrates that such data can be applied to mapping of individual rock types.

The most recent processes and climate development in Greenland are described in two papers of which one stresses the importance of applied glaciology for the exploitation of the Malmbjerg molybdenum deposit in East Greenland, because the site of a possible future mine is located between two glaciers. Future access to the mining site and removal of ore and waste rock are highly dependent on the movement of the glaciers. The second paper addresses Holocene climate variation and marine history in South Greenland, based on a number of samples collected in Bredefjord and Narsaq Sund during the Galathea 3 expedition.

A final paper on landscape development in Brazil employs the same methods of landscape mapping and apatite fission track analysis that were used to study the uplift history of the margins of Greenland and Scandinavia.

Earthquake in southern Sweden wakes up Denmark on 16 December 2008

Peter H. Voss, Tine B. Larsen, Lars Ottemöller and Søren Gregersen

A moderately strong earthquake struck southern Sweden 5 km south-west of the town of Sjöbo, 60 km east of Malmö, in the early morning at 6:20 a.m. local time on 16 December 2008. The epicentre was located in Skåne, a region that is known for its extremely low seismicity, and its location was determined to be 55.5°N and 13.6°E with an uncertainty of about 6 km. A depth of 9 km with an uncertainty of 3 km was obtained from teleseismic observations at the Yellowknife seismic array, USA. Since waveform data from the Swedish national seismic network are not yet available, depth estimation using local stations has so far not been attempted. During the period 1970–2008, only three small earthquakes were detected in the region; the largest measured 2.8 on the local Richter scale. To our knowledge none of these previous earthquakes were felt by people. The historical archives dating back to 1375 show that 14 other earthquakes have been felt in the area. The largest of these, recorded in 1894, was felt over an area of 7300 km^2 and had an epicentre 50 km east of the 16 December 2008 earthquake (Scandinavian Earthquake Archive 2003). The activity in southern Sweden is similar to that of northern Sjælland and north-western Jylland, and confirms the low seismicity of the region (Gregersen *et al.* 1991).

Even though the earthquake was unusual, the event was not totally unexpected. Northern Europe is under constant pressure from the mid-Atlantic Ridge, and the resulting stress is released in small to moderate size earthquakes. The local stress field is further modified by postglacial rebound. Earthquakes in Denmark and southern Sweden occur where there are weaknesses or faults in the subsurface. In some cases the earthquakes occur where there are no mapped faults (Gregersen *et al.* 1996).

Shaking from the earthquake was felt widely in Denmark. Strong shaking and low-frequency earthquake sounds frightened many people and caused them to abruptly leave their houses. Authorities such as the police and the Geological Survey of Denmark and Greenland (GEUS) were flooded with phone calls and e-mails from concerned citizens. Fortunately the earthquake did not cause any real damage, and no one was in danger at any time.

Macroseismic effects in Denmark

The basic physical earthquake parameters are determined from instrumental recordings. However, the effects of the earthquake on people, buildings, and nature require human inter-

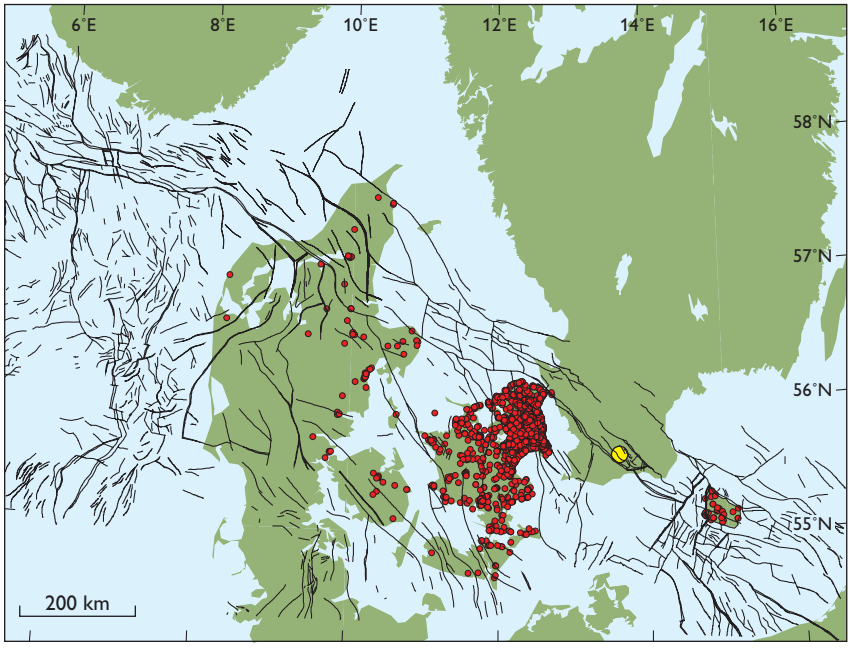

Fig. 1. Map showing the epicentre of the 16 December 2008 earthquake (yellow circle) and the locations of the first 3000 macroseismic reports received (red circles) from Denmark. Known faults are also shown.

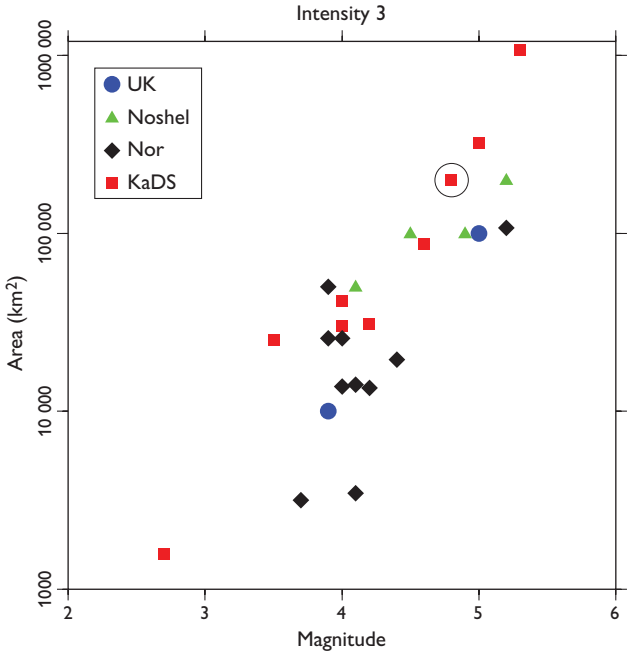

Fig. 2. Perceptibility areas for 25 selected earthquakes (area of intensity 3) correlated with their magnitudes. The red squares are for the shield region in Kaliningrad, Denmark and Sweden **(KaDS)** compared to the 16 December 2008 earthquake. These areas are larger than those in Norway **(NOR)**, on the Norwegian continental shelf **(Noshel)** and in the United Kingdom **(UK)**. The 16 December earthquake (preliminary result shown by a circle) seems to confirm the trend.

action to be delineated. Immediately following the earthquake, GEUS requested input from the public through the news media and our own web page. Our earthquake questionnaire was placed on www.geus.dk and a paper copy was mailed to those who had no internet access or who felt uncomfortable about reporting electronically. After a few days, GEUS had received more than 3000 earthquake reports (Fig. 1), and after a month the number exceeded 4000 reports. This is a large increase compared to the last widely felt earthquake in Denmark in 2001, where we received little more than 400 reports (Larsen *et al.* 2008) and the one in 1985 in Kattegat, which was almost as large as the 16 December 2008 earthquake, where we received a total of around 500 reports from Sweden and Denmark.

In Denmark alone the area where the earthquake was felt covers about 50 000 km^2 (Fig. 1). Earthquakes in Scandinavia are felt over much larger areas than in California, where C.F. Richter worked when he invented the Richter magnitude scale. Thus the attenuation in Scandinavia is lower than that in California. A comparison of local observations of 25 earthquakes in different regions and their magnitude suggests that the affected area this time will exceed 100 000 km^2 (Fig. 2).

Reports from the population are an important tool to assess the impact of an earthquake and to identify locations that are particularly vulnerable to ground shaking. This is still of great interest as earthquakes can be compared to historic events predating the era of instrumental recording. This information is used in seismic hazard studies, for example in connection with large construction projects. The GEUS questionnaire comprises the address of the observer, information about the building in which the observer was located and detailed information about shaking and other effects caused by the earthquake. Shaking is strongly amplified in tall buildings, and the European macroseismic scale (Grünthal *et al.* 1998) recommends that shaking observations above the 5th floor are not taken into account when determining the intensity of an earthquake. A detailed study of the 4000 current reports has not yet been completed, but the reports will provide valuable shake information especially for Sjælland.

In many locations the earthquake was felt strongly. Some examples, with locations shown on Fig. 3, are: Copenhagen: "walls, closet and bed were shaking", Gilleleje: "the chair I was sitting in was shaking", Humlebæk: "it was as if the bed was shaken – it felt very terrifying", Ålborg: "it felt as if someone was shaking my bed gently", Kettinge: "as when a large truck is just outside".

Some reports claim that the earthquake caused a road in Helsingør to crack. Inspection of the road confirms the presence of cracks, but it is not obvious that the cracks opened during the earthquake. New asphalt was added to the road a year earlier, and the small cracks are located in the weak zone where new asphalt overlaps with old. The road is exposed to heavy traffic and the cracks could have opened at any time. They do not look any different from other asphalt cracks. The European-Mediterranean Seismological Centre has also received information (a photo) of cracked asphalt in Sweden, but it has not been confirmed that these cracks formed during the earthquake.

Fig. 3. Map of Denmark and south-western Sweden showing the location of place names mentioned in the text.

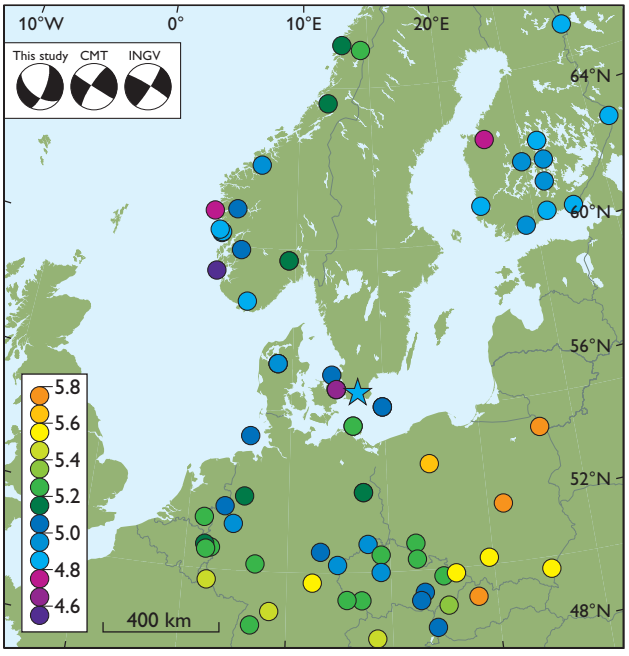

Fig. 4. Map showing magnitudes and focal mechanisms from various agencies. Each circle shows the ML estimated from the data from each seismograph. ML values are from University of Bergen, University of Helsinki, GeoForschungsZentrum in Postdam and GEUS. The 2008 epicentre is shown by a star. The focal mechanisms in the upper left corner were determined by this (preliminary) study, CMT (the global CMT project; Ekström & Nettles 2008) and INGV (The MEDNET network; Morelli *et al.* 2000).

Earthquake magnitude

Determining the magnitude of an earthquake is not straightforward. Many different definitions of magnitude are in use at seismological data centres around the world. They measure fundamentally different parameters in the seismograms, all with the intention to reproduce C.F. Richter's original magnitude measure from 1935 (Richter 1935), which is in widespread use for public information and in engineering in earthquake regions. The earthquake hazards program at the United States Geological Survey (USGS) calculates up to six different magnitude values for each registered earthquake. At GEUS, two different magnitudes are calculated: our own computation of local magnitude (ML), which should give the classical Richter number (Richter 1935) for local earthquakes, and the moment magnitude (Hanks & Kanamori 1979), which reflects the size of the fault area and the slip during the earthquake.

At GEUS, the ML is calculated from the maximum amplitude of the earthquake signal on the vertical component of the seismograph (usually the (surface) Lg wave) taking into account the distance between the earthquake and the seismograph station. When the Lg wave is observed at several seismographs, we calculate the ML as the average of the separate ML values. It requires little data to calculate and it can be calculated shortly after the earthquake. When the data quality is low, as is often the case with weak, local earthquakes, the ML is the only magnitude that can be calculated. The calculation of ML builds on experience of how effectively the shaking propagates in the area.

The variations in the ML value calculated at different seismograph stations can be large. Following the earthquake on 16 December 2008, several European agencies reported ML values for their stations. The values ranged from 4.6 to 5.8 even though the local corrections are supposed to ensure similar values for all stations (Fig. 4). Ideally the ML values estimated at seismographs map the energy released in different directions from the earthquake, but the uncertainty in the correction of damping is large, so the pattern is only determined with some uncertainty. At GEUS, a ML value of 4.8 was calculated, identical to the ML value reported by the USGS. University of Bergen reported 4.7, University of Helsinki 4.9 and Helmholtz-Zentrum Potsdam - Deutsches GeoForschungsZentrum 5.4.

The moment magnitude is based on the seismic moment of the earthquake, a physical parameter that is proportional to the area of the fault multiplied by its slip. The moment can be determined from seismological measurements, and in special cases from geodetic measurements. A large number of clear signals on seismographs surrounding the epicentre are needed to obtain a well constrained moment magnitude, using moment tensor inversion. The moment magnitude is determined by searching for the earthquake source parameters that produce synthetic seismograms that have the best possible fit to the observed seismograms. We have determined the moment tensor and a moment magnitude of 4.2 using the method by Dreger (2003). University of Uppsala, USGS and Istituto Nazionale di Geofisica e Vulcanologia reported a moment magnitude of 4.3.

Fault plane solutions determined in this preliminary study and by others all show a strike-slip movement with a normal component. The corresponding compressional stress field is orientated in a NNW–SSE direction as shown by the focal mechanisms (Fig. 4).

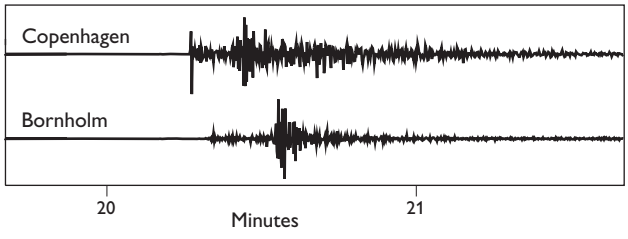

Fig. 5. Seismograms of the 16 December 2008 earthquake showing the vertical component of the broadband seismometers at Copenhagen and Bornholm, located 65 and 108 km from the epicentre, respectively.

Tectonic setting

The epicentre is located in the Sorgenfrei–Tornquist Zone, which is part of a major transition zone in Europe between (1) the old Precambrian shield of Fennoscandia and eastern Europe and (2) the younger lithosphere of central Europe (Pharaoh 1999). The earthquake activity in the Sorgenfrei–Tornquist Zone is limited, with Kattegat being the most active region. The most active area in Denmark is from north-western Jylland into Skagerrak (Gregersen *et al.* 1998). Recent studies show that many of the earthquakes cannot be referred to known faults in the Sorgenfrei–Tornquist Zone (Gregersen *et al.* 1996). This is the case even though the uncertainties in the earthquake locations are large.

Faults in the top Pre-Zechstein rocks have been mapped in the area where the earthquake occurred (Fig. 1). However, the location uncertainty (6 km) means that one cannot link the 16 December 2008 earthquake to a known fault. This is a general problem as small earthquakes occur at depth whereas faults are mostly mapped near the surface.

A re-analysis of the data recorded by the Danish seismological network shows that no foreshocks or aftershocks were observed in the months before or after the 16 December earthquake. Seismograms of the earthquake are shown in Fig. 5.

Concluding remarks

To feel an earthquake in Denmark is rare but not unlikely. Earthquakes felt in Denmark are generally small and felt in north-western Jylland or northern Sjælland (Gregersen *et al.* 1998; Larsen *et al.* 2008). Large earthquakes with epicentres located outside Denmark have also been felt in Denmark, like the earthquakes in Lissabon in 1755, Oslo in 1904 and Kaliningrad in 2004 (Gregersen *et al.* 2007). The perceptibility area in Denmark of the 16 December 2008 earthquake is comparable to the perceptibility area of the Holbæk earthquake in 2001 (Larsen *et al.* 2008), where the earthquake was felt mostly in northern Sjælland. Also, the area is not much different from that shaking in 1930 by a small earthquake in Øresund. The shaking from the Oslo earthquake in 1904 was felt in the north-eastern part of Denmark. The Kaliningrad earthquake in 2004 was felt by many in Copenhagen and in northern Sjælland, but only marginally in the rest of Denmark.

The coincidence of the perceptibility areas must be included in future evaluations of the earthquake hazard of Denmark. Denmark is located in an area of low earthquake hazard (Giardini *et al.* 2003) and the danger of any damage or injury caused by an earthquake is insignificant compared to other hazards.

Acknowledgements

University of Bergen, University of Helsinki, University of Uppsala, Deutsches GeoForschungsZentrum in Postdam and USGS provided data for this study.

References

Ekström, G. & Nettles, M. 2008: The Global CMT Project, http:// www. globalcmt.org.

Dreger, D.S. 2003: TDMT_INV: Time Domain Seismic Moment Tensor INVersion. In Lee, W.H.K., Kanamori, H., Jennings, P.C. & Kisslinger, C. (eds): International handbook of earthquake and engineering seismology **81B**, 1627 only. London: Academic Press.

Giardini, D., Jiménez, M.-J. & Grünthal, G. (eds) 2003: European-Mediterranean Seismic Hazard Map. European Seismological Commission.

Gregersen, S. 1992: Crustal stress regime in Fennoscandia from focal mechanisms. Journal of Geophysical Research **97**, 11,821–11,827.

Gregersen, S., Korhonen, H. & Husebye, E.S. 1991: Fennoscandian dynamics: present-day earthquake activity. Tectonophysics **189**, 333–344.

Gregersen, S., Leth, J., Lind, G. & Lykke-Andersen, H. 1996: Earthquake activity and its relationship with geologically recent motion in Denmark. Tectonophysics **257**, 265–273.

Gregersen, S., Hjelme, J. & Hjortenberg, E. 1998: Earthquakes in Denmark. Bulletin of the Geological Society of Denmark **44**, 115–127.

Gregersen, S., Wiejacz, P., Debski, W., Domanski, B., Assinovskaya, B., Guterch, B., Matyniemi, P., Nikulin, V., Pacesa, A. & Puura, V. 2007: The exceptional earthquakes in Kaliningrad District, Russia on September 21, 2004. Physics of the Earth and Planetary Interiors **164**, 63–74.

Grünthal, G., Musson, R.M.W., Schwarz, J. & Stucchi, M. (eds) 1998: European macroseismic scale **15**, 99 pp. Luxembourg: Cahiers du Centre Européen de Géodynamique et de Séismologie.

Hanks, T.C., & Kanamori, H. 1979: A moment magnitude scale. Journal of Geophysical Research **84**(B5), 2348–2350.

Larsen, T.B., Gregersen, S., Voss, P.H., Bidstrup, T., & Orozova-Bekkevold, V. 2008: The earthquake that shook central Sjælland, Denmark, November 6, 2001. Bulletin of the Geological Society of Denmark **56**, 1–11.

Morelli, A., Ekström, G., Mazza, S., Pondrelli, S., Boschi, E. & Dziewonski, A.M. 2000: Surface-wave centroid moment tensors in the Mediterranean region: the MEDNET-Harvard project. Orfeus Electronic Newsletter **2**, p. 4.

Pharaoh, T. 1999: Palaeozoic terranes and their lithospheric boundaries within the Trans-European Suture Zone (TESZ): a review. Tectonophysics **314**, 17–41.

Richter C.F. 1935: An instrumental earthquake magnitude scale. Bulletin of the Seismological Society of America **25**, 1–32.

Scandinavian Earthquake Archive 2003: CD with scanned reports for ICG project No. 3. ICG 3-2003-3.

Authors' addresses

P.H.V., T.B.L. & S.G., *Geological survey of Denmark and Greenland, Øster Voldgade 10, DK-1350 Copenhagen K, Denmark.* E-mail: *pv@geus.dk*

L.O., *British Geological Survey, Murchison House, West Mains Road, Edinburgh EH9 3LA, UK.*

The potential for large-scale, subsurface geological CO_2 storage in Denmark

Peter Frykman, Lars Henrik Nielsen, Thomas Vangkilde-Pedersen and Karen Lyng Anthonsen

Carbon capture and storage (CCS) is increasingly considered to be a tool that can significantly reduce the emission of CO_2. It is viewed as a technology that can contribute to a substantial, global reduction of emitted CO_2 within the timeframe that seems available for mitigating the effects of present and continued emission. In order to develop the CCS method the European Union (EU) has supported research programmes for more than a decade, which focus on capture techniques, transport and geological storage. The results of the numerous research projects on geological storage are summarised in a comprehensive best practice manual outlining guidelines for storage in saline aquifers (Chadwick *et al.* 2008). A detailed directive for geological storage is under implementation (European Commission 2009), and the EU has furthermore established a programme for supporting the development of more than ten large-scale demonstration plants throughout Europe. Geological investigations show that suitable storage sites are present in most European countries. In Denmark initial investigations conducted by the Geological Survey of Denmark and Greenland and private companies indicate that there is significant storage potential at several locations in the subsurface.

The Danish perspective in storage capacity

The ten largest point sources of CO_2 emission in Denmark account for 21 mega-tonnes per year (Mt/year). From preliminary investigations of the Danish subsurface the CO_2 storage capacity in selected subsurface structures is estimated to 2500 Mt (GeoCapacity 2009a). This corresponds to more than 100 years of storage from the ten largest emission point sources. The critical parameters of this analysis are the size of the structure, thickness, continuity and quality of the reservoir and the amount of formation water that may be displaced by the injected CO_2. The estimate is calculated assuming a surrounding aquifer volume displacement of formation water, which is limited to 50 times the trap volume (GeoCapacity 2009b).

These estimates of storage capacity are uncertain and have not yet been tested in real physical storage operation. Therefore it is difficult to evaluate to what degree the volume calculations are realistic. When a specific structure is selected for storage, a number of investigative steps are necessary, including acquisition and interpretation of new 2-D or 3-D seismic data, drilling of new wells, geological and reservoir modelling and flow simulation studies. For each step of incorporating new geological data, the site model of the reservoir is updated in the process of maturing the structure towards a storage site. This stepwise approach to site characterisation gradually leads to a research-based and relatively certain capacity estimate and an evaluation of the safety and behaviour of the site under simulated conditions, including the uncertainties of the estimates.

Assessment of geological and environmental risks can be carried out at various stages in the process. Similarly, establishment of baseline studies and monitoring strategies need to be considered along with the progress of the characterisa-

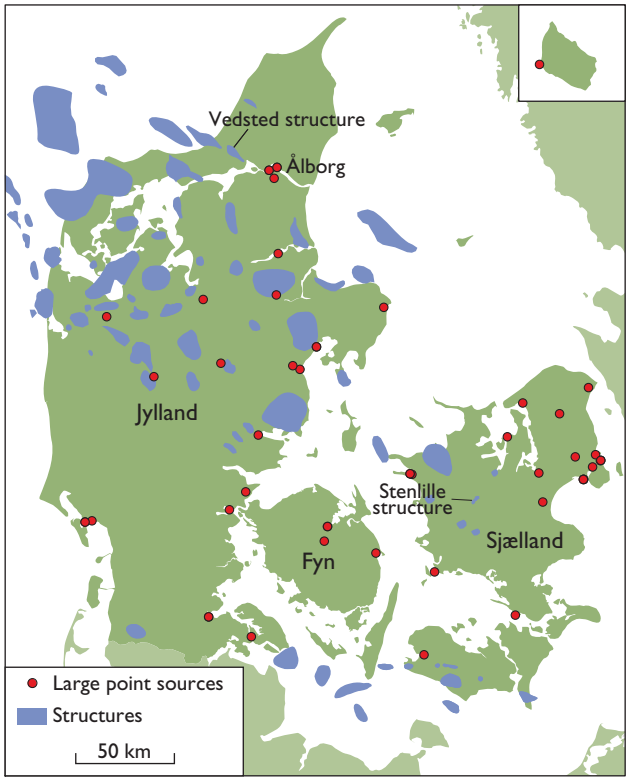

Fig. 1. Map of Denmark showing the most important point sources of CO_2 emission and prospective structures for geological storage of CO_2. The Stenlille structure is presently used for storage of natural gas; it serves to moderate seasonal fluctuations in consumption. The Vedsted structure is currently investigated for possible storage of CO_2.

tion of the storage site in order to make sure that the necessary background information is obtained before storage is initiated. In order to be reliable and operational, the baseline studies should preferably focus on measurement of conditions and properties that are stable and only show limited seasonal variations. Such studies may include groundwater-flow models and groundwater chemistry, pore water and pore gas analyses from deep wells, surface topography and natural seismicity.

A site study

Site investigations have recently been initiated of the Vedsted structure by Vattenfall A/S, with the intention of using the structure for storage of CO_2 from a nearby coal-fired power plant in Ålborg (Fig. 1; Sørensen *et al.* 2009). Existing data from oil exploration activities in the 1950s include one well in the centre of the structure and sparse 2-D seismic line data. The main target layer is the Triassic–Jurassic Gassum Formation at around 1800 m depth. The formation is widely distributed in the Danish Basin and has good reservoir properties (Fig. 2). It is currently used for storage of natural gas in the Stenlille structure on Sjælland and for geothermal energy in the Thisted area in northern Jylland.

Detailed sedimentological and sequence stratigraphic interpretations and correlations of the well logs and cores have established a robust stratigraphic framework for the Upper Triassic – Jurassic succession (Nielsen 2003). This framework forms the basis for the interpretation of the Vedsted-1 well section as well as predictions regarding the lithology of the potential reservoirs and seals in the Vedsted area (Fig. 3). The process has also underlined the necessity of acquisition of new data and more detailed modelling at several different scales.

At site scale, the optimal positioning of injection wells, as well as injectivity and capacity can be modelled and analysed, and the coupling between the operation of the power plant and the capture facility can be studied. The specific geological properties of the storage reservoir layers have consequences for the propagation and distribution of the injected CO_2 and for the storage mechanisms in the specific reservoir. Most reservoirs show both vertical and horizontal heterogeneities that will influence the distribution of the CO_2.

The preliminary reservoir model for the Vedsted structure has been investigated by simulating an injection well on its south-eastern flank and using injection rates realistic for power-plant supply rates (Frykman *et al.* 2009). After ten years of constant injection, the CO_2 distribution is as seen in Fig. 4, which clearly shows the subdivision of the migrating front into several sub-layers due to intraformational sealing layers with low permeability that also have high capillary entry pressures. The layering in the model has maximum lateral continuity, which probably overestimates the segregation to be found in real cases, but any intra-reservoir sealing layers will have such an effect on the distribution. Since this filling pattern influences the capacity, it is necessary to analyse further the properties and the continuity of the intraformational sealing layers.

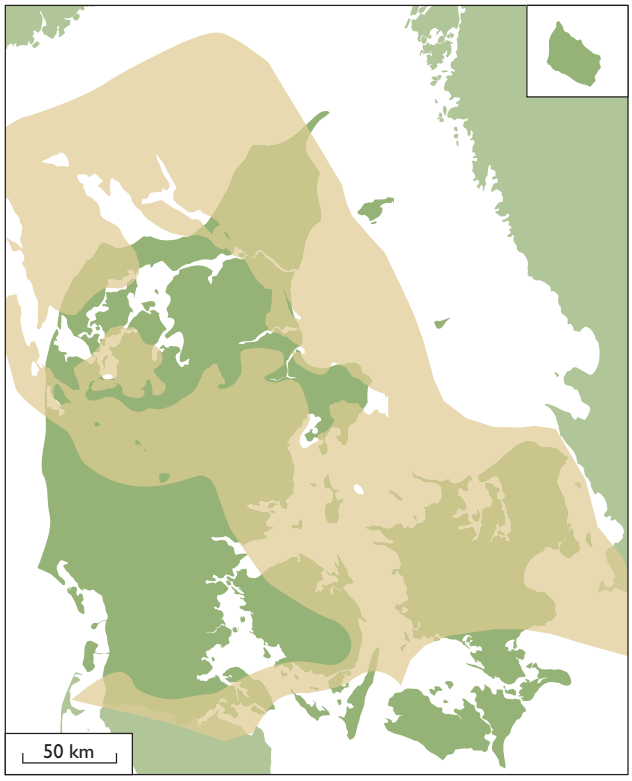

Fig. 2. Distribution of the Triassic–Jurassic Gassum Formation in the subsurface at depths between 800 m and 2400 m (yellow), the depth interval in which CO_2 exists as a supercritical phase and where burial diagenesis has not yet provoked significantly lowered porosity. At the supercritical phase the volume of CO_2 is much less than that of the CO_2 gas at the surface.

CO_2 can be trapped by several mechanisms, including structural trapping under an overlying sealing formation, dissolution of CO_2 in formation water, capillary trapping in the pore network and mineral trapping by reactions between CO_2 and mineral phases in the reservoir rock. These trapping mechanisms work on different scales both in space and time and need to be studied by designing appropriate models and experiments.

For large-scale injection of CO_2 displacing saline porewater, the propagation of the pressure field during injection outside the immediate site area is of interest. Modelling of this pressure distribution will serve to predict the amount of overpressure building up locally within the storage site, and can be used to suggest possible means of management.

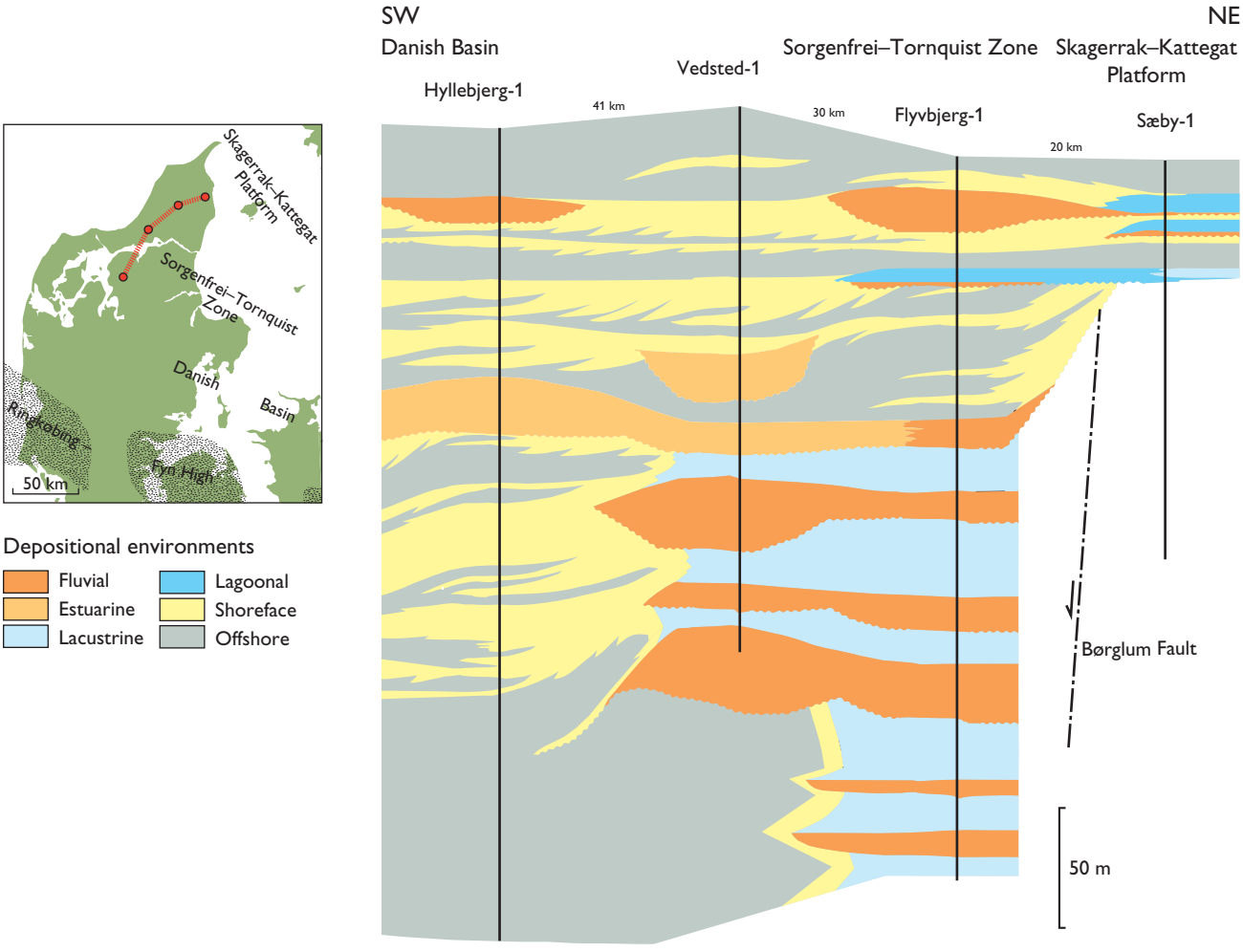

Fig. 3. SW–NE-oriented cross-section across the Danish Basin, the Sorgenfrei–Tornquist Zone and the Skagerrak–Kattegat Platform (red line on the index map). The panel shows the lower part of the Gassum reservoir which comprises fluvial, estuarine and shallow-marine deposits interbedded with offshore mudstones and some lacustrine mudstones. Shoreline fluctuations have caused interfingering of these different facies types and given rise to pronounced vertical variability. Informations from the four wells in the section about sedimentary facies have been interpreted and correlated into a sequence-stratigraphic framework. At a local site, this framework must be confirmed from detailed investigations of material from new wells drilled, and supplemented with new seismic data. Modified from Nielsen (2003).

The scale of the challenge and future perspective

The first detailed pan-European assessment of CO_2 storage capacity in the framework of the EU research project GeoCapacity has resulted in a geographic information system (GIS) database of CO_2 emissions, storage capacity estimates and geological information. The database includes information on reservoirs with a total storage capacity of 360 000 Mt CO_2, with 326 000 Mt in deep saline aquifers, 32 000 Mt in depleted hydrocarbon fields and 2000 Mt in unmineable coal beds: 116 000 Mt are onshore, and 244 000 Mt offshore (GeoCapacity 2009a). Some of the estimated storage capacity is associated with structural traps, but a very large part is in regional deep saline aquifers without identified specific traps. Almost 200 000 Mt of the total storage capacity in the database are located offshore Norway. These estimates date back to 2003 and have not been updated within the GeoCapacity project. An attempt to provide a more cautious and conservative European estimate has yielded a storage capacity of 117 000 Mt with 96 000 Mt in deep saline aquifers, 20 000 Mt in depleted hydrocarbon fields and 1000 Mt in coal beds, and with approximately 25% located offshore Norway. This must be compared to a total of 2000 Mt of CO_2 emission from large point sources, i.e. point sources emitting more than 0.1 Mt/year within Europe.

In order to illustrate the scale of the technology and infrastructure that has to be established if CCS is to become an active industry, we can look at the amount of CO_2 produced by the ten largest point sources in Denmark. There are 43 large point sources emitting 28 Mt CO_2/year, the ten largest of which are responsible for 21 Mt/year. At surface condi-

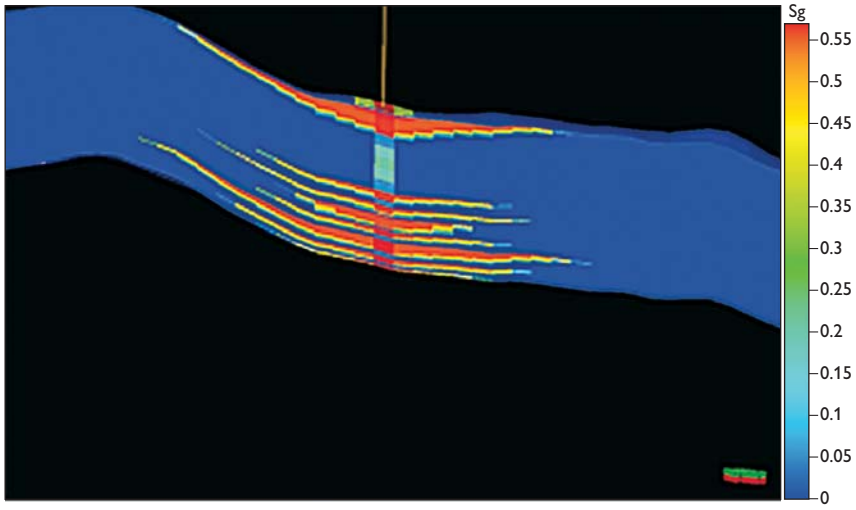

Fig. 4. Vertical NW–SE section in the Gassum reservoir model through the injection well, showing CO_2 saturation Sg (free gas-phase supercritical CO_2) after 10 years of injection. Although the model is constructed in a fairly coarse grid, the intra-reservoir sealing layers are clearly reflected and influence the spatial distribution of the injected CO_2. The sedimentary layering causes filling of the individual layers of porous sand with the injected CO_2, whereas the interbedded mudstone layers with much lower reservoir quality are not filled and also limit the vertical movement of CO_2. Model thickness 300 m, length 4800 m, vertical exaggeration 5 times. (Modified from Frykman *et al.* 2008).

tions this corresponds to 11 billion (11×10^9) m^3 CO_2 gas. The annual production of natural gas from the Danish part of the North Sea amounts to 10 billion (10×10^9) m^3 (Danish Energy Agency 2008), which is transported in pipelines and tankers and processed at plants and refineries. The comparable size of the potential volume of CO_2, to be moved around at surface and injected into the subsurface (although compressed to smaller volumes at depth), points to the large scale at which a CCS-related processing and transporting industry has to be established.

Concluding remarks

The CCS activities described here related to large-scale storage operations will involve significant physical resources and manpower. Fortunately, the work with storage-related items does not have to begin from first principles, because much of the experience already exists in the oil and gas industry, which can provide methods and tools for immediate use. The skills of geoscientists and engineers are needed in the investigation and characterisation of the sites and the subsurface conditions for storage of CO_2, and a whole new infrastructure and industry may be established. Geoscience and geo-engineering will play a major role in the analysis of the geological foundation, the assessment of site performance, and will be critical in securing the safety of the operations.

Initial investigations of the Danish subsurface indicate that suitable structural traps with a significant storage potential are present at several locations, and that the structures can accommodate the CO_2 produced from several or most of the large Danish point sources. Thus, geological storage of CO_2 may contribute considerably to the reduction of the Danish CO_2 emission, if we can be assured about safety issues, and if political and public acceptance can be obtained.

References

Chadwick, A., Arts, R., Bernstone, C., May, F., Thibeau, S. & Zweigel, P. 2008: Best practice for the storage of CO_2 in saline aquifers – observations and guidelines from the SACS and CO2STORE projects. British Geological Survey Occasional Publication **14**, 267 pp.

Danish Energy Agency 2008: Oil and gas production in Denmark 2007, 98 pp. Copenhagen: Danish Energy Agency.

European Commission 2009: Directive of the European Parliament and of the Council on the geological storage of carbon dioxide, 84 pp. Brussels: European Union.

Frykman, P., Bech, N., Sørensen, A.T., Nielsen, L.H., Nielsen, C.M., Kristensen, L. & Bidstrup, T. 2009: Geological modelling and dynamic flow analysis as initial site investigation for large-scale CO_2 injection at the Vedsted structure, NW Denmark. 9th International Conference on Greenhouse Gas Control Technologies, Washington D.C., 16–20 November, 2008. GHGT9 Energy Procedia **1**, 2975–2982.

GeoCapacity 2009a: GeoCapacity WP 2 Report, Storage capacity. EU GeoCapacity deliverable D16, 162 pp. EU GeoCapacity Consortium, Brussels.

GeoCapacity 2009b: GeoCapacity WP 4 Report, Capacity standards and site selection criteria. EU GeoCapacity deliverable D26, 45 pp. EU GeoCapacity Consortium, Brussels.

Nielsen, L.H. 2003: Late Triassic – Jurassic development of the Danish Basin and the Fennoscandian Border Zone, southern Scandinavia. In: Ineson, J.R. & Surlyk, F. (eds): The Jurassic of Denmark and Greenland. Geological Survey of Denmark and Greenland Bulletin **1**, 459–526.

Sørensen, A.T., Klinkby, L., Christensen, N.P., Dalhoff, F., Biede, O. & Noer. M. 2009: Danish development of a full-scale CCS demonstration plant in a saline aquifer. First Break **27**, 79–83.

Authors' address

Geological Survey of Denmark and Greenland, Øster Voldgade 10, DK-1350 Copenhagen K, Denmark. E-mail: *pfr@geus.dk*

Increased oil recovery from Halfdan chalk by flooding with CO_2-enriched water: a laboratory experiment

Dan Olsen

Injection of CO_2 is a method that may increase the recovery of oil from Danish chalk reservoirs in the North Sea. The method is used elsewhere, particularly in North America, but has so far not been used in the North Sea and has nowhere been used for chalk reservoirs, and the performance of the method when used for North Sea chalk is therefore uncertain. A laboratory flooding experiment was conducted at the Geological Survey of Denmark and Greenland on a sample from the Nana-1X well of the Halfdan oil field in the Danish North Sea in order to test the efficiency of CO_2-enriched water to produce additional oil from chalk. The sample is a low-permeability chalk from the Ekofisk Formation and represents rocks that are marginal to the Halfdan reservoir in an economical sense.

Outline of the experiment

For the flooding experiment, four 1.5 inch core plug samples were assembled to form a composite sample with a total length of 28 cm and a pore volume of 92 ml. The flooding experiment was conducted at a fluid pressure of 282 bars, a hydrostatic confining pressure of 429 bars, and a temperature of 85°C. These are conditions similar to those of the Halfdan reservoir. First the oil content, S_o, of the sample was adjusted to 77.7% of the pore volume (PV), the remaining pore fluid being simulated formation water. The sample was then brought to reservoir conditions, aged for three weeks to restore the wettability to reservoir conditions and then flooded with simulated formation water until oil production from the sample had ceased. After changing the flooding fluid to CO_2-enriched water, flooding was resumed and sustained until oil production had declined to a negligible level. Flooding was then stopped, the rig was cooled and depressurised, and the sample was dismounted. Both flooding operations were conducted with the sample in a vertical position from the bottom towards the top. A thorough description of the experiment is given in Olsen (2007).

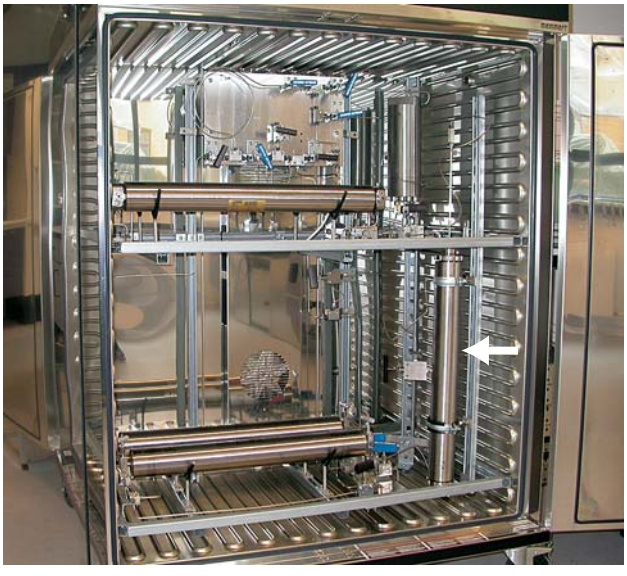

Fig. 1. Oven with high-pressure equipment used for the experiment described in this paper. The oven is 160 cm high. The arrow shows the core holder that was used for the experiment.

Experimental set-up

The experiment was conducted in a rig that simulates reservoir conditions. The rig consists of a Hassler-type core holder, a number of pressure cylinders for the experimental fluids, an acoustic separator for quantifying the fluid production, a differential pressure transducer for permeability measurement, and a high-pressure pump system for generating confining pressure, flow and pore fluid pressure. The core holder, pressure cylinders, separator, and differential pressure transducer are all situated inside a thermostatically controlled oven (Fig. 1).

Temperature and fluid pressure conditions were based on data from the adjacent Dan field reservoir, and corrected for the 250 m depth difference between the two reservoirs, Halfdan being the deeper. The temperature was corrected using a temperature gradient of 0.04°C/m. Assuming pressure correspondence between the two reservoirs, the Halfdan fluid pressure was estimated by extrapolation from the Dan field using a pressure gradient of 0.075 bar/m. Temperature, pressure and gradient values are from Jørgensen (1992). The oil used in the experiment was degassed crude oil from the Dan field. The water composition was similar to that of formation water from the Halfdan field. Fluid densities were measured at GEUS, while the water viscosity at reservoir conditions was estimated from data on the viscosity of similar brines. During the experiment differential pressure across the sample, pore fluid pressure, hydrostatic confining pressure, flow

Table 1. Flooding experiment to enhance oil recovery: sample characterisation

	Initial characterisation	Final characterisation	Change	Percent change
Dry weight (g)	613.37	609.05	–4.32	–0.70
Diameter (cm)	3.77	3.77	0.00	0.07
Length (cm)	28.32	28.24	–0.07	–0.26
Bulk volume (ml)	318.56	316.92	–1.64	–0.52
Porosity (% bulk volume)	28.77	29.09	0.32	1.10
Pore volume (ml)	91.64	92.18	0.53	0.58
Gas permeability (mD)	0.62	0.76	0.14	23

rate, cumulative injected fluid volume, produced oil volume and temperature were continuously logged. Before and after the flooding experiment the sample was characterised by measuring a number of parameters (Table 1).

Water flooding

The water flooding took place with a constant flooding rate of 0.62 ml/h and lasted 33 days with a total water injection of 490 ml or 5.35 times the pore volume. Results of the water flooding are presented in Fig. 2. Water breakthrough occurred after 77 hours when the water throughput was 0.458 times the pore volume. Before breakthrough, oil was produced from the sample at the same rate as the water was being injected. After breakthrough, the rate of oil production dropped sharply and continuously. A low oil production rate was sustained for a considerable time, but stopped completely before the flooding was terminated. A total oil volume of 0.053 times the pore volume was produced after breakthrough. Total oil production during the water flooding was 0.496 times the pore volume or 63.8% of the oil originally present in the sample.

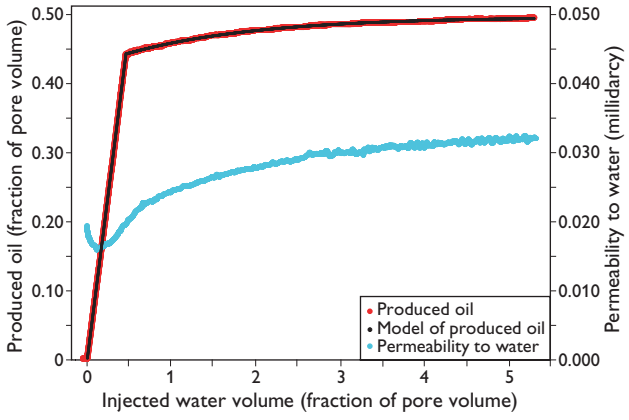

Fig. 2. Produced oil volume (N_p) versus injected water volume (V_{inj}) during flooding with water. Model before breakthrough: $N_p = 0.98 \times V_{inj}$. Model after breakthrough: $N_p = 0.50 - 0.08 \times \exp(-V_{inj}/1.57)$. Fluid saturation (fraction of pore volume): initial water saturation = 0.223, water breakthrough at water saturation = 0.666, final water saturation = 0.719, produced oil = 0.496.

A model was developed that fits the oil production (Fig. 2). Before breakthrough, the oil production shows a linear relationship with the injected water volume. After breakthrough, the oil production shows an exponentially decreasing relationship. Both relationships show a nearly perfect fit to the actual oil production.

Measurements of differential pressure across the sample were used to calculate the water permeability during the water flooding (Fig. 2). At the end of the water flooding the differential pressure had stabilised, indicating that fluid movement within the sample had stopped. Both the oil production and permeability curves show typical water-flooding development.

Flooding with CO_2-enriched water

The flooding with CO_2-enriched water was carried out at the same rate as the water flooding, i.e. at 0.62 ml/h. It lasted 64 days, and the total throughput of CO_2-enriched water was 949 ml or 10.4 times the pore volume. The CO_2-enriched water had a CO_2-content of 26.6 standard m^3 CO_2/standard m^3 water corresponding to a CO_2-saturation of 100% at 85°C and 282 bars fluid pressure (Chang *et al.* 1998).

Diffusion of CO_2 between oil, CO_2-enriched water and water without CO_2 may cause the oil within the separator to either swell or shrink as CO_2 diffuses between the fluid phases. Such volume changes are troublesome as they cannot be distinguished from oil being produced from the sample. In an attempt to establish equilibrium between separator oil and CO_2-enriched water, an amount of CO_2 was added to the separator before starting the CO_2-enriched flooding and allowed to equilibrate with the separator fluids for nine days. Using the data of Chang *et al.* (1998) the amount of CO_2 was adjusted so as to create the same CO_2-saturation in the water of the separator as in the brine used for flooding.

Figure 3 presents a plot of oil produced during the CO_2-enriched flooding versus time. The oil production curve has

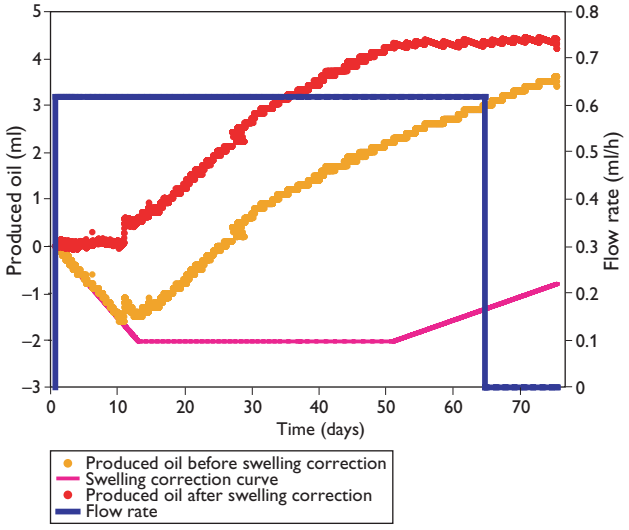

Fig. 3. Swelling correction curve for flooding with CO_2-enriched water with production curves before and after correction.

a peculiar shape with an initial negative slope, indicating that the volume of oil in the separator was reduced. As oil cannot flow from the separator, the negative slope indicates that the oil in the separator shrank in volume during the first part of the CO_2-enriched flooding. After the section with negative slope, the slope of the oil production curve changes to positive and obtains the appearance of an ordinary oil production curve with oil apparently being produced at a low rate right until the end of flooding. After cessation of the flooding the rig was left undisturbed for 10.8 days, with the conditions of the rig being the same as during the CO_2-enriched flooding, except that the fluid delivery pump was stopped. During this time the separator continued to register an increase in oil volume, at a rate that was indistinguishable from the rate during the final part of the CO_2-enriched flooding (Fig. 3). As the construction of the rig prevents oil from flowing to the separator when the delivery pump is stopped, the apparent oil production after flow-stop is considered to represent swelling of the oil within the separator. The situation appears similar to that at the beginning of the CO_2-enriched flooding, only that swelling takes place instead of shrinkage.

During flooding with CO_2-enriched water it is expected that no oil is produced from the sample before oil affected by the CO_2 has moved to the outlet end of the sample. It is therefore reasonable to assume that the initial section of the oil production curve with negative slope represents the time before breakthrough of the CO_2-enriched water and the first produced oil. The section with negative slope then represents a period without oil production and should be horizontal. The section of the oil production curve after flow-stop should also be horizontal as no oil can be produced without flow. Using these arguments a swelling correction curve has been constructed (Fig. 3). As oil shrinkage in the separator changed to oil swelling during the experiment, a section with neither shrinkage nor swelling is present in the middle part of the correction curve. This part of the curve indicates equilibrium in the separator. The correction curve of Fig. 3 therefore consists of three linear segments indicating shrinkage, equilibrium and swelling. A true correction curve probably would have a gradually changing slope, but in the absence of more information, linear line segments have been used.

The data are interpreted as follows: At the start of flooding with CO_2-enriched water, the pore space of the sample contained 66 ml of CO_2-free water while the fluids of the separator were CO_2-saturated. During the first week of the flooding, the CO_2-free water of the sample flowed to the separator and caused the oil of the separator to shrink as CO_2 diffused from oil to water. After breakthrough of CO_2-enriched water, the CO_2 content of the water in the separator gradually increased. After some time the direction of CO_2 diffusion changed, causing the oil of the separator to swell, a condition that continued after the end of the flooding.

Figure 4 presents oil production curves for flooding with CO_2-enriched water with and without correction for swelling. Compared to the water flooding, the amount of oil produced during flooding with CO_2-enriched water was small. Total oil production was 0.047 times the pore volume equivalent to 6.1% of the oil originally present in the sample, if swelling correction is applied, and 0.032 times the pore volume or 4.2% of the oil originally present in the sample, if swelling correction is omitted. The swelling correction is considered valid, and hence the corrected values are preferred.

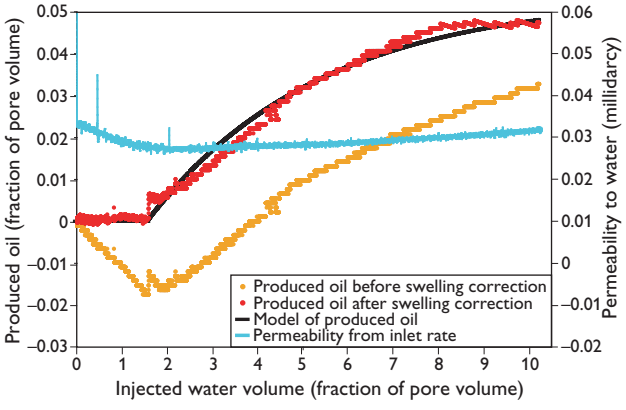

Fig. 4. Produced oil volume (N_p) versus injected fluid volume (V_{inj}) during flooding with CO_2-enriched water compared to production curves with and without correction for swelling. Model before breakthrough: $N_p = 0$. Model after breakthrough: $N_p = 0.05 - 0.08 \times \exp(-V_{inj}/3.8)$. Fluid saturation (fraction of pore volume): water saturation before CO_2 flood = 0.719. **With** swelling correction: water saturation after CO_2 flood = 0.767, oil production during CO_2 flood = 0.047. **Without** swelling correction: water saturation after CO_2 flood = 0.752, oil production during CO_2 flood = 0.032.

Fig. 5. The inlet end of the composite sample showed a dissolution structure after flooding with CO_2-enriched water. The star-like shape is governed by the arrangement of the distributor channels in the end pieces of the core holder.

A model has been developed that approximates the oil production profile (Fig. 4). The fit is reasonable, although inferior to the fit obtained for the water flooding (Fig. 2). The inferior fit is at least partly caused by the smaller volume changes compared to the water flooding, causing a greater relative experimental uncertainty.

Dissolution effects

The bulk volume of the sample was reduced by 1.64 ml during the experiment (Table 1), equivalent to a grain volume loss of 1.17 ml. This is attributed to a distinct dissolution structure that was found at the inlet end face after the experiment (Fig. 5). The structure was due to dissolution of the chalk by the CO_2-enriched water. Dissolution structures were not visible on the other surfaces of the sample. Porosity of the sample increased by 0.32% of the bulk volume during the experiment (Table 1), which indicates that 1.01 ml of grain material were dissolved from the interior of the sample during the experiment. Combining the bulk volume loss and the porosity increase indicates a total dissolution of 2.18 ml of grain material, which is equivalent to the loss of 5.91 g of calcite. The measured weight loss was 4.32 g, which is considered to agree within the experimental uncertainty (Table 1).

The gas permeability increased by 23% during the experiment (Table 1), which is remarkable compared to the modest increase in porosity. The increase in both porosity and permeability was evenly distributed among the four subsamples, indicating a certain amount of dissolution throughout the sample (Olsen 2007). The evidence shows that dissolution took place both close to where the CO_2-enriched water entered the sample and within the sample. A small length reduction (Table 1) occurred due to the formation of the dissolution structure.

Conclusions

Water flooding of a low-permeable Ekofisk chalk sample from the Nana-1X well in the Danish North Sea resulted in an oil saturation of 28.0% of the pore volume with an oil recovery of 63.8% of the oil originally present in the sample. Flooding with CO_2-enriched water corresponding to 10.4 times the pore volume increased the oil recovery by 6.1% of the oil originally present in the sample, resulting in a final oil saturation of 23.3% of the pore volume. Compared to the water flooding, the flooding with CO_2-enriched water increased the final oil recovery by 9.6%. A correction procedure was applied to correct for diffusion processes within the separator of the rig. At the inlet end of the sample a dissolution structure was created by the CO_2-enriched water. The rest of the sample was visually unaffected by the flooding, but the injection resulted in a 1.1% increase in porosity and a 23% increase in gas permeability, which shows that some dissolution took place within the pore space of the sample.

Acknowledgements

Financial support was received from the Ministry of Science, Technology and Innovation, and from the European Network of Excellence on Geological Storage of CO_2 that is co-funded by the European Commission within the 6th Framework Programme.

References

Chang, Y., Coats, B.K. & Nolen, J.S. 1998: A compositional model for CO_2 floods including CO_2 solubility in water. SPE Reservoir Evaluation & Engineering **1**, 155–160.

Jørgensen, L.N. 1992: Dan Field – Denmark, Central Graben, Danish North Sea. In: Foster, N.H. & Beaumont, E.A. (eds): Atlas of oil and gas fields. Structural traps VI, 199–218. Tulsa: American Association of Petroleum Geologists.

Olsen, D. 2007: Increased oil recovery from the Danish North Sea chalk fields. Flooding experiment OCD1. Danmarks og Grønlands Geologiske Undersøgelse Rapport **2007/30**, 20 pp.

Author's address

Geological Survey of Denmark and Greenland (GEUS), Øster Voldgade 10, DK-1350 Copenhagen K, Denmark. E-mail: *do@geus.dk*

Ladinian palynofloras in the Norwegian–Danish Basin: a regional marker reflecting a climate change

Sofie Lindström, Henrik Vosgerau, Stefan Piasecki, Lars Henrik Nielsen, Karen Dybkjær and Mikael Erlström

The Triassic – lower Cretaceous sedimentary succession of the Norwegian–Danish Basin has for a long time been of exploration interest, and numerous studies have been carried out. However, high-resolution correlation within the basin remains necessary, especially between the Danish and Norwegian parts of the basin. A variety of litho- and biostratigraphic schemes have been applied to the succession over the years, but lack of consistency in terminology has often led to confusing interpretations of the geological development. In this study a sequence stratigraphic scheme has been developed for the Danish Basin and a compiled palynological event stratigraphy is applied to a number of wells connecting the Danish and Norwegian parts of the basin and new marker horizons are identified. One of the aims of this study is to reach consistency in order to facilitate correlation within the basin and we also emphasise the recognition of a potentially important mid-Triassic event in the basin.

Geological setting

The intracratonic Permian–Cenozoic Norwegian–Danish Basin is bounded to the south by the Ringkøbing–Fyn High and to the north by the strongly faulted Sorgenfrei–Tornquist Zone (Fig. 1). The basin was formed by Late Carboniferous – Early Permian crustal extension followed by thermal sagging, local faulting and salt tectonics. The syn-rift succession consists of Rotliegendes volcaniclastic rocks, alluvial conglomerates and sandstones as well as lacustrine mudstones. The overlying Zechstein–Cenozoic post-rift succession consists of two major sequences separated by an early Middle Jurassic unconformity that reflects regional uplift and erosion (Nielsen 2003). The lower sequence comprises Zechstein salt, Triassic sandstones, mudstones, marls and carbonates and Lower Jurassic claystones, while the upper sequence encompasses Middle Jurassic – Lower Cretaceous clastic rocks,

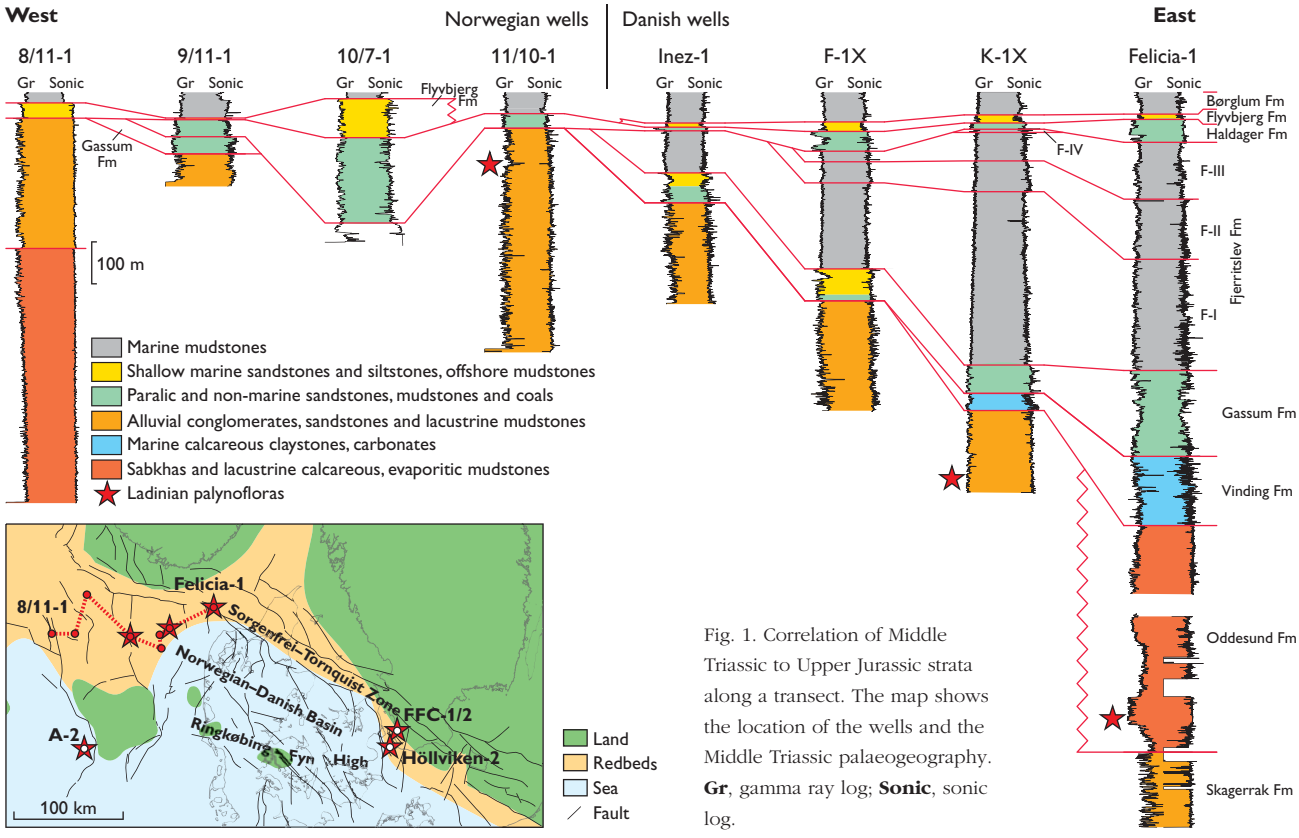

Fig. 1. Correlation of Middle Triassic to Upper Jurassic strata along a transect. The map shows the location of the wells and the Middle Triassic palaeogeography. **Gr**, gamma ray log; **Sonic**, sonic log.

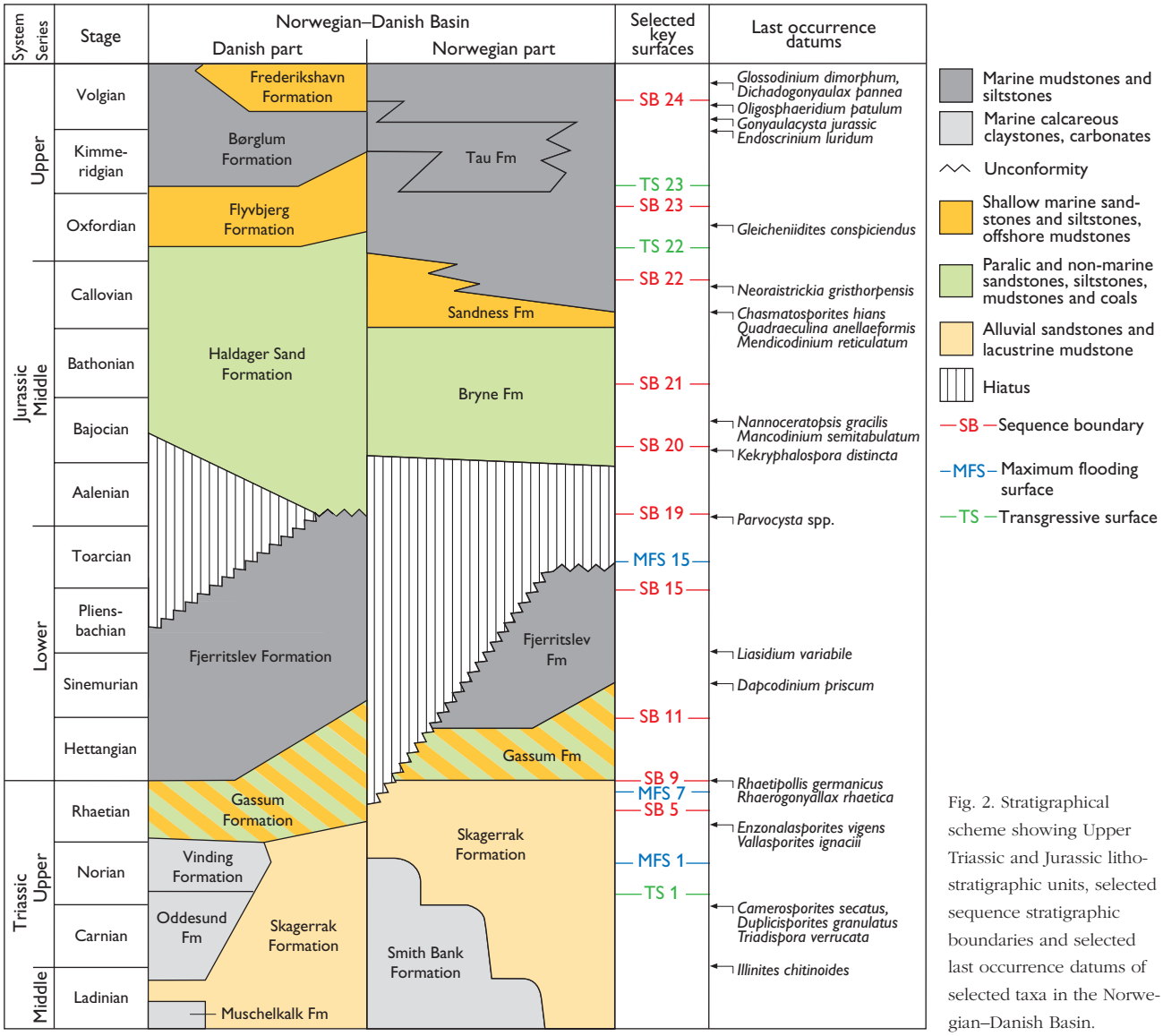

Fig. 2. Stratigraphical scheme showing Upper Triassic and Jurassic litho-stratigraphic units, selected sequence stratigraphic boundaries and selected last occurrence datums of selected taxa in the Norwegian–Danish Basin.

Upper Cretaceous Chalk and Cenozoic clastic rocks. Large parts of the lower sequence are difficult to date accurately by biostratigraphy owing to the predominantly continental strata deposited during a hot and arid climate, whereas the upper sequence is dominated by marine fossiliferous deposits, which are easier to date.

The investigated succession and the stratigraphic approach

The principal reservoir rocks and potential source rocks of the basin were formed during Late Triassic – Late Jurassic times (Petersen *et al.* 2008). Different lithostratigraphic terminologies are used for the Norwegian and Danish areas (Fig. 2). An inconsistent mixture of lithostratigraphic names from both Norwegian and Danish schemes is commonly used by the operators in well reports, and in some cases, lithostratigraphic names normally applied to units in the Norwegian Central Graben further contribute to the confusion. A robust sequence stratigraphic scheme established in the Danish Basin by Nielsen (2003) and a compiled palynostratigraphic event scheme are applied to a number of wells (Felicia-1, K-1, F-1, Inez-1, 11/10-1, 10/7-1, 9/11-1 and 8/11-1) situated along an E–W trending transect from the Fjerritslev Fault NW of Jylland to the border of the Norwegian Central Graben (Fig. 1). Based on characteristic well-log patterns supported by lithological descriptions from well reports, formation tops and sequence stratigraphic surfaces were identified and integrated with palynological events identified in this study. The latter events are based on established spore–pollen and dinoflagellate cyst stratigraphies for the Triassic – Early Cretaceous of western Europe. Selected important palynostratigraphic events and sequence stratigraphic surfaces are shown in Fig. 2.

The results of the correlation show that lithostratigraphic units and key sequence stratigraphic surfaces can be followed across the Danish and Norwegian areas indicating that the general depositional development along the transect largely follows the pattern described by Nielsen (2003). Hence, the sequence stratigraphic and lithostratigraphic schemes established for the Danish part were successfully applied to the Norwegian wells, as exemplified in Figs 1, 2.

However, the lack of readily recognisable sequence stratigraphic key surfaces and biostratigraphic events within the Middle – Upper Triassic succession is a major problem for reliable stratigraphic analyses.

The Middle Triassic – an unsuitable climate for palynomorph preservation

During the Middle Triassic the Norwegian–Danish Basin was situated around 35°N. The arid to semi-arid conditions that had prevailed during the Early Triassic continued, as signified by mainly fluvial and lacustrine, heterogeneous, siliciclastic rocks of the Skagerrak Formation (Michelsen & Clausen 2002). Marine calcareous mudstones and carbonates of the Muschelkalk Formation in the North German Basin expanded northwards during a transgressive event in the Anisian to early Ladinian (Michelsen & Clausen 2002). Arid to semi-arid climatic conditions continued during early Late Triassic times, with deposition of variegated, calcareous, anhydritic and pyritic mudstones in sabkhas and ephemeral lakes. In the deep central part of the basin more permanent lakes were established. The deposits are included in the Oddesund (Danish area) and Smith Bank (Norwegian area) formations. Towards the basin margins in the north and north-east these deposits pass into alluvial fans and fluvial sediments of the Skagerrak Formation. The combination of large lateral variations in depositional environment and the absence of extensive marine-flooding surfaces and marked unconformities hinder identification of reliable and regional sequence stratigraphic key surfaces.

Whereas Middle to lower Upper Triassic successions of the Arctic, Alpine and Tethys regions show evidence of fairly rich and diverse vegetation, the pre-Rhaetian Triassic redbeds of the Norwegian–Danish Basin only contain sparse palynomorphs. However, this does not necessarily mean that there were no plants growing in the area at the time of deposition. Most arid areas today host some vegetation adapted to such a hostile climate, but conditions for preservation of palynomorphs are generally poor due to oxidation of the sediments. Nevertheless, the present study indicates that during a restricted interval in the latest Middle Triassic the area hosted a relatively rich vegetation and the climatic conditions in the area were better suited for palynomorph preservation.

Ladinian spore–pollen floras

Well-preserved, typical Middle Triassic palynofloras were found in ditch cuttings from the lowermost part of the Oddesund Formation in the Felicia-1 well, and in the lower part of the Skagerrak Formation in K-1 and 11/10-1. These assemblages are distinguished from caved Rhaetian–Cretaceous material by their generally darker colour. All the assemblages contain *Illinites chitonoides*, a pollen species that has a last appearance datum at the top of the Ladinian in northern Europe, and within the Carnian in the Arctic region (de Graziansky *et al*. 1998). The assemblage from Felicia-1 is dominated by the bisaccate pollen *Ovalipollis ovalis /pseudoalatus*, which has its first common appearance datum at the base of the late Ladinian (de Graziansky *et al*. 1998). In addition, members of *Protodiploxypinus*, e.g. *P. fastidioides* and *P. macroverrucosus*, and *Triadispora*, mainly *T. crassa, T. plicata, T. verrucata*, are common constituents of the palynofloras. The co-occurrence of *Angustisulcites klausii, Kuglerina meieri, Podosporites amicus, Staurosaccites quadrifidus, Rimaesporites aquilonalis, Aratrisporites* spp., *Camerosporites secatus, C. verrucatus, Duplicisporites granulatus* and *Enzonalasporites vigens* also suggests a late Ladinian age (de Graziansky *et al*. 1998; Schulz & Heunisch 2005). The presence in Felicia-1 of the typical Triassic chlorococcalean coenobium *Plaesiodictyon mosellanum* with a known stratigraphical range from late Anisian to latest Norian indicates brackish to freshwater conditions.

In the easternmost parts of the Norwegian–Danish Basin comparable palynofloras are present in core samples from the Höllviken-2 well and two other wells in southern Sweden. The Höllviken-2 palynoflora is dominated by monolete (*Aratrisporites* spp.) and trilete (e.g. *Calamospora* spp. and *Anapiculatisporites* spp.) spores, but bisaccate pollen are also abundant and diverse. Both abundant *Aratrisporites* spores and species of *Protodiploxypinus* suggest a latest Muschelkalk – early Keuper (i.e. Ladinian) age, and this range is further limited to early Keuper by the presence of *Retisulcites perforatus* (last appearance datum in earliest Carnian), *Nevesisporites lubricus*, and *Ovalipollis brutus*. A banana-shaped acritarch, *Dactylofusa* sp., is present in the palynoflora from FCC-1.

Comparable palynofloral assemblages were found in well A-2 in the Danish Central Graben containing e.g. *Aratrisporites saturni, Angustisulcites klausii, Illinites chitonoides, Triadispora* spp., *Protodiploxypinus fastidioides, P. granulatus, Protodiploxypinus* spp., and *Striatoabieites aytugii* (Bertelsen 1975). Thus, typical Ladinian palynofloras appear to be present within a relatively restricted time interval along the northern margin of the mid-Triassic Muschelkalk sea.

Remarks on stratigraphy, environment and climate

The Höllviken-2 assemblages are recorded in a succession of dark, fine-grained sediments (Maglarp-C member) with fossiliferous intervals containing fossil fish, ostracods and characean algae. Previous biostratigraphy based on the latter correlates the succession with late Muschelkalk to early Keuper, i.e. mainly of Ladinian age (Kozur 1974). The characean algae suggest limnic to possibly brackish environments, while the fish fauna vary from limnish-brackish (e.g. *Paleobates* spp.) to fully marine (e.g. *Birgeria* spp. and *Hybodus* spp.). The ostracods (*Bairdia* spp.) indicate warm, shallow littoral environments. Hence, the combined macrofossil evidence suggests a shallow marine environment with brackish to limnic lagoons behind the coast. The palynoflora recorded in the Höllviken-2 core supports a Ladinian age.

All the contemporaneous palynofloras described here contain several elements typical of warm and dry conditions. For instance, *Aratrisporites* is a common constituent in arid to semi-arid Triassic palynofloras worldwide. The parent plants, pleuromeiacean lycopsids, appear to have been opportunistic and saline-tolerant inhabitants of intertidal environments (Retallack 1975). The taeniate bisaccates, e.g. *Lunatisporites* and *Striatoabieites*, are generally regarded to have been produced by pteridosperms, and adapted to warm and dry conditions. The bisaccate pollen of *Triadispora, Protodiploxypinus, Ovalipollis, Illinites* and *Staurosaccites*, as well as the monosaccate pollen *Enzonalasporites,* and pollen of the Circumpolles group, i.e. *Duplicisporites* and *Camerosporites*, are all believed to come from conifers. The Circumpolles group is only recorded in some of the investigated assemblages. They are regarded as relatives to the cheirolepids, a group of conifers often associated with warm and dry conditions. In palynofloras of similar age from central and south Europe, pollen of the Circumpolles group tend to be much more abundant.

The diverse Ladinian spore–pollen flora described above indicates a generally warm and dry climate, but the diversity and preservation suggest a change towards more humid conditions favouring preservation of palynomorphs during this interval. In Germany and Poland the uppermost Ladinian, known as the Lettenkeuper, is interpreted as reflecting more humid conditions. It seems plausible that the palynofloras recorded in this study reflect the same change to more humid conditions.

Conclusions

The recorded Ladinian palynofloras from the Maglarp-C member in southern Sweden, the lowermost Oddesund Formation in Denmark, and from the middle Skagerrak Formation in both Denmark and Norway, enable correlation between these units in the otherwise poorly dated Triassic succession in the Norwegian–Danish Basin. The fact that the palynofloral assemblages are recognisable even in ditch cutting material of exploration wells makes them very useful markers. The palynoflora contains many elements indicating a warm and dry climate, and deposition in fresh to brackish water in coastal environments. The preservation of the palynoflora probably reflects a climatic event with a change to more humid conditions, similar to that recorded in northern and central Europe.

Acknowledgement

We thank Talisman Energy Norway A/S for allowing us to publish results from the Norwegian wells.

References

Bertelsen, F. 1975: Triassic palynology and stratigraphy of some Danish North Sea boreholes. Danmarks Geologiske Undersøgelse Årbog **1974**, 17–32.

de Graziansky, P.-C., Hardenbol, J., Jacquin, T. & Vail, P.R. (eds) 1998: Mesozoic and Cenozoic sequence stratigraphy of European basins. Society for Sedimentary Geology (SEPM) Special Publication **60**, 786 pp.

Kozur, H. 1974: Biostratigraphie der germanischen Mitteltrias. Freiberger Forschungshefte C**280** Paläontologie, Teil I, II & Anlagen, 56 pp. + 71 pp.

Michelsen, O. & Clausen, O.R. 2002: Detailed stratigraphic subdivision and regional correlation of the southern Danish Triassic succession. Marine and Petroleum Geology **19**, 563–587.

Nielsen, L.H. 2003: Late Triassic – Jurassic development of the Danish Basin and the Fennoscandian Border Zone, southern Scandinavia. In: Ineson, J.R. & Surlyk, F. (eds): The Jurassic of Denmark and Greenland. Geological Survey of Denmark and Greenland Bulletin **1**, 459–526.

Petersen, H.I., Nielsen, L.H., Bojesen-Koefoed, J.A., Mathiesen, A. & Dalhoff, F. 2008: Evaluation of the quality, thermal maturity and distribution of potential source rocks in the Danish part of the Norwegian–Danish Basin. Geological Survey of Denmark and Greenland Bulletin **16**, 66 pp.

Retallack, G.J. 1975: The life and times of a Triassic lycopod. Alcheringa **1**, 3–29.

Schulz, E., & Heunisch, C. 2005: Palynostratigraphische Gliederungsmöglichkeiten des deutschen Keupers. Courier Forschungsinstitut Senckenberg **253**, 43–49.

Authors' addresses

S.L., J.H.V., L.H.N., S.P., & K.D., *Geological Survey of Denmark and Greenland, Øster Voldgade 10, DK-1350 Copenhagen K, Denmark.* E-mail*: sli@geus.dk*
M.E.*, Geological Survey of Sweden, Kiliansgatan 10, S-223 50 Lund, Sweden.*

Fingerprinting sediments along the west coast of Jylland: interpreting provenance data

Christian Knudsen, Thomas Kokfelt, Troels Aagaard, Jesper Bartholdy and Morten Pejrup

The Danish North Sea coast is a dynamic sedimentary environment experiencing erosion, transport and re-deposition of sand along the coast. Because of the natural and economic value of the coastal zone expensive protection measures such as nourishment of the coast are undertaken. The present study utilises provenance analysis techniques developed at the Geological Survey of Denmark and Greenland (GEUS) to characterise the coastal sand bodies by fingerprinting the heavy minerals in the sand. The aims of the study are to test these new methods in an active sedimentary environment and to develop an understanding of transport pathways along the coast. A total of *c*. 40 samples have been collected and analysed as part of the project. This paper gives an outline of the project and provides examples of the methods used based on six samples from the Husby profile on the west coast of Jylland (Fig. 1). The study is a collaboration project involving GEUS and the Department of Geography and Geology (DGG) at Copenhagen University; GEUS is responsible for the analyses and DGG for sample collection.

Provenance analysis based on modal abundance and composition of heavy minerals is used to understand the dispersal of sand in ancient siliciclastic systems, with focus on problems relevant to the petroleum industry (e.g. Larsen *et al.* 2006; Morton *et al*. 2007). Investigation of present-day processes and sedimentary environments may provide a key to understand how provenance indicators can be used to describe and interpret fossil clastic sedimentary systems. It is well known that properties such as grain shape and density are important factors in the processes controlling transport and deposition of mineral grains. As the heavy minerals used in provenance analysis have a wide range of densities and shapes, it is important to include these properties in studies of their dynamics in the environment. Therefore GEUS has focused on developing computer-controlled scanning electron microscopy (CC-SEM), which provides information on mineralogy and mineral chemistry together with grain size and shape (Keulen *et al.* 2008). Furthermore, the development of laser ablation inductively coupled mass spectrometry (LA-ICP-MS) analysis has focused on a single, robust mineral species, zircon. These analyses also yield information on the age of the zircon mineral grains, and the age distribution of zircon grains is used to fingerprint the sand (Knudsen *et al.* 2005; Frei *et al.* 2006). Saye & Pye (2005) have described variations in the bulk chemical composition and particle size of coastal sands in Denmark. The work outlined here is a continuation of this work, but using different methods focusing on the modal mineralogy of the heavy minerals in the sand as well as the age distribution of detrital zircon grains.

Sample sites

Samples have been collected from three settings. (1) From coastal cliffs that are being actively eroded and accordingly supply sediment to the littoral drift system along the coast of Jylland. The sampling aims at fingerprinting some of the potential sources of sand mainly from till beds and glacio-fluvial sediments. (2) From four profiles orientated perpendicular to the coast; the samples represent lower shoreface, upper shoreface, beach and dunes (profiles at Bovbjerg, Husby, Vejers and Skallingen; Fig. 1). The aim is to study the variation of the sediment fingerprint between the different sedimentary facies along the coast as well as the variation within identical sedimentary environments. The profiles are situated along the southward-directed net littoral drift of sand that exists between Bovbjerg and Skallingen. (3) From the Vejers/ Skallingen/Grådyb area samples will be analysed to investigate if the littoral drift sediment bypasses Horns Rev and to characterise the sedi-

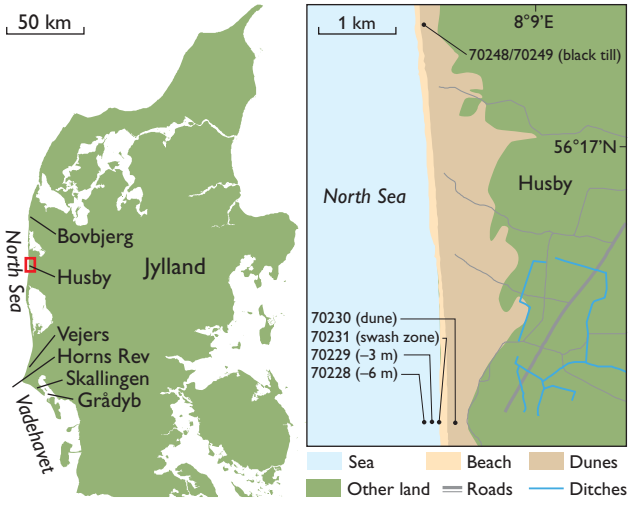

Fig. 1. Map of western Denmark showing the location of the Husby area (red box) and place names mentioned in the text. The map to the right shows the Husby area with sample sites marked.

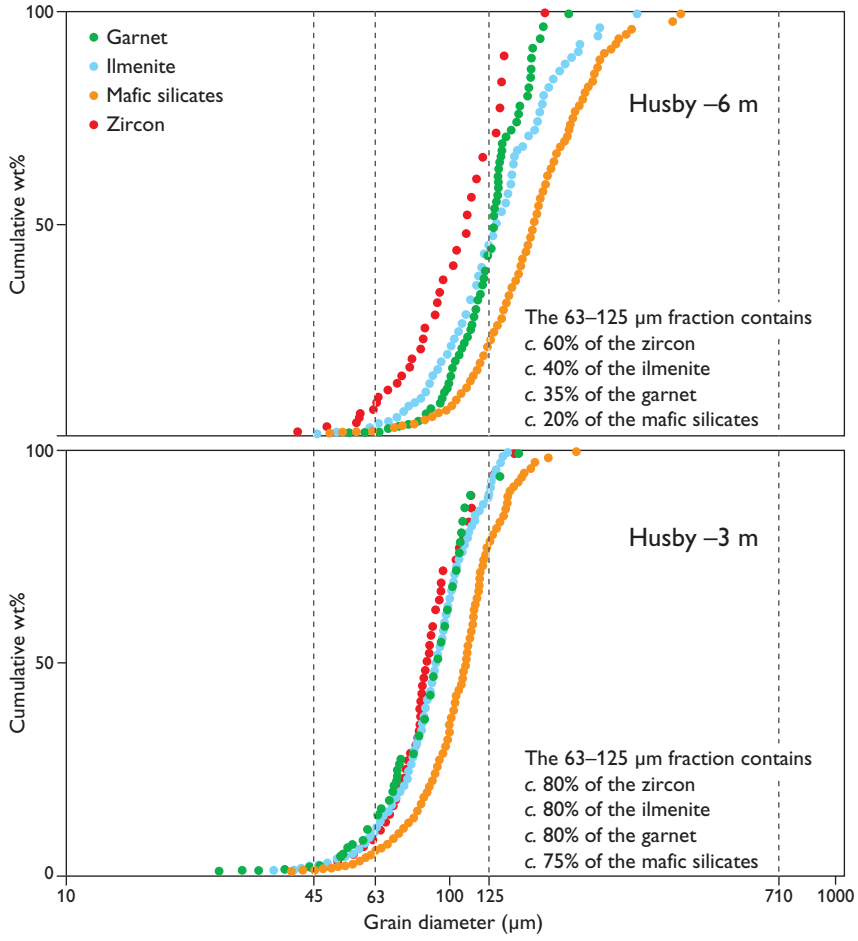

Fig. 2. Grain-size distribution curves for zircon, garnet, ilmenite and mafic silicates in two samples from Husby taken at 3 and 6 m water depth. Note that if only the 63 to 125 µm fraction of the heavy mineral fraction was analysed, the modal proportions of the heavy mineral species would not represent the actual proportions in the sand.

ment exchange between the North Sea and Vadehavet (Danish Wadden Sea) relative to other sources and sinks in the area. Here we present data from the profile at Husby.

Computer-controlled scanning electron microscopy (CCSEM)

CCSEM is used at GEUS to analyse the composition and properties of detrital mineral grains. Sediment samples are sieved and the fraction between 45 and 710 µm analysed. The samples are separated using heavy liquid (2.89 g/cm^3) and the heavy mineral fraction is used for analysis. The grains are mounted in epoxy in such a way that the grains do not touch one another. The mount is polished and analysed by CCSEM to determine the chemical composition of *c.* 1200 individual heavy mineral grains, together with their size and shape. The result of the chemical analysis of each grain is compared with a library of mineral compositions. The results are stored in a database and properties such as modal mineralogy, mineral chemistry and grain-size distributions of the individual species can be displayed (Figs 2, 3). The CCSEM analytical procedure is described in further detail by Knudsen *et al.* (2005), Keulen *et al.* (2008) and Bernstein *et al.* (2008).

LA-ICP-MS fingerprinting of zircon

When using the modal proportions of heavy minerals for characterising the provenance of the sand, it is important to recognise potential hydrodynamic effects due to, e.g. grain density. In addition, the size and shape characteristics of the grains of the different heavy mineral species may influence their response to sedimentary processes. Furthermore, the relative sensitivity of the heavy mineral species to

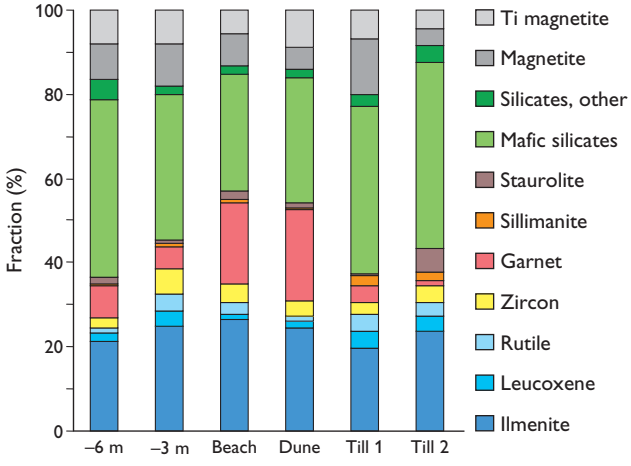

Fig. 3. The heavy mineral proportions in the six samples from Husby recorded by CCSEM. The samples from the shoreface (–3, –6 m) are characterised by low contents of garnet (*c.* 7%) in contrast to the samples from the beach and dune that are characterised by high garnet contents (*c.* 20%).

chemical and physical decomposition depends on the stability of the different minerals. To overcome these problems, it is advisable in provenance analysis to focus analysis on one mineral species because differences in hydrodynamic behaviour or weathering can thereby be discounted. For this purpose the extremely stable mineral zircon is very well suited. A key property of zircon in provenance analysis is the relatively high content of uranium, which makes the mineral well suited for dating. At GEUS the measurements are carried out on a laser ablation inductively coupled mass spectrometer (LA-ICP-MS; Frei *et al.* 2006; Frei & Gerdes 2009). The sand is physically separated using a shaking table to concentrate the very heavy minerals. From this concentrate, the zircon is picked out and mounted (*c.* 150 zircon grains per sample) in epoxy. The mount is polished and introduced to the laser ablation system. A *c.* 30 µm diameter spot is ablated with the laser in the core of each zircon grain, and the ablated material is introduced into the ICP-MS, in which the ratios between the different U and Pb isotopes are measured.

Results from Husby

Some results of analyses of six samples collected near Husby (Fig. 1) are discussed here. Two samples are from till beds exposed in the coastal cliff, one is from a dune, one is from the active swash zone and two samples are from the shoreface, at water depths of 3 and 6 m.

The grain-size distribution varies among the different heavy mineral species (Fig. 2). Zircon with the highest density is finer-grained than lighter minerals such as ilmenite and garnet, and the mafic silicates (amphibole, pyroxene and epidote) are the most coarse-grained of the heavy minerals. This is in close accordance with that predicted by Stokes' law, and implies that grain-size sorting has acted according to grain-fall velocity. The steepness of the grain-size distribution curves also varies among the different minerals. The garnet curve is steeper and narrower than that of, for example,

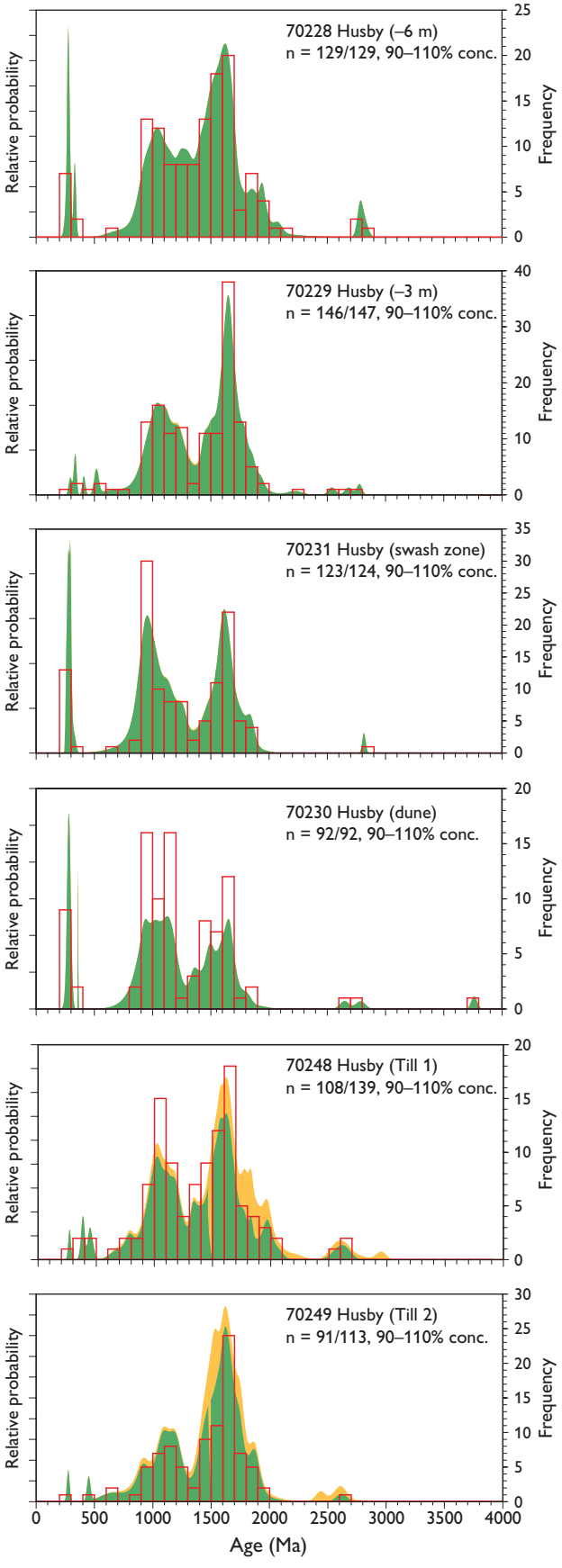

Fig. 4. Age distribution of zircons in the samples from Husby. The frequency (red histograms) indicates the number of zircons in the age brackets (100 Ma). The green area indicates the content of concordant grains whereas the yellow area indicates the discordant grains (only present in the till samples). The samples from the shoreface (–3, –6 m) are characterised by two main populations, one with ages between 1000 Ma and 1300 Ma and one with ages between 1400 Ma and 1900 Ma, the latter being the most abundant. Samples from the beach and dune contain the same populations, but are characterised by more equal proportions of the two populations. It can also be noticed that the samples from the till in the cliff behind the beach are characterised by a pattern similar to the samples from the shoreface.

ilmenite or mafic silicates. This could be caused by differences in grain shape, and one of the aims of the project is to investigate how the grain-size distribution varies among the different sedimentary environments along the west coast of Jylland.

In provenance analysis it is often assumed that ratios between the heavy mineral species can be used as provenance indicators. Due to analytical constraints, or chosen standard procedures, a given size-fraction (typically 63 to 125 µm; Hallsworth & Chisholm 2008; Yang *et al*. 2009) is often used for such analysis, regardless of the fact that the sands which are compared have different overall grain-size distributions. As can be seen on Fig. 2, for example, the modal proportions of the heavy minerals would not reflect the true values if only the fraction between 63 and 125 µm was analysed. The sample Husby –6 m would be characterised by its finer part, with zircon being over-represented whereas the sample Husby –3 m would be close to the modal value. In Fig. 3, the modal proportions of the heavy minerals show that the composition of the heavy mineral fraction in the shoreface sands (–6 and –3 m) is similar but different to the beach sand and dune sands, which in turn resemble each other. The main difference between these two pairs is that garnet is more abundant in the beach and dune sands than in the shoreface sand. The heavy mineral assemblages from the tills exposed in the cliff are different to the beach and dune sands, but similar to the sand from the shoreface.

Figure 4 shows the age distributions of the zircon grains in the six samples. The samples show roughly the same spectra: a few Archaean (>2500 Ma) grains, an Early Proterozoic maximum (*c*. 2000–1500 Ma), a Middle Proterozoic maximum (*c*. 1400–900 Ma) and a Caledonian peak (*c*. 400–300 Ma). It is a characteristic feature of the shoreface sands and the till samples that Early Proterozoic zircons are more abundant than Middle Proterozoic zircons. In contrast, the two populations are equally represented in the beach and dune samples. The Middle Proterozoic zircons were probably derived from the Sveco-Norwegian orogen in southern Norway and western Sweden to the north of Jylland whereas the Early Proterozoic zircons were probably derived from Jotnian and Sveco-Fennian sources to the east.

Both the mineral paragenesis data and the zircon age distributions suggest that the shoreface sands have a provenance that is distinct from the beach and dune sands at Husby. This is surprising, and further work will concentrate on explaining these patterns, with the aim of understanding the processes responsible for the observed distribution of these sands. In addition, the distribution of heavy mineral assemblages along the shore will be analysed.

References

Bernstein, S., Frei, D., McLimans, R.K., Knudsen, C. & Vasudev, V.N. 2008: Application of CCSEM to heavy mineral deposits: source of high-Ti ilmenite sand deposits of South Kerala beaches, SW India. Journal of Geochemical Exploration **96**, 25–42.

Frei, D., Hollis, J.A., Gerdes, A., Harlov, D., Karlsson, C., Vasquez, P., Franz, G., Johansson, L. & Knudsen, C. 2006: Advanced *in situ* geochronological and trace element microanalysis by laser ablation techniques. Geological Survey of Denmark and Greenland Bulletin **10**, 25–28.

Frei, D. & Gerdes, A. 2008: Precise and accurate *in situ* U-Pb dating of zircon with high sample throughput by automated LA-SF-ICP-MS. Chemical Geology **261**, 261–270.

Hallsworth, C.R. & Chisholm J.I. 2008: Provenance of late Carboniferous sandstones in the Pennine Basin (UK) from combined heavy mineral, garnet geochemistry and palaeocurrent studies. Sedimentary Geology **203**, 196–221.

Keulen, N.T., Frei, D., Bernstein, S., Hutchison, M.T., Knudsen, C. & Jensen, L. 2008: Fully automated analysis of grain chemistry, size and morphology by CCSEM: examples from cement production and diamond exploration. Geological Survey of Denmark and Greenland Bulletin **15**, 93–96.

Knudsen, C., Frei, D., Rasmussen, T., Rasmussen, E. S. & McLimans, R. 2005: New methods in provenance studies based on heavy minerals: an example from Miocene sands in Jylland, Denmark. Geological Survey of Denmark and Greenland Bulletin **7**, 29–32.

Larsen, M., Knudsen, C., Frei, D, Frei, M., Rasmussen, T. & Whitham, A.G. 2006: East Greenland and Faroe–Shetland sediment provenance and Palaeogene sand dispersal systems. Geological Survey of Denmark and Greenland Bulletin **10**, 29–32.

Morton, A.C., Herries, R. & Fanning, C.M. 2007: Correlation of Triassic sandstones in the Strathmore Field, west of Shetland, using heavy mineral provenance signatures. In: Mange, M. & Wright, D.T. (eds): Heavy minerals in use. Developments in Sedimentology **58**, 1037–1072.

Saye, S.E. & Pye, K. 2006: Variations in chemical composition and particle size of dune sediments along the west coast of Jutland, Denmark. Sedimentary Geology **183**, 217–242.

Yang, S., Wang, Z., Guo, Y., Li, C. & Cai, J. 2009: Heavy mineral compositions of the Changjiang (Yangtze River) sediments and their provenance-tracing implication. Journal of Asian Earth Sciences **35**, 56–65.

Authors' addresses

C.K. & T.F.K., *Geological Survey of Denmark and Greenland, Øster Voldgade 10, DK-1350 Copenhagen K, Denmark.* E-mail: *ckn@geus.dk*

T.A., J.B. & M.P., *Department of Geography and Geology, University of Copenhagen, Øster Voldgade 10, DK-1350 Copenhagen K, Denmark.*

Structural development of Maglevandsfald: a key to understanding the glaciotectonic architecture of Møns Klint, SE Denmark

Stig A. Schack Pedersen and Peter Gravesen

The Møns Klint Glaciotectonic Complex (Fig. 1) exposed in the N–S-trending chalk cliff on the east coast of the island of Møn in south-east Denmark is one of the most famous glaciotectonic geosites in the world. People of all nationalities are attracted to the site, which has more than 300 000 visitors per year. Many of them may not realise the uniqueness of the glaciotectonic framework, and are probably more fascinated by the spectacular view of the white cliff and chalk peaks separated by the deep green gorges. However, without the glaciotectonic deformation the cliffs would never have formed. Instead the Cretaceous chalk would still have been resting horizontally below the seabed, covered by glaciofluvial sand, glaciolacustrine clay and clayey till.

In the summer 2007, a new natural science exhibition centre, GeoCenter Møns Klint, was opened. The exhibition focuses on the geology of Denmark with special reference to the chalk cliffs of Møns Klint. Prior to the decision to build the centre, the Geological Survey of Denmark and Greenland was asked to provide an evaluation of the landslide risk for the site, because landslides regularly occur along the cliff section (Pedersen 2003). A detailed structural analysis was consequently carried out at the planned site of the centre just above the Maglevandsfald gorge (Fig. 1). During this investigation it became obvious that understanding the glaciotectonic framework was a prerequisite for the geological risk analysis. Thus the structural details at Maglevandsfald became a key point for the glaciotectonic model of Møns Klint which we present in this paper.

Geological setting of Møns Klint

The Cretaceous chalk represents the oldest bedrock affected by glaciotectonic thrusting in Denmark. The chalk consists of a fine-grained matrix of coccoliths and remains from invertebrates (Surlyk & Håkansson 1999). The chalk at Møn is correlated with the upper part of the Tor Formation in the North Sea and the Danish Basin (Surlyk *et al.* 2003).

An erosional unconformity on top of the chalk represents a hiatus of about 60 million years. Due to erosion, the unconformity is found at gradually lower and lower levels towards the southern part of the cliff, which indicates that the pre-Quaternary relief probably contributed to the formation of glaciotectonics in the area. In some parts of Møn the pre-Quaternary unconformity is overlain by a Saalian till, marine Eemian clay and three Weichselian tills intercalated by glaciolacustrine and glaciofluvial deposits (Houmark-Nielsen 1994). However, at Møns Klint an old Weichselian till is the oldest Quaternary deposit recognised at present (Pedersen & Gravesen 2006). This till is a grey and reddish sandy till that grades up into a gravelly, stone-rich top surface indicating terrestrial conditions. We tentatively correlate this unit with the Ristinge Klint Till (Houmark-Nielsen 1987, 1994), which was deposited by a Baltic ice stream in the early part of the Weichselian (*c.* 60 000 years BP) from a source area in the Baltic Sea. When the Baltic Ice Stream melted back the depression became occupied by a huge lake, in which dark glaciolacustrine mud rich in dropstones was deposited (Houmark-Nielsen 1994; Houmark-Nielsen & Kjær 2003).

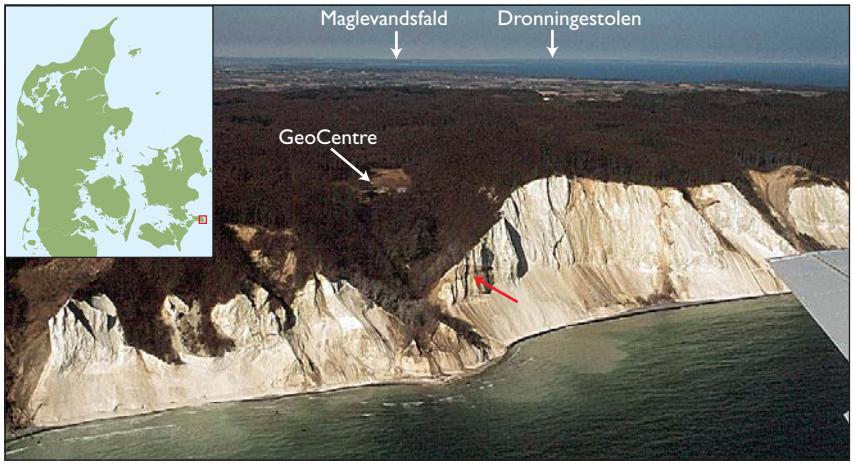

Fig. 1. Aerial photograph of Møns Klint. The highest cliff in the centre is Dronningestolen. To the left the Maglevandsfald gorge leads from the location of GeoCenter Møns Klint down to the beach. At the left side of Dronningestolen a wedge-shaped structure is seen (red arrow), which was formed in the first deformation phase of the glaciotectonic complex. The thrust structures to the right of Dronningestolen were thrust to the SW during the last deformation phase. The location of Møns Klint is shown on the inset map of Denmark.

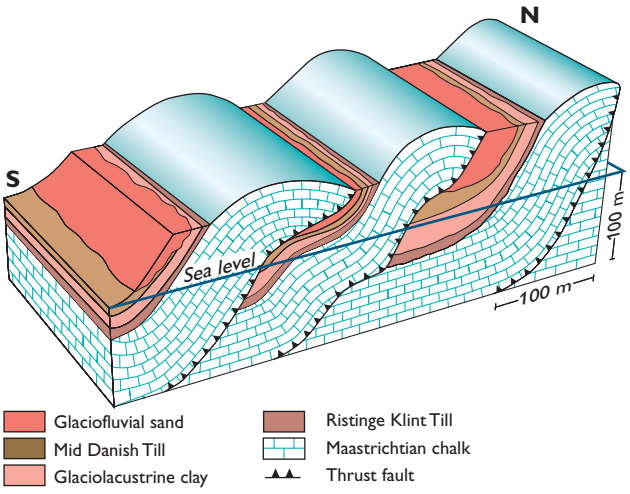

Fig. 2. Stratigraphical and structural framework of the southern imbricate fan at Møns Klint. The thickness of the lithological units is variable, and especially the glaciofluvial sand above the Mid Danish Till increases in thickness, where the sand was deposited in piggyback basins during the thrust-fault deformation. From Pedersen & Gravesen (2006).

The unit is informally called the elephant clay due to its characteristic erosion features. At the Late Weichselian glacial maximum the Swedish Ice advanced over the eastern part of the Danish Basin onto the Main Stationary Line depositing the Mid Danish Till on Møn (Fig. 2; Houmark-Nielsen 1987; Pedersen & Gravesen 2006).

At about 18 000 years BP the Young Baltic Ice Stream reached Møn (Houmark-Nielsen & Kjær 2003). The pressure from the ice was directed away from the central axis of the ice stream towards both north and south, where it thrust up the chalk sheets at Møns Klint. The glaciotectonic structures at Møns Klint can be divided into three architectural elements. In the southern part the thrust sheets form an imbricate fan with thrust faults striking E–W, in the central part the structures form an antiformal stack, and farthest to the north the thrust sheets dip gently to the south in the foreland regime of the thrust deformation (Fig. 3; Pedersen 2000). Towards the end of the Weichselian the Scandinavian ice sheet melted back. However, a readvance from southern Sweden reached Møn from east-north-east at a time between 17 000 and 15 000 years BP, which was responsible for superimposed deformation of the glaciotectonic complex (Pedersen 2000).

Photogrammetric mapping and a borehole investigation

A 3-D terrain model of the area was developed for the risk evaluation. The data for the model were provided by a photogrammetric survey and a digital model was constructed, in which the trace of the glacial deposits, interbedded between the unconformity on top of the chalk and the base of an overthrust chalk sheet, was positioned (Fig. 4). In addition, a borehole was drilled to investigate whether karst cavities or an unforeseen thrust-fault zone with dip towards the cliff and beach were present. If a fault zone exists below the location it could be a candidate for a landslip similar to the one that destroyed the Store Taler chalk peak in January 2007 (Fig. 5). The borehole was placed on top of the cliff 100 m above sea level close to the old Hotel Store Klint (Fig. 6). The uppermost 16.3 m consist of glacial sediments resting upon the chalk unconformally. The oldest unit in the glacial succession is a 1 m thick till that is correlated with the Ristinge Klint Till. This formation is overlain by 2.3 m glaciolacustrine mud, which grades into the nearly 2 m thick Mid Danish Till. A 7.7 m thick unit of glaciofluvial sand and gravel overlies the Mid Danish Till; the upper part of the glacial succession is a 3.5 m thick, sandy till that was deposited by the Young Baltic Ice. Below the unconformity the drilling penetrated 48 m of Cretaceous chalk, after which the drilling was

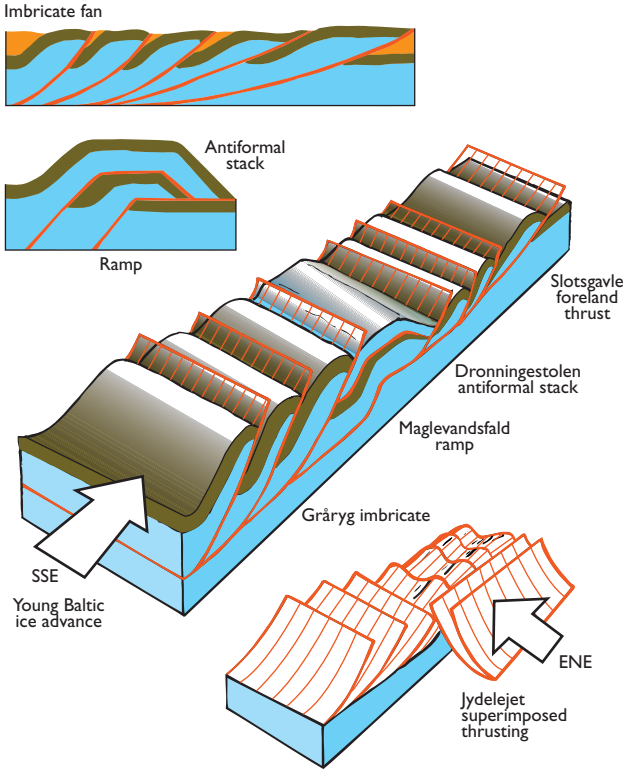

Fig. 3. Principal structural framework of the Møns Klint Glaciotectonic Complex. Blue: chalk; brown and orange: Quaternary deposits. Red lines outline the thrust faults. To the south the E–W-trending ridges represent an imbricate fan, and in the central part an antiformal stack is responsible for the formation of Dronningestolen. Two principal sketches of the structures are shown in the top left corner. In the distal part of the complex to the north a gently dipping imbricate fan was formed in the near-foreland regime. The structures from the distal regime to Maglevandsfald were strongly affected by superimposed deformation caused by a re-advance of ice from Skåne. After Pedersen (2000).

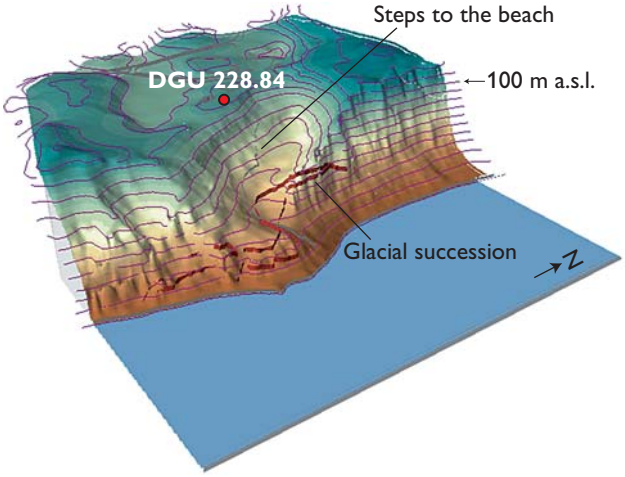

Fig. 4. 3-D model of the Maglevandsfald gorge. The position of the exploratory borehole DGU 228.84 is indicated with a dot, located between the exhibition centre and the old hotel. The upper and lower boundaries of the glacial succession are shown with a brown line. Contour interval 10 m.

Fig. 5. The landslide at Store Taler took place at the end of January 2007. A volume of more than 100 000 m^3 was displaced along an inherited thrust-fault surface formed during the last phase of deformation at Møns Klint. Store Taler is located in the northern part of Møns Klint.

unfortunately stopped for logistic reasons. It would have been perfect if the borehole had reached the level of the lower thrust fault and the underlying glacial succession. However, the data demonstrate that neither a karst cavity nor an eastward dipping thrust-fault zone was present.

Thrust-fault tectonics and superimposed deformation

The structures in the Møns Klint Glaciotectonic Complex are directly comparable to structures in thin-skinned thrust-fault belts formed by gravity spreading (Pedersen 2005). The geomorphological expression of a mountain range is clearly seen in the parallel-ridged landscape of Høje Møn (the eastern, hilly part of Møn). For detailed structural analysis five cross-sections were constructed across the Maglevandsfald (Figs 6, 7). The data for the cross-sections were taken from the photogrammetric survey combined with a structural investigation of the cliff section immediately south of Maglevandsfald. In the cross-sections two horizons of glacial successions are shown (Fig. 7). The lower glacial horizon rests on the unconformity on top of the chalk. The top of the glacial deposits is bordered by a thrust fault, where the base of the chalk sheet can be classified as a hanging-wall flat related to the earliest glaciotectonic deformation. Farther to the south this flat can be followed into a hanging-wall ramp, which dips into the subsurface below the beach. This ramp strikes E–W, indicating that it is part of the antiformal stack structure (Fig. 3). As the décollement zone must be situated at the base of the chalk unit, which in Fig. 7 can be seen to be about 60 m thick, the depth to this zone must be of similar magnitude, probably about 75 m below sea level. Therefore the chalk below the lower glacial unit is also interpreted as a thrust sheet lifted up from the décollement zone.

The lower glacial unit is folded in a SW-verging overturned structure, which has been deformed by the second glaciotectonic event. The structure is partly hidden by soil and vegetation in the Maglevandsfald gorge, but the upper limb of the structure is exposed at the cliff edge of Maglevandsnakken (Fig. 7), where the unit continues into the wedge-shaped feature in the southern part of the Dronningestolen cliff section (Fig. 1). The wedge-shaped feature was formed during the foreland-dipping thrusting of the antiformal stack (compare with Fig. 3). The thrust-fault flat

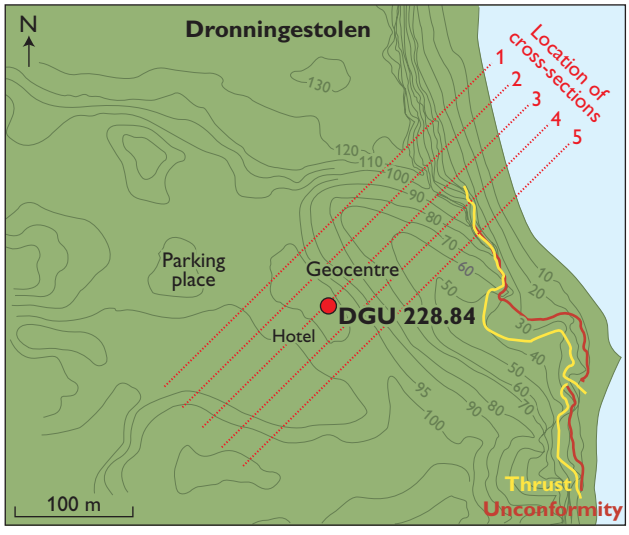

Fig. 6. The Maglevandsfald area with location of the exploratory borehole mentioned in the text and the cross-sections applied in the structural analysis.

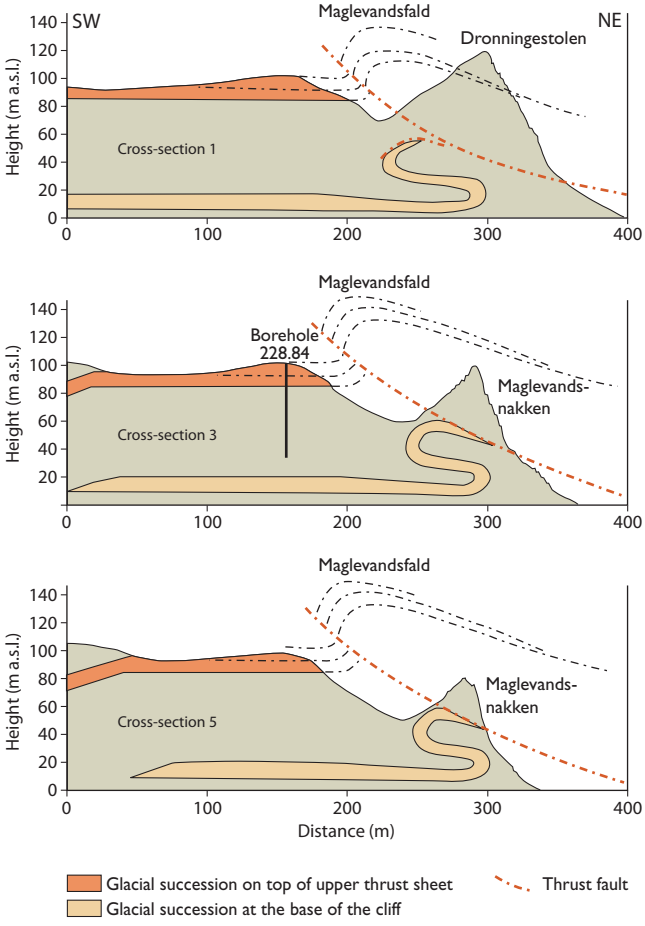

Fig. 7. Three of the cross-sections across the Maglevandsfald gorge (for location see Fig. 6). The cross-sections were constructed perpendicular to the fold axis of the last deformation, which created a recumbent anticline and syncline pair below a thrust fault with a displacement of 20 m. The folding is outlined in the glacial units below the thrust-fault flat of the first deformation, which is responsible for the wedge-shaped feature in the top of the fold. The strike of the first deformation thrust is oblique to the second phase fold axis, and therefore the position of the wedge changes from cross-section to cross-section. In cross-section 5 the tip of the thrust wedge touches the cliff edge, which corresponds to the exposure of the wedge seen in Fig. 1 immediately to the right of Maglevandsfald.

above the glacial unit is folded in the Maglevandsfald gorge structure with a fold axis trending NW–SE, which demonstrates the superimposed deformation. A similar wedge-shaped structure is present just below the edge of the Dronningestolen cliff, which may indicate that a thrust sheet existed even higher in the antiformal stack before the Young Baltic Ice truncated the structure during the advance towards NNW.

Final remarks

Møns Klint is one of the most famous glaciotectonic localities in the world. The structures in the Møns Klint Glaciotectonic Complex are comparable to structures in thin-skinned thrust-fault belts formed by gravity spreading. The glaciotectonic complex is responsible for the parallel-ridge landscape known as Høje Møn, where Aborre Bjerg (143 m) represents the highest hill in eastern Denmark. A combination of an imbricate fan and an antiformal stack is responsible for the impressive tectonic complex. Its main architecture was formed during the Young Baltic Ice Stream advance dated to about 18 000 years BP, but a readvance of ice from southern Sweden from 17 000 to 15 000 years BP is responsible for the superimposed deformation of the complex.

The most impressive unit forming the thrust sheets is the Maastrichtian chalk. The chalk is part of the huge carbonate platform that spread over northern Europe during the late Cretaceous. The top surface of the chalk, the pre-Quaternary unconformity, was originally situated more than 20 m below sea level, and the décollement zone for the thrusting is probably located about 80–100 m below sea level in a marl-rich variety of the chalk.

References

Houmark-Nielsen, M. 1987: Pleistocene stratigraphy and glacial history of the central part of Denmark. Bulletin of the Geological Society of Denmark **36**, 1–189.

Houmark-Nielsen, M. 1994: Late Pleistocene stratigraphy, glacial chronology and Middle Weichselian environmental history from Klintholm, Møn, Denmark. Bulletin of the Geological Society of Denmark **41**, 181–202.

Houmark-Nielsen, M. & Kjær, K. 2003: Southwest Scandinavia, 40–15 kyr BP: palaeography and environmental change. Journal of Quaternary Science **18**, 769–786.

Pedersen, S.A.S. 2000: Superimposed deformation in glaciotectonics. Bulletin of the Geological Society of Denmark **46**, 125–144.

Pedersen, S.A.S. 2003: Vurdering af skredrisiko for området oven for Maglevandsfaldet på Møns Klint. Strukturel undersøgelse af de glacialtektoniske forhold i klintområdet ved Hotel Storeklint, Møns Klint, Møn. Danmarks og Grønlands Geologiske Undersøgelse Rapport **2003/50**, 31 pp.

Pedersen, S.A.S. 2005: Structural analysis of the Rubjerg Knude Glaciotectonic Complex, Vendsyssel, northern Denmark. Geological Survey of Denmark and Greenland Bulletin **8**, 192 pp.

Pedersen, S.A.S. & Gravesen, P. 2006: Geological map of Denmark, 1:50 000, Møn. Copenhagen: Geological Survey of Denmark and Greenland.

Surlyk, F. & Håkansson, E. 1999: Maastrichtian and Danian strata in the southeastern part of the Danish Basin. In: Pedersen, G.K. & Clemmensen, L.B. (eds): IAS Field trip guidebook. Contribution to Geology, 29–58. Copenhagen: Geological Museum, University of Copenhagen.

Surlyk, F., Dons, T., Clausen, C.K. & Higham, J. 2003: Upper Cretaceous. In: Evans, D. *et al.* (eds): The millennium atlas: Petroleum geology of the central and northern North Sea, 213–233. London: The Geological Society of London.

Authors' address

Geological Survey of Denmark and Greenland, Øster Voldgade 10, DK-1350 Copenhagen K, Denmark. E-mail: *sasp@geus.dk*

Fracture valleys in central Jylland – a neotectonic feature

Peter Roll Jakobsen and Stig A. Schack Pedersen

Geomorphological indications of tectonic activity in the Danish glacial landscape were pointed out already by Milthers (1916, 1948). He described a conspicuous system of N–S-trending, narrow valleys in central Jylland and interpreted them as fault-generated features (fracture valleys). The valleys occur in the area between Ulstrup and Hammel and in a smaller area near Skjød (Fig. 1). The most significant valley system is found near Hvorslev, and it is here referred to as the Hvorslev lineaments (Fig. 1).

An alternative interpretation of the genesis of the Hvorslev lineaments was presented by Hansen (1970). He argued that the N–S-trending valleys were formed by backward erosion from E–W-orientated erosional valleys in a former drainage system related to former higher groundwater table. However, Milther's interpretation that the valleys have a tectonic origin was later supported by Larsen & Kronborg (1994) and Torp (2001).

Former interpretations of the lineaments were primarily based on morphological studies and arguments. Recently the area with the Hvorslev lineaments was mapped as part of the systematical geological mapping of Denmark by the Geological Survey of Denmark and Greenland. The mapping of the surface lithology has added new information, and along with available seismic data it provides a framework for a well-founded interpretation of the elongated valleys, which is presented in this paper. We conclude that the fracture valleys are tectonic features, based on their morphology and because they are situated above a fault zone.

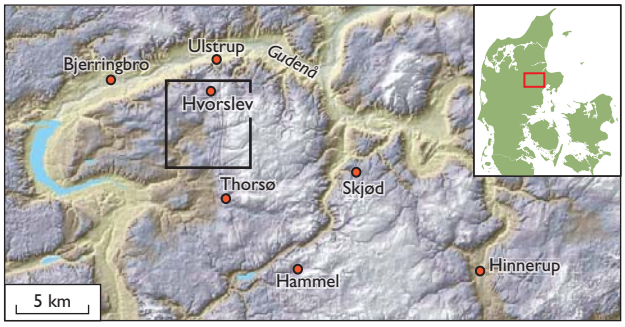

Fig. 1. Digital elevation model of the Hvorslev region with place names mentioned in the text. The focus area is the northern part of the valley system between Ulstrup and Hammel near Hvorslev. The difference in elevation from the valleys to the highest areas is around 90 m. The rectangle shows the location of Fig. 3, and the inset map of Denmark shows the location of the model.

Geological setting

The highest levels in the region are covered by a till unit, mainly a clayey till, but with patches of sandy till (Fig. 2). On

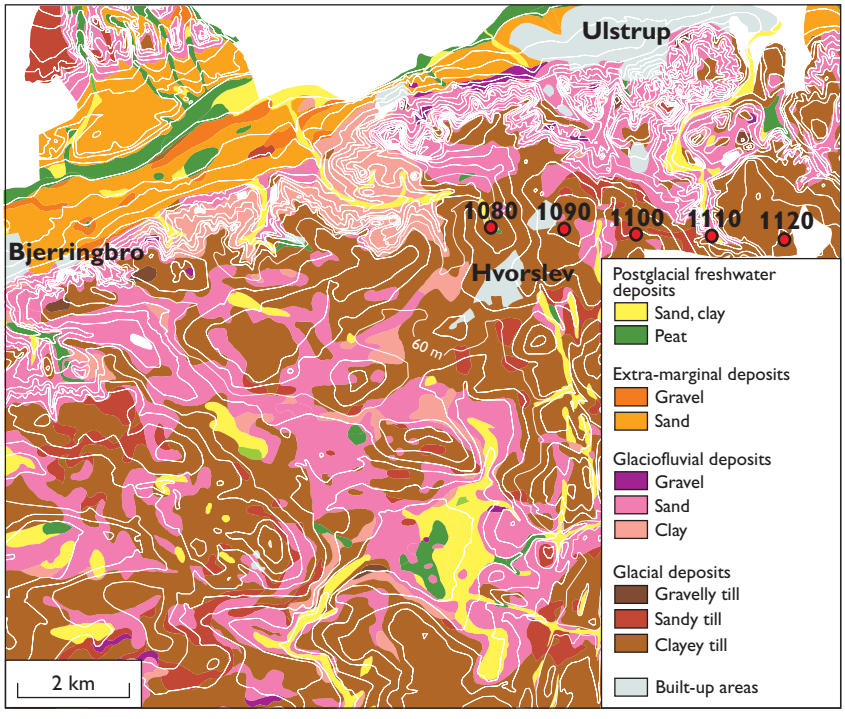

Fig. 2. Geological map of the Hvorslev area (extract from the digital map, see Jakobsen & Hermansen (2007). Contour interval 5 m. The location of the seismic line 73203 is shown with dots, which indicate the position of every 10th geophone.

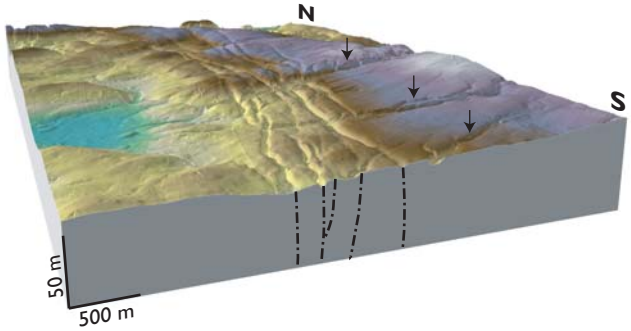

Fig. 3. Block diagram of the Hvorslev lineaments. The inferred faults are drawn on the frontal south-facing side of the block diagram. The arrows mark some of the erosional valleys.

the steep slopes of the Gudenå valley, glaciofluvial deposits are found below the till unit. Smaller outcrops of glaciofluvial sand appear in the till unit representing erosional windows in the till surface. Thus the uppermost lithostratigraphy in the region comprises a glaciofluvial unit overlain by a till. This succession is also recorded in boreholes in the region (Gravesen 1991). In most wells a clayey till is present at the top below which the glaciofluvial sand has a thickness of up to 20 m. The sand rests mainly on Oligocene mica clay and in a few places on Oligocene quartz sand.

The glaciofluvial unit is correlated with the Teppestrup Formation (Larsen *et al.* 1977; Pedersen & Petersen 1997), which was deposited on an outwash plain in front of the ice advancing from the north-east. The clayey till is interpreted as deposited by the ice advance from the north-east that reached the Main Stationary Line in Jylland. The till is correlated with the Mid Danish Till of Houmark-Nielsen (1987) and its correlative the Fårup Till of Kronborg *et al.* (1990), which date to around 23 000–21 000 years before present in this part of Denmark (Houmark-Nielsen & Kjær 2003).

Morphology

The parallel alignment of valleys in the Ulstrup–Hammel area suggests that they can be characterised as fracture valleys (Fig. 1). The length of the valley system between Ulstrup and Hammel is about 17 km. The most prominent part of the system is located at Hvorslev, where the valleys trend N–S with a spacing of 125 m to 250 m. The individual valleys are up to about 9 km long and 6 m deep. The width of the zone with fracture valleys is 800–1100 m wide (Figs 1, 3). The valleys cut hills and erosional valleys without any change of direction and are therefore not controlled by the general landscape morphology. Even one of the highest hills in the area is cut at the top by one of the valleys.

The individual valleys show an undulating floor in the longitudinal direction, occasionally with small depressions containing bogs and lakes. Most cross-sections of the individual valleys display a U-shaped morphology; in some places an asymmetrical shape is seen with a steep eastern slope and a gently dipping western slope.

The trends of the westernmost valleys south of Hvorslev are concave towards the west, curving around a depression which is filled with postglacial freshwater deposits. Downhill towards this depression, and almost perpendicular to the Hvorslev lineaments, a system of erosional valleys cuts into the surface with a gentle fall towards the west. The most prominent erosional valley system is first order valleys with branching second order valleys. The major first order valley cuts through the Hvorslev lineaments and a stream starts in its lower part where one of the N–S-trending valleys intersects the erosional valley. The second order valleys are not as deep as the first order valleys, and are cut by the Hvorslev lineaments. Some of them are hanging valleys on the sides of the N–S-trending valleys.

The E–W-trending erosional valleys were generated shortly before the Hvorslev lineaments. Most of them are dry valleys that formed at a time when surface drainage was greater than now, most likely shortly after deglaciation. Erosion within the first order valleys was so strong that it sustained the effect of the formation of the Hvorslev lineaments, which were apparently almost penecontemporaneous with the erosional valleys.

Seismic records

The seismic section 73203 shows an E–W cross-section across the Hvorslev lineaments south-east of Bjerringbro (Fig. 4). The features between geophone positions 1090 and 1112 are inter-

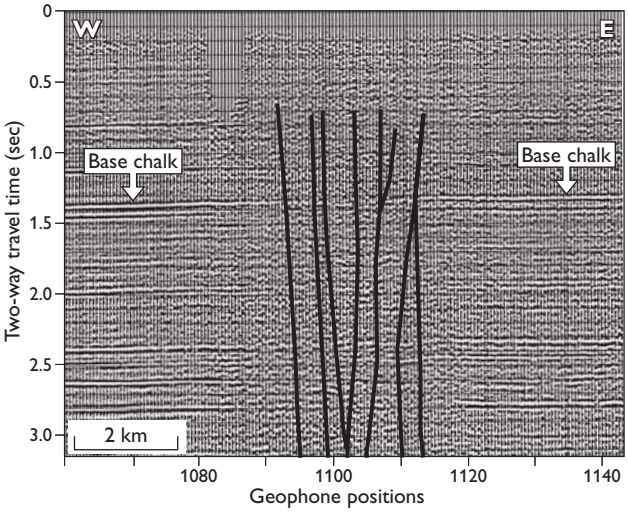

Fig. 4. Part of the seismic section 73203 in the Hvorslev region (for location see Fig. 2). The fault zone is situated between geophone positions 1090 and 1112, and the faults are marked with black lines. The height of the section corresponds to *c.* 3000 m.

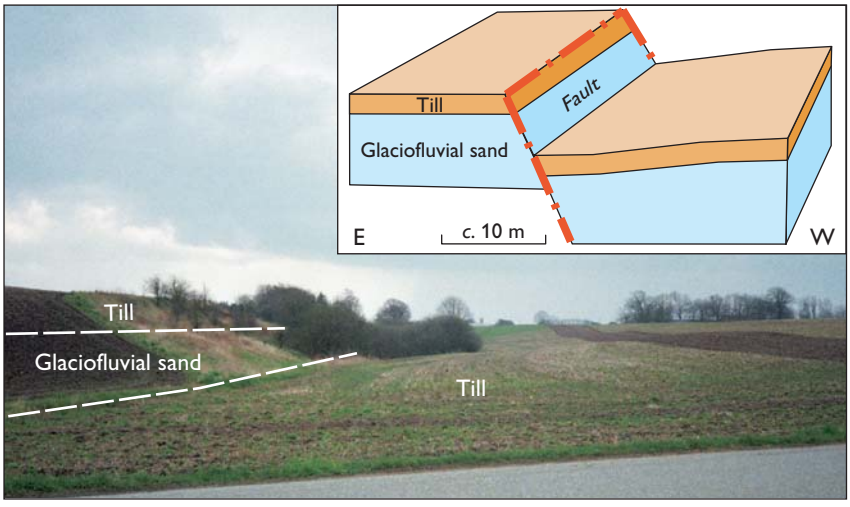

Fig 5. Photograph of one of the asymmetric valleys (viewed southwards). In the west-facing, steep slope, glaciofluvial sand is present below a clayey till. The height of the steep slope is 6 m. On the gently dipping slope clayey till drapes the surface down to the bottom of the valley. The inserted block diagram illustrates the interpretation of the valley as generated by faulting.

preted as faults. They occur over a zone *c.* 2.5 km wide situated directly below the Hvorslev lineaments. The overall structure is interpreted as a negative flower structure, where extension caused downfaulting of segments into a minor graben bounded by marginal faults. Across the inferred fault zone downfaulting towards W predominates. The largest normal fault displacement is 0.05 second at 1.4 second two-way travel time measured on the reflector of the Base chalk, which corresponds to a downthrow of *c.* 50 m at 1400 m depth. East of the fault zone the reflector is horizontal, and to the west it dips weakly towards W.

Indications of faulting at the surface

Most of the area around the Hvorslev lineaments is covered by till. Along the steepest slopes of the asymmetrical valleys, glaciofluvial sand is recorded below clayey till and on the gently dipping slopes clayey till drapes the surface all the way to the bottom of the valley (Fig. 5). Our interpretation of this distribution of the lithological units is that the upper till unit has been displaced by a normal fault down to the floor of the valley, whereby the glaciofluvial sand is exposed in the footwall (Fig. 5). The fault planes dip steeply W with a vertical displacement of *c.* 6 m.

Discussion

The correlation between the Hvorslev lineaments and the faults inferred from the seismic section indicates that the lineaments are surface traces of deep-seated faults. The Hvorslev lineaments strike N–S, which most likely corresponds to the orientation of the faults.

The Himmerland Graben is located to the north of the Hvorslev lineaments (Fig. 6; Vejbæk 1990). It is a deep-seated structure outlined by two major N–S-trending basement-attached faults, which is associated with the Sorgenfrei–Tornquist Zone (Fig. 6). Dextral strike-slip faulting in the Sorgenfrei–Tornquist Zone has resulted in E–W extension across the Himmerland Graben and led to normal faulting. The major tectonic events which caused syn-rift subsidence within the Himmerland Graben occurred during the Triassic and in the late Cretaceous.

The Hvorslev lineaments are situated south of the eastern fault of the Himmerland Graben and probably form a southern continuation of this fault. The indication of downthrow towards W within the Hvorslev lineaments corroborates this assumption. This implies that the fault activity in the Himmerland Graben continues to the south into the central part of Jylland.

The fault-related valleys formed after deposition of the youngest till in the area, because the till is cut by faults (Fig. 5). The youngest glaciation of the area was during the main Weichselian ice advance, during which the Mid Danish Till was deposited. Because the fracture valleys and the erosional valleys were formed at the same time, the faulting probably occurred shortly after the recession following the main Weichselian ice advance. The deglaciation of the region occurred around 21 000 years ago, which gives a maximum age for the formation of the fracture-valley system in central Jylland.

Two different causes can be suggested for the generation of the faults. Either the fault activity was a response to the glacio-static rebound after the last deglaciation, or the faulting is related to the neotectonic extension responsible for the general graben subsidence in the Danish Basin. This question cannot be answered unambiguously on the basis of the available data, but the trend of the lineaments and graben faults are oblique to the general trend of the postglacial marine limit in the region (Mertz 1924) and hence are probably not linked to postglacial isostatic movements. The fact that the asymmetrical valleys show a downthrow towards W indicates that the valleys were formed in connection with tectonic activities in the Himmerland Graben. Moreover, the long length of the fault-related valleys also supports a tectonic origin.

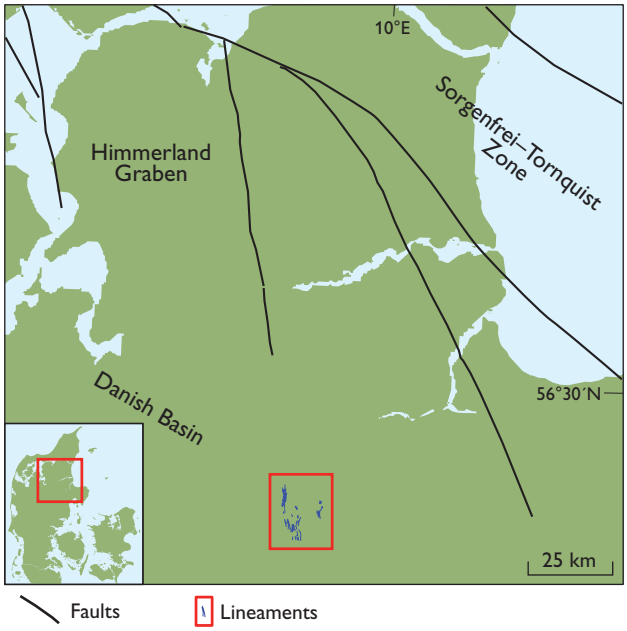

Fig. 6. Map of central Jylland showing the tectonic outline of the region. Fault-related valleys (red box) after Milthers (1916) are located in the continuation of the eastern boundary fault of the Himmerland Graben. Faults after Vejbæk (1990) and Sigmond (2002).

In addition to the fracture-valley system between Ulstrup and Hammel, another system of similar valleys occurs near Skjød, as pointed out by Milthers (1916, 1948). Fracture valleys are also found farther to the east near Hinnerup (Fig. 1; Czakó 1994). Morphologically they are similar to the Hvorslev lineaments, although they are more curved. Nevertheless, we suggest that they are fault-controlled.

Conclusions

We suggest that the system of long, straight and narrow valleys in central Jylland is related to a fault zone recognised on a seismic section across the valley system. Hence the valleys are regarded as surface traces of a deep-seated fault zone.

The faulting resulted in downfaulting of the surface-forming till along normal faults with downthrow mainly to W. The faulting occurred at a time when surface drainage was greater than at present, shortly after the last deglaciation that occurred around 21 000 years ago. The deformation is consequently a neotectonic activity. The fracture valleys indicate that the Himmerland Graben continues farther to the south than previously outlined, and that crustal deformation related to this tectonic feature took place during the late Quaternary. Fault-related valleys as described in this paper are geomorphological elements that characterise some parts of the Danish landscape. It is important to consider their potential implications for geological and hydrological models developed for the Quaternary deposits.

References

Czakó, T. 1994: The photogeological map and the map of surface water flow net of Grundfør. Explanations, preliminary results. DGU data-dokumentation **3**, 18 pp.

Gravesen, P. 1991: Geological map of Denmark, 1:50 000. Map sheet Bjerringbro. Geological basic data map. Danmarks Geologiske Undersøgelse Kortserie **32**.

Hansen, K. 1971: De miltherske spaltedale i Jylland. Dansk geologisk Forening, Årsskrift for **1970**, 47–53.

Houmark-Nielsen, M. 1987: Pleistocene stratigraphy and glacial history of the central part of Denmark. Bulletin of the Geological Society of Denmark **36**, 1–189.

Houmark-Nielsen, M. & Kjær, K. 2003: Southwest Scandinavia, 40–15 kyr BP: palaeogeography and environmental change. Journal of Quaternary Science **18**, 769–786.

Jakobsen, P.R. & Hermansen, B. 2007: Danmarks digitale jordartskort 1:25 000, version 3.0. Danmarks og Grønlands Geologiske Undersøgelse Rapport **2007/84**, 27 pp.

Kronborg, C., Bender, H., Bjerre, R., Friborg, R., Jacobsen, H.O., Kristiansen, L., Rasmussen, P., Sørensen, P.R. & Larsen, G. 1990: Glacial stratigraphy of east and central Jutland. Boreas **19**, 273–287.

Larsen, G., Jørgensen, F.H. & Priisholm, S. 1977: The stratigraphy, structure and origin of glacial deposits in the Randers area, eastern Jutland. Danmarks Geologiske Undersøgelse II. Række **111**, 36 pp.

Larsen, G. & Kronborg, C. 1994: Geologisk set, det mellemste Jylland. En beskrivelse af områder af national geologisk interesse. 272 pp. Odense: Geografforlaget.

Mertz, E.L. 1924: Oversigt over de Sen- og Postglaciale Niveauforandringer i Danmark. Danmarks Geologiske Undersøgelse II. Række **41**, 49 pp.

Milthers, V. 1916: Spaltedale i Jylland. Danmarks Geologiske Undersøgelse IV. Række **1**(3), 16 pp.

Milthers, V. 1948: Det danske Istidslandskabs Terrænformer og deres Opstaaen. Danmarks Geologiske Undersøgelse III. Række **28**, 234 pp.

Pedersen, S.A.S. & Petersen, K.S. 1997: Djurslands geologi, 96 pp. Copenhagen: Geological Survey of Denmark and Greenland.

Sigmond, E.M.O. 2002: Geological map, land and sea areas of northern Europe, scale 1:4 million. Trondheim: Geological Survey of Norway.

Torp, S. 2001: De Miltherske spaltedale – landskabsdannelse og laserscanning i Midtjylland. Geologisk Nyt **3**(1), 28–29.

Vejbæk, O.V. 1990: The Horn Graben, and its relationship to the Oslo Graben and the Danish Basin. Tectonophysics **178**, 29–49.

Authors' address

Geological Survey of Denmark and Greenland, Øster Voldgade 10, DK-1350 Copenhagen K, Denmark. E-mail: *prj@geus.dk*

Soil erosion and land-use change during the last six millennia recorded in lake sediments of Gudme Sø, Fyn, Denmark

Peter Rasmussen and Jesper Olsen

The Danish landscape is characterised by low relief and consequently the risk of soil erosion is low compared to many central and southern European countries with more variable terrain (European Environment Agency 2000; Van der Knijff *et al.* 2000). However, even in countries with less intensive erosion, water-induced soil erosion is recognised as an increasingly important environmental issue due to its role in the transport of nutrients, pesticides and other contaminants to rivers, lakes and coastal waters (e.g. Stone 2000).

There are relatively few monitoring programmes of sediment erosion in Denmark and those that exist typically only cover the last few decades (Veihe *et al.* 2003). Therefore, it is difficult to identify long-term trends and baseline conditions. However, the geological record provides insight into patterns and rates of soil erosion through time. Lake and fjord sediment archives are especially useful because they can provide continuous and undisturbed sediment successions that can be analysed at high temporal resolution. These sediment records can be examined using a variety of approaches that include sedimentological, geochemical and biological analyses and thus generate important insight into baseline states, trajectories and responses to forcing mechanisms over long timescales, which would otherwise be difficult to obtain. The records are typically limited to yielding insight only into the average rate of erosion and they often provide little information about the spatial extent or distribution of erosional processes within a catchment area.

In this paper we present an example of a long-term erosional record from Gudme Sø, Fyn (Fig. 1). Numerous archaeological excavations have been undertaken near Gudme Sø, and the Geological Survey of Denmark and Greenland has carried out analyses of sediments from the lake to provide a continuous picture of landscape changes. Sediment accumulation rates of minerogenic matter and pollen analysis are here used to explore the erosional response to changes in land-use.

Study site and methods

Gudme Sø is located on south-east Fyn *c.* 5 km from the sea in a gently undulating terrain with surface deposits consisting of clay till (Fig. 1). The lake has a surface area of 9 ha, a mean water depth of 0.5 m, and a catchment area of 48 ha. It has no major natural inlets or outlets. An 11.8 m long sediment core of slightly humic gyttja with low calcareous content and varying silt and clay contents was retrieved from the lake. Age determination was provided by radiocarbon dating, and the chronology at the top of the core was further refined by linear interpolation, using the first occurrence of spheroidal carbonaceous fly-ash particles and the date of the sediment surface (i.e. the year of coring) as bracketing ages (Fig. 2).

Sediment accumulation rates of minerogenic matter (SAR-min in mg/cm^2 per year) were calculated and used as proxies of soil erosion from the catchment area to the lake (e.g. Mackereth 1966). The changes in SAR-min values were compared to pollen-inferred changes in vegetation and land-use from the same sediment core. The increases and decreases in non-arboreal pollen (NAP) were used as a record of changes in the proportion of open land. It is assumed that the variation in the sum of taxa of cultivated plants and *Plantago lanceolata* (ribwort plantain) reflects changes in the extent of arable land, and pastures or meadows, respectively (Behre 1981; Gaillard 2007). The record of colonies of the green algae *Pediastrum* sp. is used as proxy evidence for in-lake productivity (Bradshaw *et al.* 2005).

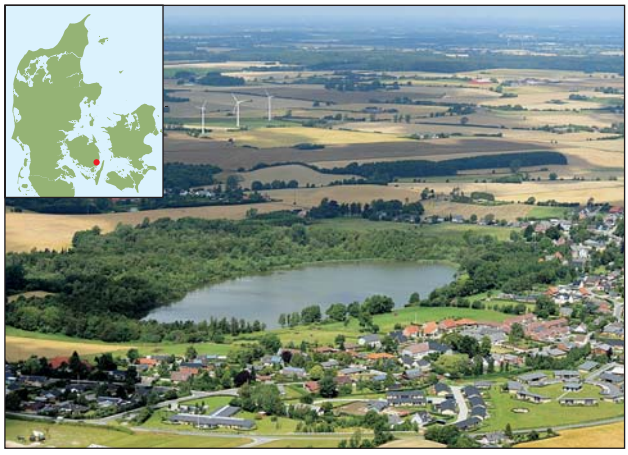

Fig. 1. Aerial photograph of Gudme Sø seen from the south-east. The lake size is *c.* 490 × 250 m. Today the lake catchment area (48 ha) consists of 50% tilled, 25.8% natural and 24.2% built-up area. Photograph courtesy of The Royal Danish Air Force.

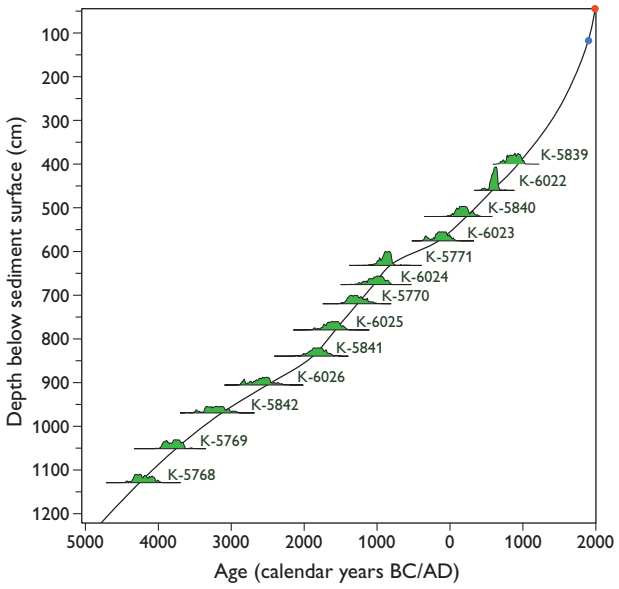

Fig. 2. Age–depth model for the Gudme Sø sediment succession based on 13 calibrated ^{14}C dates, the date of the first occurrence of spheroidal carbonaceous fly-ash particles (blue dot at AD 1900; Odgaard 1993) and the age of the sediment surface (red dot at AD 1989). The K-numbers are the laboratory numbers for the dated samples. The small diagrams show probability distributions of the calibrated ages. The age–depth model was established using the programme Bpeat (Blaauw & Christen 2005).

Results and discussion

Chronology

The ^{14}C dates from the Gudme Sø sediment core are based on bulk sediment samples and may overestimate their actual ages due to the hard-water effect (Björck & Wohlfarth 2001). However, the $CaCO_3$ content of the sediments is very low and the ages of key-pollen, stratigraphical levels at Gudme Sø are in agreement with other independent ages from corresponding levels in Danish bogs where the dated peat is unaffected by hard water (Table 1). Hence, we consider the Gudme Sø age–depth model to be reasonably accurate and reliable within *c.* 100 years. In the following, all ages are given in calendar years BC/AD.

Incipient landscape disturbance

In Fig. 3 the history of the last *c.* 6000 years of soil erosion to the Gudme Sø basin is compared with contemporary changes in vegetation and land-use. Coincident increases in total NAP and taxa of cultivated plants and in SAR-min suggest a causal link between agricultural activities and soil loss.

The low SAR-min values in the late Mesolithic (*c.* 4200–3900 BC) suggest a low level of soil disturbance, which is in good agreement with the pollen data. Very low NAP values (*c.* 2%) indicate that the landscape was dominated by closed-canopy forests with only a sparse field layer vegetation (Iversen 1973). During the Mesolithic, anthropogenic impact on the vegetation appears to have been negligible, and landscape disturbance was driven by natural agencies, implying that the sediment flux to the lake at this time represents a 'natural' baseline state.

In Denmark the cultural shift from the Mesolithic (hunting-fishing-gathering) to the Neolithic (farming) way of living took place *c.* 3900 BC. Approximately 200 years later (*c.* 3650–3500 BC) a marked increase in both SAR-min and NAP values at Gudme Sø indicate an erosional event clearly triggered by deforestation that was associated with incipient agricultural activities. At that time the first pollen types unambiguously indicative of crop cultivation and pastoral farming occurred (cereals and *Plantago lanceolata*, respectively). Interestingly, the data indicate that catchment disturbance and agricultural activities precede accelerated erosion rates by *c.* 150–200 years, thus showing a delay or threshold effect in the system's response.

Between *c.* 3350 and 3200 BC soil erosion rates increased again, although this time not correlated with pollen evidence of land clearance or intensified agriculture. Low soil erosion rates between *c.* 3200 and 2650 BC and low NAP values indicate catchment stability. At about 2650 BC a renewed and short-lived (*c.* 2650–2550 BC) deforestation was accompanied by intensified agricultural activities reflected in high percentages of NAP, *Plantago lanceolata* and cultivated taxa. Despite the apparent intensity of this brief land clearance episode, the erosional response was moderate. This might be

Table 1. ^{14}C dates of pollen-analytical levels in Gudme Sø and three Danish raised bogs

	Gudme Sø	Fuglsø Mose	Abkær Mose	Holmegaard Mose
1st *Centaurea cyanus* (cornflower)	AD 1320	AD 1360	AD 1240	AD 1350
1st *Secale cereale* (rye)	170 BC	80 BC	80 BC	80 BC
Fagus sylvatica (beech) 3–5%	960 BC	890 BC	240 BC	920 BC
Fagus sylvatica (beech) > 0.5–1%	1460 BC	1320 BC	1320 BC	1400 BC
1st *Plantago lanceolata* (ribwort plantain)	3650 BC	3630 BC	3000 BC	3800 BC
Elm decline	3990 BC	3830 BC	3870 BC	3500 BC

Data partly from Odgaard (1994).

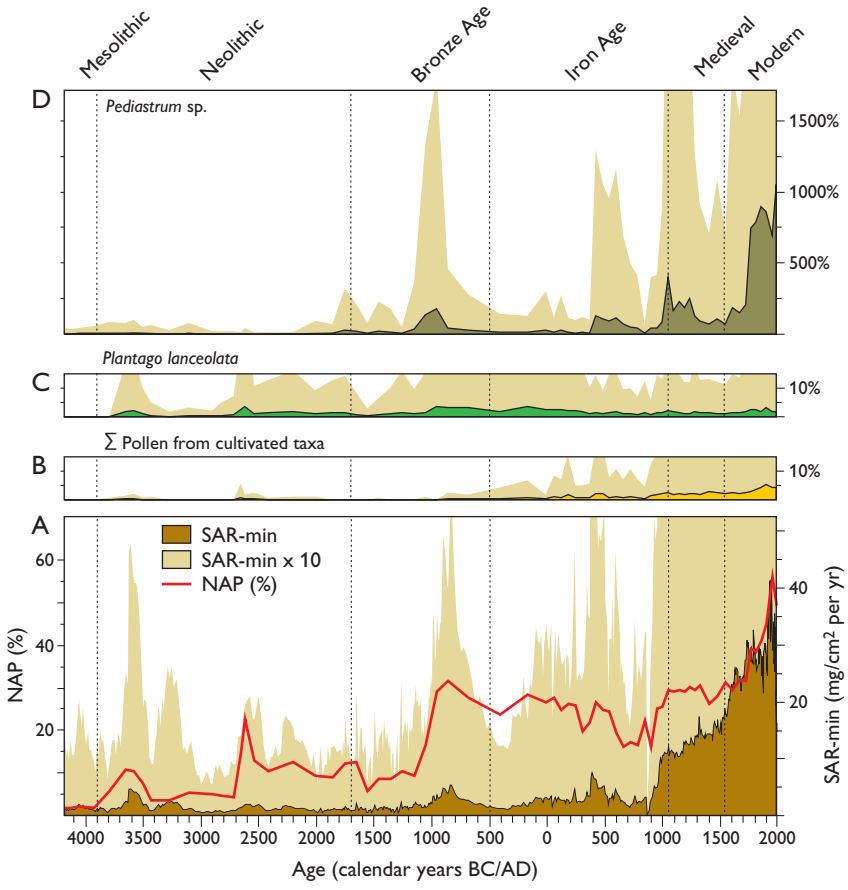

Fig. 3. **A**: Sediment accumulation rate of minerogenic matter (SAR-min; proxy of soil erosion rate) and non-arboreal pollen (NAP; proxy for open land). The results of the pollen analysis are presented as percentages of the total sum of pollen and spores from terrestrial plants. **B**: Pollen percentages of the sum of cultivated taxa. **C**: Pollen percentages of *Plantago lanceolata* (ribwort plantain). **D**: Percentages of the green algae *Pediastrum* sp. (calculated on the basis of the terrestrial pollen and spore sum). For B, C and D the dark-coloured curves are percentages and the light-coloured areas represent 10 times exaggeration.

due to the type of land-use at a time when subsistence economy most likely was predominantly based on pastoral farming. In contrast to arable farming, such land-use implies the maintenance of permanently grass-covered pasture that would be less prone to erosion than cultivated fields (Veihe *et al.* 2003). After 2550 BC, low soil erosion rates indicate a long period of relative stability in the catchment area, which lasted until the middle of the Bronze Age at *c.* 1000 BC.

Landscape transformation

For *c.* 150 years, between 1000 and 850 BC, the landscape around Gudme Sø changed drastically and became far more open than previously as suggested by the increase in NAP. Extensive forest clearance and expansion of areas used for livestock grazing and crop cultivation led to comprehensive landscape disturbance and a marked increase in erosion rates to the lake. The contemporary increase in *Pediastrum* sp. indicates a larger nutrient loss from the catchment area to the lake due to soil in-wash, which enhanced the in-lake productivity. After *c.* 200 years, the sediment influx to the lake gradually declined and stabilised, despite a continued high anthropogenic impact on the landscape as indicated by the continued high NAP values.

In the Iron Age around 100 BC, the erosion rates increased slightly and remained almost constant until *c.* AD 400. Thereafter, there was a short-lived disturbance period around AD 400–500 with intensified arable farming (increased abundances of cultivated taxa), accelerated soil erosion, and higher lake productivity (raised percentages of *Pediastrum* sp.). High percentages of *Cannabis*-type pollen in this period (not shown) indicate that the lake was used for retting hemp, a process in which stems are soaked in water to free their bast fibres from the surrounding tissue in order to produce fibres for example for cloth and rope making. Hemp-retting in the lake most likely contributed to the increased input of minerogenic material, as plants for retting may have been placed in the lake with roots; this could also have contributed to the nutrient enrichment of the lake at that time (Odgaard 1994).

Between *c.* AD 600 and 900 the soil erosion rate to the lake decreased, in agreement with the reduced anthropogenic impact on the landscape as reflected in the decreasing NAP values. At this time, the use of the lake for hemp-retting almost ceased and the percentage value of *Pediastrum* sp. declined. Between AD 950 and 1050, i.e. in the second half of the Viking Age, the pollen data suggest renewed deforestation followed by greatly intensified arable farming (elevated percentages of cultivated taxa). This marked change in land-use led to an unprecedented increase in soil erosion that likely caused eutrophication of the lake involving blooms of *Pediastrum* sp. The nutrient enrichment of the lake may have been further intensified by resumption of hemp-retting in the lake, a procedure which continued to around AD 1900.

During the Medieval period, the anthropogenic impact on the landscape increased significantly as land clearance in-

creased and crop cultivation intensified. The cultivation of large new areas was facilitated by the introduction of new farming technology such as the mouldboard plough and ridge-and-furrow. At Gudme Sø, the intensive arable farming in the Middle Ages led to steadily increasing sediment yields. The abundance of *Pediastrum* sp. at this time suggests continued eutrophication.

In Modern time (AD 1536 to the Present) the area around the lake was further cultivated at the expense of woodland. From *c*. AD 1500 to 1950, NAP values increased from *c*. 30% to 55% indicating widespread agricultural activities predominantly characterised by crop cultivation. The high and increasing human impact during this period corresponds closely to a dramatic and unprecedented increase in soil erosion, which peaked around AD 1950 contemporaneously with the highest NAP values in the entire record. A rapid and marked increase in the percentage of *Pediastrum* sp. at the beginning of the 18th century signifies the onset of a major nutrient enrichment of the lake.

Concluding remarks

The investigation of the lake sediments from Gudme Sø provides a 6000-year-record of soil erosion rates as well as contemporary pollen-inferred changes in vegetation and land-use. The study demonstrates a close correlation between changes in agricultural activity and rates of soil erosion in the catchment area of the lake. Prior to the late Viking Age, erosion to the lake occurred in pulses triggered by episodes of land clearance followed by periods of relative stability in the catchment area. After the late Viking Age, soil erosion accelerated continuously and reached a peak in the mid-20th century with erosion rates approximately 30 times higher than the pre-disturbance rates in the Mesolithic. The study demonstrates that after the introduction of agriculture, soil erosion was mainly caused by human activity rather than climate. This general result has also emerged from other lake-based studies of long-term erosion in Denmark (Rasmussen & Bradshaw 2005) and southern Sweden (Dearing 1991). According to current climate models we can expect an increase in precipitation, more rainfall in the winter season and a higher frequency of extreme precipitation events in the future (Christensen *et al*. 2006). Given these predictions, climate will undoubtedly be of growing significance as a forcing mechanism for soil erosion.

Acknowledgement

The Gudme Sø investigation is part of an archaeological research project funded by A.P. Møller og Hustru Chastine Mc-Kinney Møllers Fond til almene Formaal.

References

Behre, K.-E. 1981: The interpretation of anthropogenic indicators in pollen diagrams. Pollen et Spores **23**, 225–245.

Björck, S. & Wohlfarth, B. 2001: ^{14}C chronostratigraphic techniques in paleolimnology. In: Last, W.M. & Smol, J.P. (eds): Tracking environmental change using lake sediments: basin analysis, coring, and chronological techniques **1**, 205–245.

Blaauw, M. & Christen, J.A. 2005: Radiocarbon peat chronologies and environmental change. Journal of the Royal Statistical Society, Series C (Applied Statistics) **54**, 805–816.

Bradshaw, E.G., Rasmussen, P., Nielsen, H. & Anderson, N.J. 2005: Mid- to late-Holocene land-use change and lake development at Dallund Sø, Denmark: trends in lake primary production as reflected by algal and macrophyte remains. The Holocene **15**, 1130–1142.

Christensen, J.H., Christensen, O.B., Guldberg, A. & Stendel, M. 2006: Modeller for klimaets udvikling. In: Søndergaard, M., Kronvang, B., Pejrup, M. & Sand-Jensen, K. (eds): Vand og vejr om 100 år – klimaforandringer og det danske vandmiljø, 40–54. Højbjerg: Forlaget Hovedland.

Dearing, J.A. 1991: Erosion and land use. In: Berglund, B.E. (ed.): The cultural landscape during 6000 years in southern Sweden. Ecological Bulletins **41**, 283–292.

European Environment Agency 2000: Down to earth: soil degradation and sustainable development in Europe. A challenge for the 21st century. Environmental Issue Series **16**, 32 pp. Luxembourg: Office for Official Publications of the European Communities.

Gaillard, M.-J. 2007: Pollen methods and studies – Archaeological applications. In: Elias, S.A. (ed.): Encyclopedia of Quaternary science **3**, 2570–2595. Oxford: Elsevier Science.

Iversen, J. 1973: The development of Denmark's nature since the last glacial. Danmarks Geologiske Undersøgelse V. Række **7-C**, 126 pp.

Mackereth, F.J.H. 1966: Some chemical observations on post-glacial lake sediments. Philosophical Transactions of the Royal Society of London, Series B, **250**, 165–213.

Odgaard, B.V. 1993: The sedimentary record of spheroidal carbonaceous fly-ash particles in shallow Danish lakes. Journal of Paleolimnology **8**, 171–187.

Odgaard, B.V. 1994: The Holocene vegetation history of northern West Jutland, Denmark. Opera Botanica **123**, 171 pp.

Rasmussen, P. & Bradshaw, E. 2005: Mid- to late-Holocene land-use change and lake development at Dallund Sø, Denmark: study aims, natural and cultural setting, chronology and soil erosion history. The Holocene **15**, 1105–1115.

Stone, M. (ed.) 2000: The role of erosion and sediment transport in nutrient and contaminant transfer. International Association of Hydrological Sciences Publication **263**, 308 pp.

Van der Knijff, J.M., Jones, R.J.A. & Montanarella, L. 2000: Soil erosion risk assessment in Europe, 34 pp. EUR 19044 EN. Ispra: European Soil Bureau, Joint Research Centre and Space Applications Institute.

Veihe, A., Hasholt, B. & Schiøtz, I.G. 2003: Soil erosion in Denmark: processes and politics. Environmental Science & Policy **6**, 37–50.

Authors' addresses

P.R., *Geological Survey of Denmark and Greenland, Øster Voldgade 10, DK-1350 Copenhagen K, Denmark.* E-mail*: per@geus.dk*

J.O., *Department of Earth Sciences, Aarhus University, Høegh-Guldbergs Gade 2, DK-8000 Århus C, Denmark.*

Geophysical methods and data administration in Danish groundwater mapping

Ingelise Møller, Verner H. Søndergaard and Flemming Jørgensen

Groundwater mapping in Denmark has high priority. It was initiated in the 1990s when the pressure on groundwater resources increased due to urban development and pollution from industrial and agricultural sources. In some areas, the groundwater mapping included survey drillings, modelling based on existing knowledge and geophysical mapping with newly developed methods that made area coverage on a large scale possible. The groundwater mapping that included development of new geophysical methods showed promising results, and led to an ambitious plan to significantly intensify the hydrogeological mapping in order to improve the protection of the Danish groundwater resources. In 1999 the Danish Government initiated the National Groundwater Mapping Programme with the objective to obtain a detailed description of the aquifers with respect to localisation, extension, distribution and interconnection as well as their vulnerability to pollution (Thomsen *et al.* 2004). This mapping programme covers around 40% of the area of Denmark designated as particularly valuable water abstraction areas. Water consumers finance the mapping programme by paying 0.04 € per cubic metre of consumed water. At the end of the programme in 2015, the total cost is estimated to be about 250 000 000 € with a significant part spent on geophysical mapping.

The mapping programme is administered by seven local offices under the Ministry of Environment, but most of the practical work is carried out by private consulting companies, and involves the use of geophysical survey methods, survey drillings, well logging, water sampling and hydrological mapping, as well as geological and groundwater modelling. In major parts of the particularly valuable water abstraction areas, it is important to obtain spatially dense geophysical data covering large continuous areas.

Geophysical methods used in the hydrogeological mapping

The choice of geophysical methods depends on the geological setting of the aquifers. Those of interest for drinking water are primarily found within the upper 250 m of the subsurface. The aquifers can be grouped into three main types. In

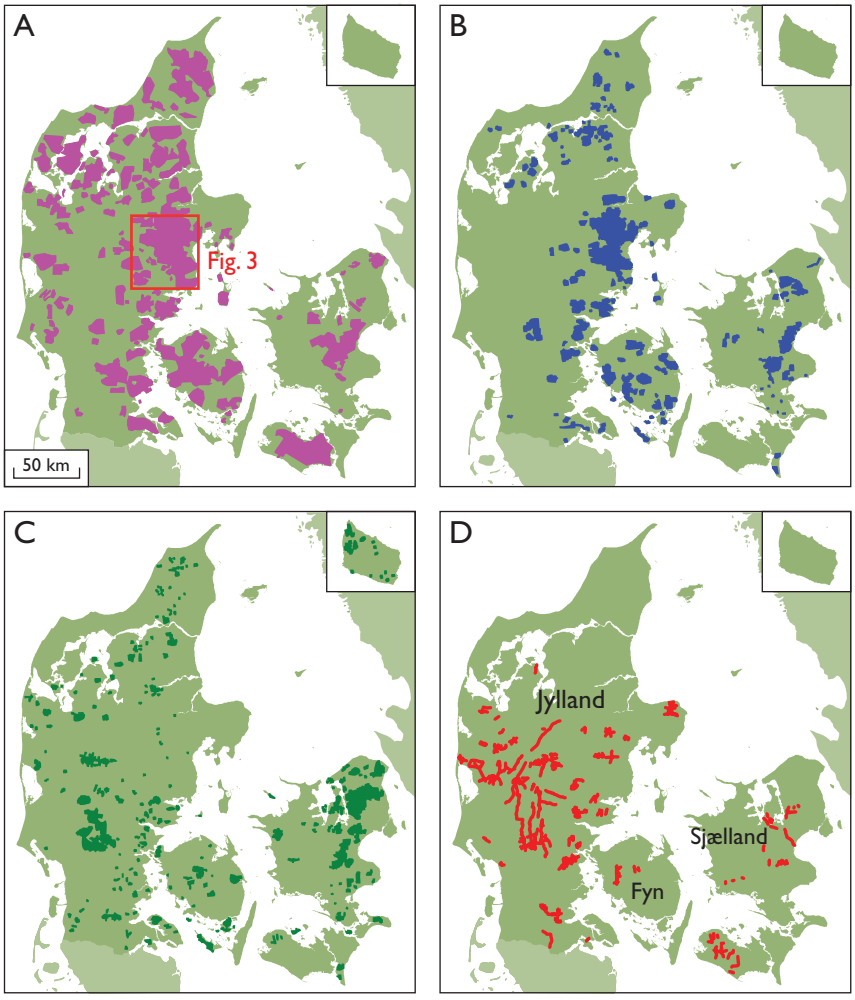

Fig. 1. Areal extent of data collected by the end of 2008. **A**: Areas with TEM and SkyTEM soundings, **B**: Areas with PACES profiles, **C**: CVES profiles. **D**: Seismic profiles.

the western part of Denmark, extensive Quaternary and Pre-Quaternary sand deposits dominate. In the central part, the most important groundwater resources are located in Quaternary sand deposits often found in Quaternary valley structures deeply eroded into Palaeogene clay deposits. In the northern and eastern parts of the country, most of the important aquifers are found in Upper Cretaceous and Danian limestone.

The most important geophysical methods are electrical and electromagnetic methods, combined with reflection seismic profiling and borehole logging at selected localities. Differences in electrical properties between sandy aquifers and clay sediments favour the use of the electrical and electromagnetic methods (Sørensen *et al.* 2005), but the ability of seismic methods to reveal detailed internal structures within the aquifers is also important.

The most commonly used geophysical method in the groundwater mapping programme is the airborne transient electromagnetic method, SkyTEM (Sørensen & Auken 2004), which is one of the new methods that has been developed to improve and optimise groundwater mapping. The first SkyTEM groundwater mapping project was carried out in 2003. Since then the SkyTEM method has been developed further and has proved faster and more powerful than the ground-based, single-site transient electromagnetic method, TEM, which was previously widely used. The SkyTEM method is used for mapping to a maximum depth of 250–300 m. Numerous buried valleys have been mapped in Denmark by the TEM method, in particular in the central parts of the country, where highly impermeable and low-resistive Palaeogene clay layers form the lower boundaries of the aquifers and the valleys are easily detected. At the end of 2008, TEM and SkyTEM data cover an area of more than 11 000 km^2 (Fig. 1A), which is about one quarter of the area of Denmark.

Electrical methods are used for near-surface mapping purposes. The pulled array continuous electrical sounding method (PACES; Sørensen 1996) has been extensively used to map layers within the upper 20–30 m. This method works well in combination with TEM measurements, and the combined methods provide data from the surface down to 200–300 m. This combination of methods has mainly been used in eastern Jylland and on Fyn. A total of around 9000 effective line kilometres of PACES data have been collected, corresponding to a coverage of more than 3000 km^2 (Fig. 1B).

The continuous vertical electrical sounding method (CVES; e.g. Dahlin 1996) is used in areas where it is unnecessary to map deeper layers, and where the subsurface resistivity values are too high for the SkyTEM method. About 4000 line kilometres have been collected, mainly in the central part of Jylland and on the eastern part of Sjælland (Fig. 1C).

The reflection seismic method is also of great value as a geophysical groundwater mapping tool, particularly following the development of a land-streamer and a new vibroseismic system (e.g. Vangkilde-Pedersen *et al.* 2006). Although the reflection seismic method is expensive, it can be successfully combined with SkyTEM measurements, and the decision about where to acquire seismic data can be based on the SkyTEM results (Jørgensen *et al.* 2003). Successful mapping of the outline of buried valleys and their internal structures has been based on the interpretations of seismic profiles; SkyTEM data do not allow such interpretations. The reflection seismic method has also been used successfully to map Palaeogene and Neogene sediments in the western part of Denmark (Rasmussen *et al.* 2007), where thick and extensive layers of sandy deposits constituting important aquifers are bounded by thinner layers of clayey deposits, and to map faults in Danian and Cretaceous limestone in the eastern part of Denmark. Around 1400 km of seismic lines have been collected, particularly in the western and central parts of Jylland (Fig. 1D).

Borehole logs are crucial for the geological and hydrological interpretation of boreholes. It is now common practise to log boreholes following survey drilling, and older water supply wells have also been logged. Particularly in areas with chalk and limestone or Neogene groundwater reservoirs log stratigraphy has provided valuable information. About 1500 boreholes have been logged.

Administration of the geophysical data

The Groundwater Mapping Programme is split up into many smaller areas to ease the administrative handling and to be able to meet priority criteria. Careful and standardised treatment of data is required to ensure that the resulting 'patchwork' is of high and uniform quality and has no visible seams. Therefore, standards and guidelines are worked out for geophysical data acquisition, calibration of instruments, data processing, interpretation (e.g. HydroGeophysics Group 2007a) and geological modelling (Jørgensen *et al.* 2008).

Without a predefined system of archiving the geophysical data and modelling results, the data logistics of the groundwater mapping programme would be overwhelming. The national GEophysical Relation DAtabase (GERDA; http://gerda.geus.dk) hosted at the Geological Survey of Denmark and Greenland (GEUS), is used for archiving these geophysical data. The development of the database began more than ten years ago. The database contains geophysical data of various types such as Wenner profiles, Schlumberger soundings, pulled array continuous electrical soundings, continuous vertical electrical soundings and induced polarisation, transient electromagnetic data including the airborne SkyTEM data,

frequency domain electromagnetic data, reflection seismic profiles and borehole logs. Various kinds of 1-D models and 2-D models resulting from inversion of electrical and electromagnetic data are also saved, securing an immediate use of the results. All information about data acquisition, data processing and inversion can be stored, which facilitates reprocessing of data and makes the inversion and interpretation of data transparent.

GEUS also hosts another database (Jupiter; http://jupiter.geus.dk) for borehole data. Jupiter contains information on, for example, geological and lithological descriptions, groundwater level and water quality observations. Both the Jupiter and GERDA databases have web-based graphical user interfaces, where any user can search for and download data free of charge.

Geophysical data are handled from data processing to geological interpretation in an integrated system formed by the GERDA and the Jupiter databases and two software packages, the Aarhus Workbench and the Geoscene3D in combination with a geological model database hosted at GEUS (Fig. 2; Møller *et al.* in press). The Aarhus Workbench (HydroGeophysics Group 2007b) has modules for handling, processing, inverting, interpreting and visualising electrical and electromagnetic data, all combined on a common GIS platform and a common database. The Aarhus Workbench enables anybody to work with the geophysical data in the GERDA database without having to know the complicated data model of GERDA or to be able to carry out a database query. By using the GIS platform at the Aarhus Workbench it is easy to produce various types of maps compiled from the geophysical data.

The different maps are entered into the 3-D visualisation and modelling tool Geoscene3D (I-GIS, http://www.i-gis.dk) together with all the geophysical data stored in GERDA and the borehole information stored in Jupiter, and the geophysical data are ready to be used in the geological modelling process carried out in Geoscene3D.

An example of the strength of the integrated data handling system is illustrated for a 50 × 60 km^2 area in eastern Jylland (Fig. 3). Large parts of this area are covered by TEM soundings (*c.* 83 000 soundings), collected during more than 90 mapping campaigns (Fig. 3B) and with five different TEM methods (Fig. 3C) over a time span of more than ten years. Figure 3A shows a map of the surface of the deepest low-resistive model layer based on interpretation of all the TEM soundings in the area. The deepest low-resistive model layer represents Palaeogene clay deposits except in the north-eastern corner, where it represents salty pore water in Danian limestone. The most prominent features found in the area are a large number of buried valleys incised into the Palaeogene clay deposits. The buried valleys show no direct correlation to

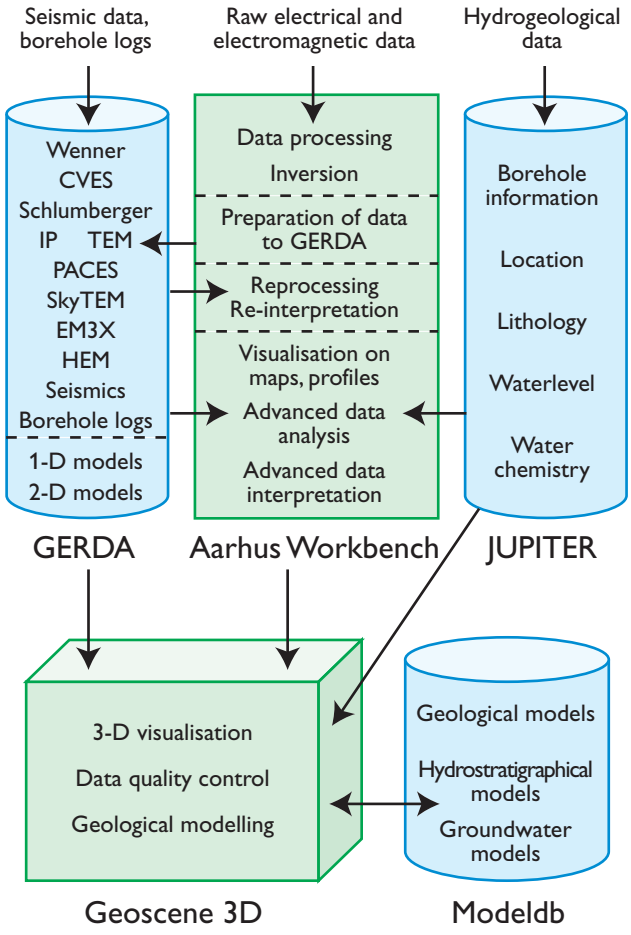

Fig. 2. Sketch of the integrated system of databases and program packages handling geophysical data and geological modelling. The arrows show the flow of data between the geophysical database GERDA, the borehole database Jupiter, the Aarhus Workbench program package, the Geoscene3D visualisation and modelling tool and the geological model database Modeldb.

the overall topography. Even though the data have been acquired by different companies, with different instruments and methods, and at different times, the data can be combined without showing any discrepancies at survey borders.

Concluding remarks

Geophysical measurements play an important role in the National Groundwater Mapping Programme and have contributed significantly to the mapping of aquifers in Denmark. In heterogeneous regions the data density needs to be high in order to provide acceptable mapping results. Geophysical methods like TEM/SkyTEM and electrical methods can provide sufficient data density and reflection seismic profiles can resolve internal structures in specific areas in combination with detailed borehole information such as lithological descriptions, geophysical logs, data on water chem-

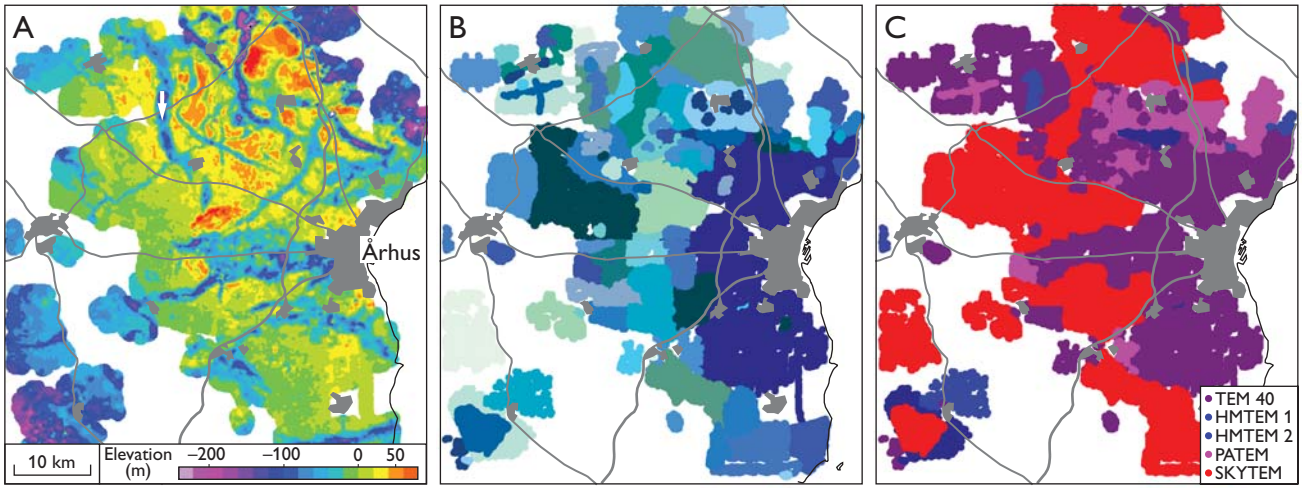

Fig. 3. Data coverage and results from an area in eastern Jylland. For location see Fig. 1. **A**: Map showing the elevation of the surface of the deepest low-resistive layer in the area relative to sea level. **B**: The data come from 94 different mapping projects (shown by different colours). **C**: Five different TEM methods were used to produce map A.

istry and hydraulic parameters. These data form the basis for detailed hydrogeological models. An integrated data handling system makes it possible to merge geophysical data acquired over long periods by different companies with different instruments. This is of great value for future mapping and administrative purposes.

References

Dahlin, T. 1996: 2D resistivity surveying for environmental and engineering applications. First Break **14**, 275–283.

HydroGeophysics Group 2007a: Guide to processing and inversion of SkyTEM data. Version 1.2. Århus: Department of Earth Sciences, University of Aarhus. http://www.hgg.geo.au.dk/HGGSoftware/work-bench/Workbench_SkyTEM.pdf.

HydroGeophysics Group 2007b: Aarhus Workbench A-Z Reference, Version 2.2. Århus: Department of Earth Sciences, University of Aarhus. http://www.hgg.geo.au.dk/HGGSoftware/workbench/Workbench_A-Z_reference.pdf.

Jørgensen, F., Lykke-Andersen, H., Sandersen, P.B.E., Auken, E. & Nørmark, E. 2003: Geophysical investigations of buried Quaternary valleys in Denmark: an integrated application of transient electromagnetic soundings, reflection seismic surveys and exploratory drillings. Journal of Applied Geophysics **53**, 215–228.

Jørgensen, F., Kristensen, M., Højberg A.L., Klint, K.E.S, Hansen, C., Jordt, B.E., Richardt, N & Sandersen, P. 2008: Opstilling af geologiske modeller til grundvandsmodellering. Geo-Vejledning **3**, 176 pp. Copenhagen: Geological Survey of Denmark and Greenland.

Møller, I., Søndergaard, V.H., Jørgensen, F., Auken, E. & Christiansen, A.V. in press: Integrated management and utilisation of hydrogeophysical data on a national scale. Near Surface Geophysics.

Rasmussen, E.S., Vangkilde-Pedersen, T. & Scharling, P. 2007: Prediction of reservoir sand in Miocene deltaic deposits in Denmark based on high-resolution seismic data. Geological Survey of Denmark and Greenland Bulletin **13**, 17–20.

Sørensen, K. 1996: Pulled array continuous electrical profiling. First Break **14**, 85–90.

Sørensen, K.I. & Auken E. 2004: SkyTEM – A new high-resolution helicopter transient electromagnetic system. Exploration Geophysics **35**, 191–199.

Sørensen, K.I., Auken, E., Christensen, N.B. & Pellerin L. 2005: An integrated approach for hydrogeophysical investigations. New technologies and a case history. In: Butler, D. (ed.): Near-surface Geophysics Part II, SEG Investigations in Geophysics Series **13**, 585–603. Tulsa: Society of Exploration Geophysicists.

Thomsen, R., Søndergaard, V.H & Sørensen, K.I. 2004: Hydrogeological mapping as a basis for establishing site-specific groundwater protection zones in Denmark. Hydrogeology Journal **12**, 550–562.

Vangkilde-Pedersen, T., Dahl, J. F. & Ringgaard, J. 2006: Five years of experience with landstreamer vibroseis and comparison with conventional seismic data acquisition. Proceedings of the 19th Annual SAGEEP Symposium on the Application of Geophysics to Engineering and Environmental Problems, Seattle, USA, 2–6 April, 2006. (Published on CD-ROM, 1086–1093).

Authors' address

Geological Survey of Denmark and Greenland, Lyseng Allé 1, DK-8270 Højbjerg, Denmark. E-mail: *ilm@geus.dk*

Water budget of Skærsø, a lake in south-east Jylland, Denmark: exchange between groundwater and lake water

Bertel Nilsson, Peter Engesgaard, Jacob Kidmose, Sachin Karan, Majken Caroline Looms and Mette Cristine Schou Frandsen

The European Union's Water Framework Directive aims to achieve a 'good' ecological status for groundwater bodies, for groundwater-dependent terrestrial ecosystems, and for aquatic surface water bodies by the year 2015. In Denmark, this goal will most likely not be fulfilled within such a short time frame due to the current poor ecological condition of Danish lakes (Søndergaard *et al.* 2008). However, public concern about the protection of aquatic environments has increased, and so has interest in improving lake water quality by reducing nutrient loading. Effective and sustainable lake restoration and conservation depend on the ability to (1) point out sensitive catchment areas for the lake, (2) estimate its total water and nutrient budgets and (3) relate observed differences in seepage rates to the abundance and distribution of macrophytes in the lake and to the topography and land-use of the surrounding terrain. In seepage lakes, i.e. lakes without inlets or outlets, the influence of the surrounding terrain, regional hydrogeology and lake geometry on the overall lake water budget has been studied in some detail (Krabbenhoft *et al.* 1990; Anderson & Cheng 1993; Cheng & Anderson, 1994; Kratz *et al.* 1997;

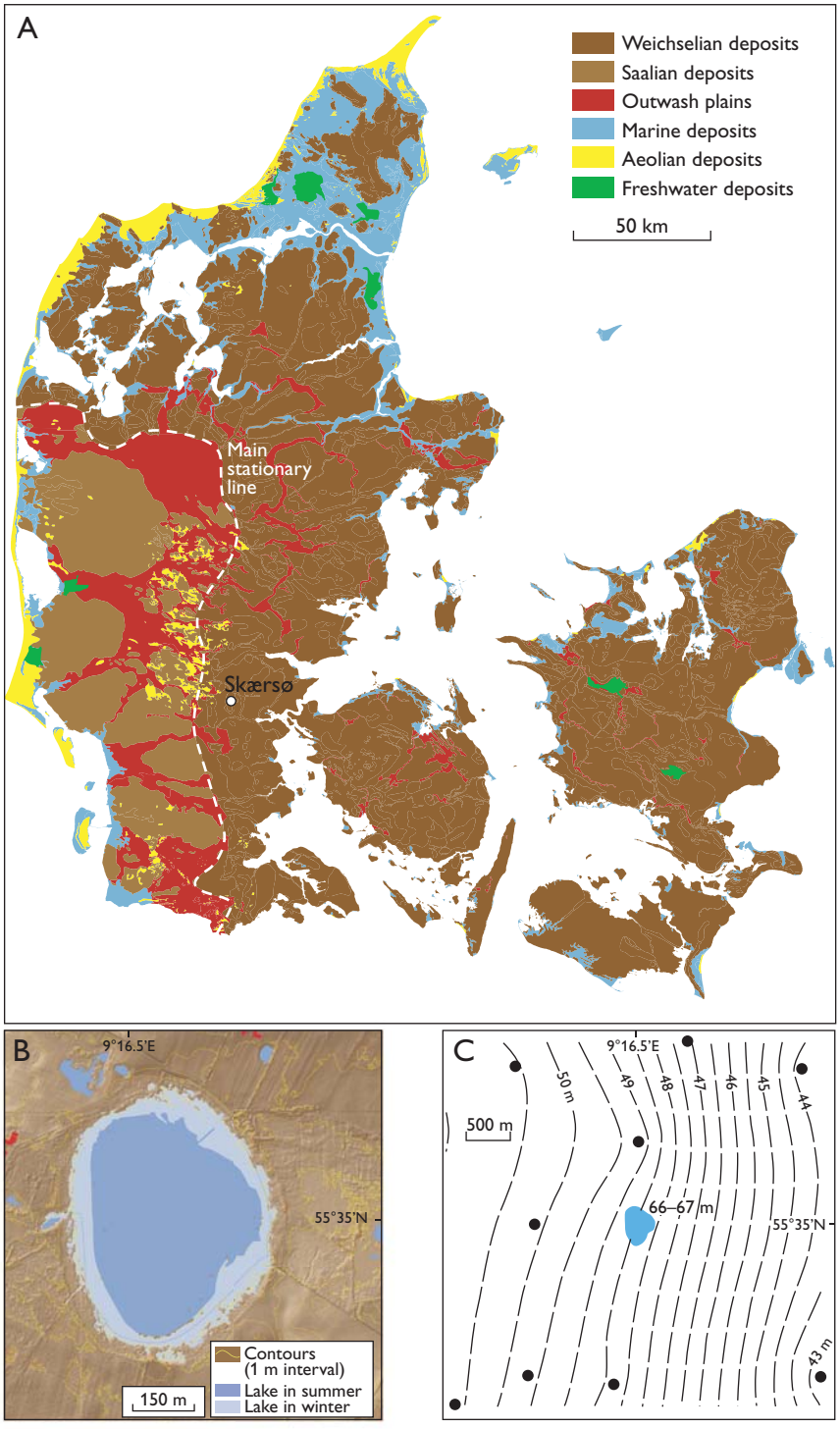

Fig. 1. **A**: Location of Skærsø east of the main stationary line in Jylland. **B**: Lake area in summer (dark blue) and winter (light blue). **C**: Map of the lake Skærsø area showing the groundwater level of the regional aquifer and the water level of Skærsø. Black dots show the locations of wells used to construct the map.

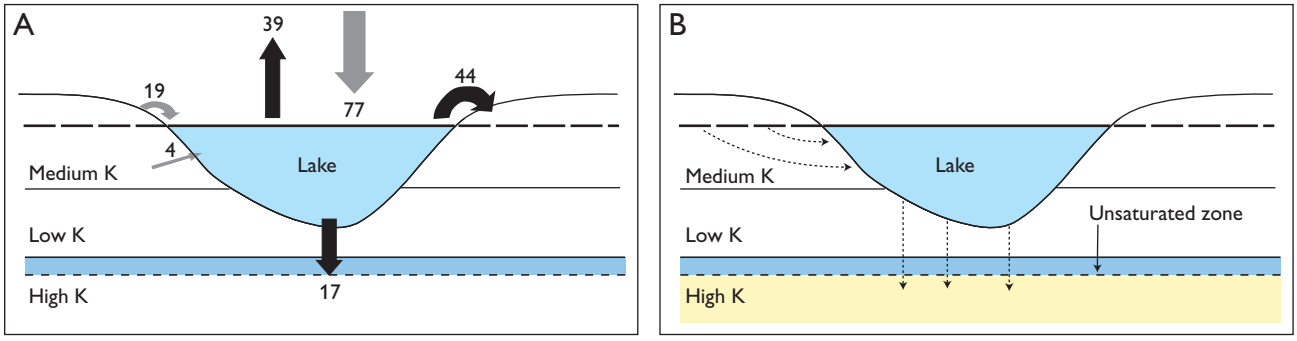

Fig. 2. **A**: Preliminary model of the water balance of Skærsø. Grey arrows show influx, black arrows loss. Numbers in per cent. **B**: Conceptual hydrogeological model of a perched lake disconnected from the underlying aquifer.

Winter 1999; Townley & Trefry 2000). However, little effort has been made to understand and quantify how riparian zones (wetlands) surrounding lakes may control the water flow and nutrient transport to the lakes. Although groundwater inflow to seepage lakes is suspected to be smaller than inflow from drainage ditches, it may still account for a significant nutrient influx.

This paper focuses on field work carried out 2007 and 2008 at Skærsø, a lake in the upper part of the Kolding Å catchment area in south-east Jylland (Fig. 1A). Field studies at Skærsø have shown that seepage can vary on different scales in both space and time. The purpose of this study is to link measurements of lake seepage rates and lake precipitation or evaporation to the catchment hydrogeology. The project is conducted by the Centre for Lake Restoration, which includes participants from University of Southern Denmark, National Environmental Research Institute, University of Copenhagen and Geological Survey of Denmark and Greenland.

Towards a lake typology

The Centre for Lake Restoration is developing a typological classification of Danish lakes using a multidisciplinary approach that integrates interactions between groundwater and lake water. The classification is based on geological, hydrological, hydrogeological, geomorphological, botanical and chemical aspects. The botanical part focuses on plant indicator species in the lakes, and the chemical part addresses water and sediment chemistry. Two or three main lake types are currently distinguished on the basis of geological, hydrological, hydrogeological and geomorphological criteria. New lake types will probably be defined in the coming years as biological and chemical indicators are also included in the classification.

Location and setting of Skærsø

Skærsø is located a few kilometres east of the main stationary line that formed during the last glacial maximum around 20 000 years ago. The lake is situated in the upper part of the

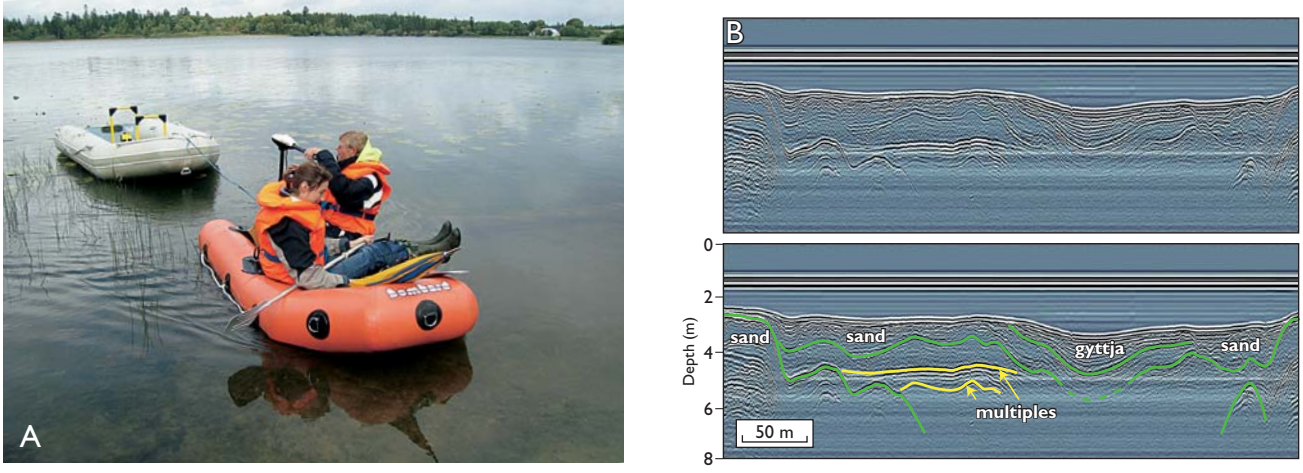

Fig. 3. **A**: Mapping of lake sediments using reflection ground penetrating radar (GPR). The radar equipment is contained in the grey rubber boat. **B**: An example of a GPR reflection profile with a preliminary interpretation.

Kolding Å catchment area (Fig. 1A) that is dominated by glacial and glaciofluvial deposits. Around Skærsø a 2–7 m thick sand layer overlies an approximately 10 m thick clayey till that is underlain by a regional sandy aquifer. The riparian zone around Skærsø has a width of 30–50 m and a thickness of 0.1–0.5 m, and consists of organic-rich fine sand and silt. The water table of the lake varies seasonally about 0.5 m, and in the winter or early spring the riparian zone around the lake is flooded (Fig. 1B). During flooding, organic particles and solutes are transported to the lake and cause a significant decrease in the transparency of the water. Below Skærsø, the groundwater table of the regional sand aquifer is 48–49 m above sea level, whereas the surface of the lake is 66–67 m above sea level. This difference indicates that there is a hydraulic connection between the lake and the regional aquifer (see below and Fig. 1C).

The area of Skærsø is approximately 16 ha , and its average water depth is 1.5 m, with a maximum depth of about 8 m. It is characterised as a mesotrophic, low-alkaline, clear-water lake. Until the 1980s, Skærsø was a clear-water heath lake, dominated by submerged macrophytes including *Lobelia dortmanna* that grew to a depth of 1.5 m. At the end of the 1980s, Skærsø suffered from organic-rich, acidic, unclear water, resulting in almost complete disappearance of the submerged macrophytes. After almost 19 years of unsuccessful attempts at lake restoration, the conditions in Skærsø are still deteriorating. A recent study showed that changes in light conditions in the lake are not as strongly coupled to changes in the external nutrient loading as expected (Frandsen & Stæhr 2007). Changes in the hydrology of the riparian zone have led to a seasonal flush of dissolved coloured organic matter into the lake which causes decreased water transparency, decreased light penetration and release of nutrients. However, the mechanisms that affect water transparency require further investigation.

Hydrogeological model

The hydrogeological model of the lake is characterised by the setting of shore and wetland (the riparian zone) with an upper, local groundwater aquifer in sediments of low to moderate permeability showing low hydraulic gradients. The deeper part of the lake is probably connected to a lower permeable layer with high hydraulic gradients (Fig. 1C). Because the surface of Skærsø is almost 20 m above the hydraulic head of the regional sand aquifer, we expect leakage of water from the lake through its bottom into the underlying regional aquifer.

The water supply to Skærsø is dominated by precipitation (77%) and inflow from the catchment area (19%). A limited portion (4%) comes from the shallow, local groundwater aquifer. Water flux from the lake is dominated by outflow via outlets (44%; mainly an artificial ditch) and evaporation (39%). We suggest that the remaining 17% is lost by leakage to the underlying aquifer (Fig. 2A). Thus Skærsø can be conceptualised as a perched lake, a lake which is disconnected from the underlying aquifer by an unsaturated zone between the lake bottom and the aquifer (Fig. 2B).

Ground penetrating radar

In order to investigate the structure and thickness of the sediments below the lake, a ground penetrating radar survey was carried out (Fig. 3A). Thick layers of organic-rich sediments such as lake mud (gyttja) or peat generally reduce groundwater seepage, whereas sandy sediments can promote interaction between groundwater and lake water (Fig. 3B). Ground penetrating radar can help to identify areas of potential groundwater seepage, which may then be verified using more traditional point measurements such as coring. The application of ground penetrating radar to map lake sediments is new in Denmark, and the interpretation of the radar profiles is still uncertain and needs to be checked against data from coring. However, according to our preliminary interpretation of the radar data, sandy sediments are widespread below the lake, whereas gyttja is probably restricted to a small area (Fig. 3B).

Multidisciplinary approach to estimate the groundwater flux

Seepage to or from Skærsø to the upper, local groundwater aquifer was measured using various tracers (heat, stable isotopes), direct measurements of water flux, as well as nutrients sampled from piezometer transects. The combined use of different tracers and methods at different scales provides a good understanding of the physical, chemical and biological behaviour of the entire lake. Figure 4 shows three types of field equipment that were used to quantify the flux from the local aquifer to Skærsø, and the estimated groundwater fluxes (specific discharges) to Skærsø are summarised in Table 1.

The flux values estimated by the three different methods are not consistent. The highest estimated fluxes (using the Darcy

Table 1. Groundwater discharge into Skærsø

Method	Flux	Specific discharge (m/sec)
Seepage meter	q_{seep}	$10^{-7} – 3 \times 10^{-7}$
Temperature	q_T	$10^{-8} – 10^{-7}$
Darcy[1]	q_D	$10^{-7} – 10^{-6}$

[1] $q_D = K \times i$, where K is the saturated hydraulic conductivity of the lake-shore sediment (i.e. fine sand and silt in the upper 2 m) equivalent to $K = 10^{-4} – 10^{-5}$ m/sec, and *i* is the hydraulic gradient measured by a potentiomanometer to about ± 0.01.

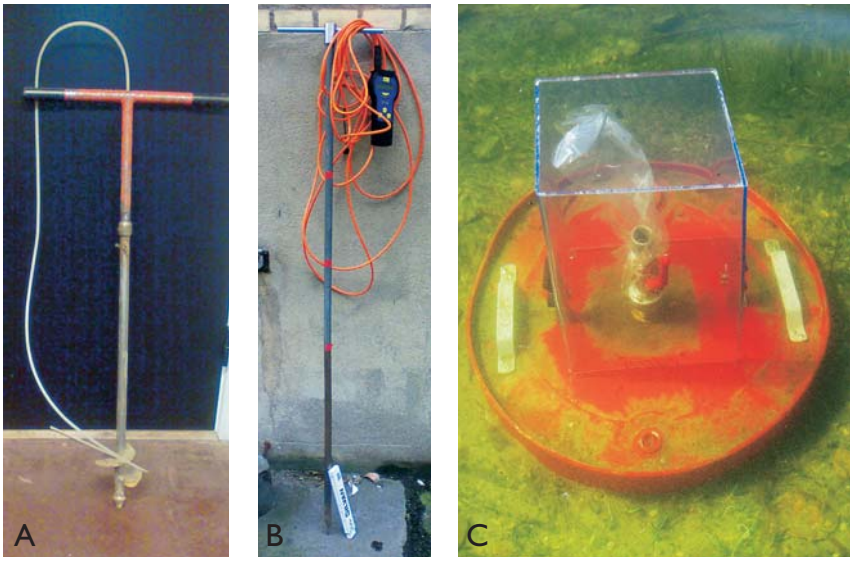

Fig. 4. Equipment used for field determination of groundwater seepage. **A**: Modified 1 m long potentiomanometer used to measure the water pressure in the subsurface (Winter *et al.* 1988). **B**: Multi-level, 1.25 m long temperature probe used to measure the temperature at multiple levels in the sediment (Schmidt *et al.* 2005). **C**: A steel drum seepage meter, 0.5 m in diameter, used to measure the flow of groundwater through the lake bottom (Lee 1977). From Nilsson *et al.* (2008).

(transect) method) are 10–100 times higher than the lowest estimated fluxes (using the temperature method). Despite this difference, the data indicate a low inflow from the shallow groundwater aquifer and, as mentioned above, we suggest that 4% of the inflow to the lake comes from the shallow aquifer, based on the average value obtained by the applied methods. We have no data on leakage through the lake bottom to the underlying aquifer, but we consider this process likely and suggest a flux value of 17% based on the difference between the other fluxes. However, this figure is highly uncertain. Especially the figure for the evaporation from the lake may be underestimated if investigations of other lakes in Jylland are considered. Nevertheless, we conclude that exchange between groundwater and lake water plays an important role in the water budget of lake Skærsø.

Acknowledgement

Villum Kann Rasmussen Fonden is gratefully acknowledged for funding the Centre for Lake Restoration (CLEAR), which is a Villum Kann Rasmussen Centre of Excellence.

References

Anderson, M.P. & Cheng, X. 1993: Long- and short-term transience in a groundwater/lake system in Wisconsin, USA. Journal of Hydrology **145**, 1–18.

Cheng, X. & Anderson, M.P. 1994: Simulating the influence of lake position on groundwater fluxes. Water Resources Research **30**, 2041–2049.

Frandsen, M.C.S. & Stæhr, A.P. 2007: Differentieret analyse af lysmiljøet i Skærsø, 24 pp. Unpublished report, Freshwater Biological Laboratory, University of Copenhagen, Hillerød, Denmark.

Krabbenhoft, D.P., Bowser, C.J., Anderson, M.P. & Valley, J.W. 1990: Estimating groundwater exchange with lakes. 2. Calibration of a three-dimensional, solute transport model to stable isotope plume. Water Resources Research **26**, 2455–2462.

Kratz, T.K., Webster, K.E., Bowser, C.J., Magnuson, J.J. & Benson, B.J. 1997: The influence of landscape position on lakes in northern Wisconsin. Freshwater Biology **37**, 209–217.

Lee, D.R. 1977: A device for measuring seepage flux in lakes and estuaries. Limnology and Oceanography **22**, 140–147.

Nilsson, B., Engesgaard, P., Kidmose, J. & Karan, S. 2008: Groundwater – lake exchange at lake Skærsø in western Denmark. Proceedings of 36th IAH Congress, October 2008, Toyama, Japan. Integrating Groundwater Science and Human Well-Being. Extended abstract on CD-ROM.

Schmidt, C., Bayer-Raich, M. & Schirmer, M. 2005: Characterization of spatial heterogeneity of groundwater – stream water interactions using multiple depth streambed temperature measurements at the reach scale. Hydrology and Earth System Sciences **10**, 849–859.

Søndergaard, M., Liboriussen, L., Pedersen, A.E. & Jeppesen, E. 2008: Lake restoration by fish removal: short- and long-term effects in 36 Danish lakes. Ecosystems **11**, 1291–1305.

Townley, L.R. & Trefry, M.G. 2000: Surface water – groundwater interaction near shallow circular lakes: flow geometry in three dimensions. Water Resources Research **36,** 935–949.

Winter, T.C. 1999: Relation of streams, lakes, and wetlands to groundwater flow systems. Hydrogeology Journal **7**, 28–45.

Winter, T.C., LaBaugh, J.W. & Rosenberry, D.O. 1988: The design and use of a potentiomanometer for direct measurement of differences in hydraulic head between groundwater and surface water. Limnology and Oceanography **33**, 1209–1214.

Authors' addresses

B.N., *Geological Survey of Denmark and Greenland, Øster Voldgade 10, DK-1350 Copenhagen K, Denmark.* E-mail*: bn@geus.dk*

P.E., J.K., S.K. & M.C.L., *Department of Geography and Geology, University of Copenhagen, Øster Voldgade 10, DK-1350 Copenhagen K, Denmark.*

M.C.S.F., *Freshwater Biological Laboratory, Biological Institute, University of Copenhagen, Helsingørsgade 51, DK-3400 Hillerød, Denmark.*

Geological observations in the southern West Greenland basement from Ameralik to Frederikshåb Isblink in 2008

Nynke Keulen, Anders Scherstén, John C. Schumacher, Tomas Næraa and Brian F. Windley

In 2008, the Geological Survey of Denmark and Greenland began a project in collaboration with the Bureau of Minerals and Petroleum of Greenland with the aim to publish a web-based, seamless digital map of the Precambrian bedrock between 61°30′ and 64°N in southern West Greenland. Such a map will be helpful for the mineral exploration industry and for basic research. Producing an updated digital map requires additional field work revisiting key localities to collect samples for geochemistry, geochronology and metamorphic petrology. The new data will help us to test and refine existing models and improve general understanding of the geological evolution of the area. Here we summarise some results from the 2008 field activities between Ameralik in the north and Frederikshåb Isblink in the south (Fig. 1). The area was mapped in the 1960s and 1970s, and although the 1:100 000-scale maps are of excellent quality, they do not include more recent developments in geochronology, thermobarometry and geochemistry. A notable exception is the Fiske- næsset complex (Fig. 1), which has received considerable attention after it was first mapped (Ellitsgaard-Rasmussen & Mouritzen 1954; Windley *et al.*, 1973; Windley & Smith, 1974; Myers 1985). New tectonic models have been developed since the original 1:100 000 maps were produced, and the tectonic evolution has been commonly explained in terms of terrane accretion (Friend *et al.* 1996). Friend's model defines a number of boundaries that separate terranes of different age and origin and which might have contrasting tectono-metamorphic histories prior to terrane accretion. The current project area includes the northern part and proposed boundary of the Tasiusarsuaq terrane, which was amalgamated with the terranes to the north at 2.72 Ga, when regional metamorphism affected the region (Friend *et al.* 1996). In addition, Windley & Garde

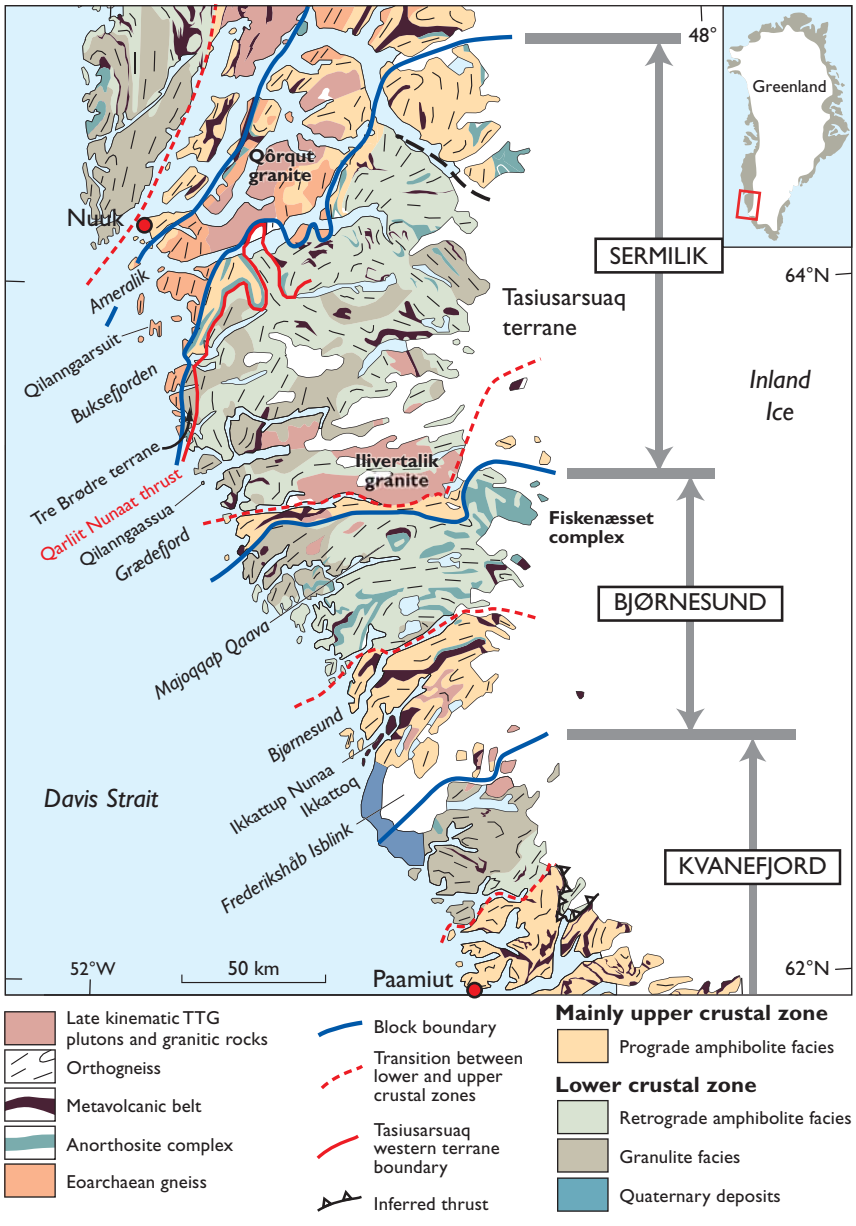

Fig. 1. Simplified geological map of the central part of the North Atlantic craton in southern West Greenland showing the main rock components, patterns of metamorphic facies and three crustal blocks (modified after Windley & Garde 2009).

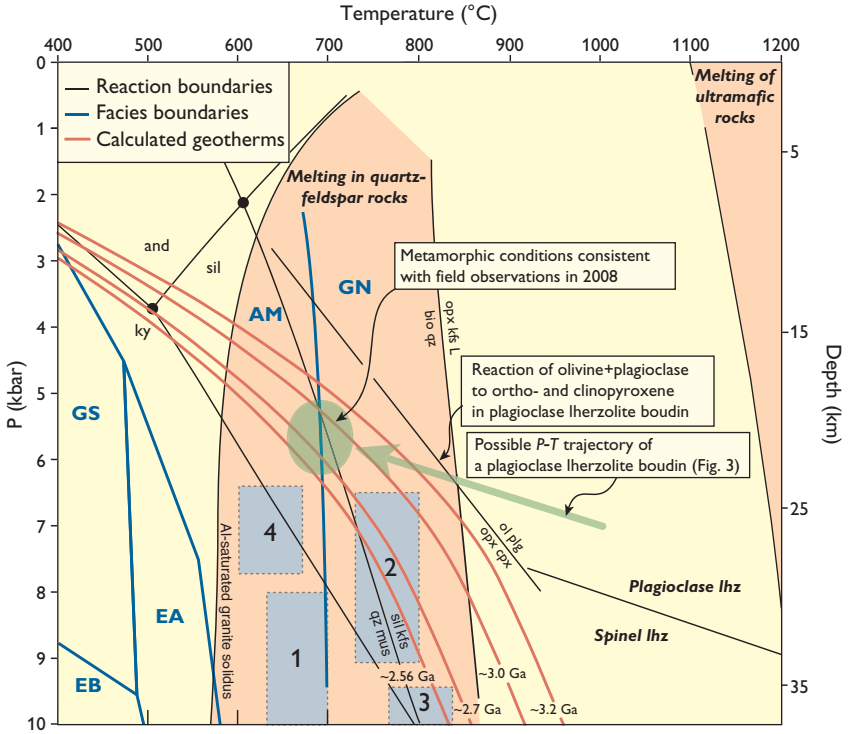

Fig. 2. Ranges of *P–T* estimates from previous work by Wells (1979), Griffin *et al.* (1980) and Riciputi (1990); geotherms based on measured and estimated contents as a function of time of radiogenic elements in basaltic and felsic Greenland rocks using methods of Kamber *et al.* (2005). The calculations are based on a crustal thickness of 40 km and a two-layer model with 10 km of mafic rocks at the base of the crust overlain by 30 km of felsic rocks. Depths in kilometres are based on an average crustal density of 2.75 g/cm^3. Parameters: mantle heat flow: 20 mW/m^2; mafic and felsic rock-heat production are: 0.262 and 3.478 µW/m^3 at 3.2 Ga (possible maximum age for this part of the terrane), 0.244 and 3.254 µW/m^3 at 3.0 Ga, 0.220 and 2.945 µW/m^3 at 2.7 Ga, 0.210 and 2.811 µW/m^3 at 2.56 Ga (age of the Qôrqut granite). The numbered blue fields represent the ranges of *P–T* estimates: 1 = Sermilik (Griffin *et al.* 1980); 2 = Sermilik and Qilanngaassua (Riciputi *et al.* 1990); 3 = Sermilik (Wells 1979); 4 = Qilanngaarsuit (Wells 1979). **AM**, amphibolite facies; **and**, andalusite; **bio**, biotite; **cpx**, clinopyroxene; **EA**, epidote-amphibolite facies; **EB**, epidote-blueschist facies; **GN**, granulite facies; **GS**, greenschist facies; **kfs**, K-feldspar; **ky**, kyanite; **l**, liquid; **lhz**, lherzolite; **mus**, muscovite; **ol**, olivine; **opx**, orthopyroxene; **plg**, plagioclase; **qz**, quartz; **sil**, sillimanite.

(2009) proposed a model in which a series of blocks represent crustal sections that (except for the Sermilik block; Fig. 1) display a systematic metamorphic progression from amphibolite facies to granulite facies rocks from south to north. Each block represents a number of island and continental arcs that were amalgamated by collision into the growing North Atlantic craton. In their model, the project area consists of the Sermilik, Bjørnesund and Kvanefjord blocks, where each block represents a combination of lateral and vertical crustal growth. However, contrary to the terrane model, two blocks can have a common origin.

Quartzo-feldspathic rocks

Grey tonalite-trondhjemite-granodiorite-type gneisses (TTG) have intrusive ages of 2.92–2.84 Ga that represent the main crust-generating period (Schiøtte *et al.* 1989; Næraa & Scherstén 2008). There is growing evidence from zircon U-Pb-Hf geochronology for an older previously unrecognised Mesoarchaean crustal component within the Tasiusarsuaq terrane (Næraa & Scherstén, unpublished data). The extent of the older component is currently unclear, but it is apparently most widespread in the northern part of the terrane. In addition, a number of strongly deformed and veined tonalitic gneisses of presumed early Neoarchaean age are younger, about 2.72 Ga, and formed from older pre-existing crust.

Granite (*sensu lato*) intrusions are variably deformed but post-date the majority of the grey gneisses. The main granite, the Ilivertalik augen granite, has feldspar megacrysts, and is in some places orthopyroxene-bearing and has been dated to 2.8 Ga (Pidgeon & Kalsbeek 1976; Næraa & Scherstén, unpublished data). The main volume of this granite intrudes the Sermilik block, but satellite intrusions, including the type locality at Ilivertalik mountain, are found in the Bjørnesund block, implying that these blocks were a single crustal unit by 2.8 Ga. At Ilivertalik mountain, Kalsbeek & Myers (1973) suggested that the intrusion was charnockitic and was emplaced under granulite-facies conditions.

Mica schists, commonly with garnet or sillimanite, occur throughout the area. These were originally mapped as having sedimentary protoliths. To our knowledge, all recognised structures in these rocks are tectono-metamorphic, and their supracrustal origin seems to have been mostly inferred from their common relationship with amphibolites or their aluminium-rich or quartzitic compositions.

Amphibolites and metagabbro-anorthosites

Supracrustal rocks with a range of compositions occur throughout the area, but are dominated by amphibolites. Preservation varies, with readily identified primary textures in

some areas and amphibolite lenses in others. The Ikkattup Nunaa belt on the islands in the Ikkattoq fjord just north of Frederikshåb Isblink (Fig. 1) is one of the best-preserved volcanic belts in the region (Andersen & Friend's 1973 Ravns Storø belt). Pillow lavas and volcanic bombs are well preserved here, and these rocks likely formed in shallow water with partly explosive volcanism. Rocks with calc-alkaline basaltic to andesitic compositions predominate (K. Szilas *et al.*, unpublished data 2009), and analytical results suggest a convergent margin setting with an age of 2.91 ± 0.01 Ga (Nutman *et al.* 2004). In 2008 we discovered that some major amphibolite belts at Majoqqap Qaava (Fig. 1) contain two components, namely lithic tuff-dominated, metavolcanic rocks and massive homogeneous amphibolite sheets, which are similar to the two main components of the Ikkattup Nunaa belt, thus a common arc origin is likely.

The Fiskenæsset complex is a layered igneous complex containing ultramafic rocks, gabbros, leucogabbros, anorthosites and chromitites, which formed largely by cumulate processes (Myers 1985). In 2008, we established that the lower main ultramafic unit, best exposed at Majoqqap Qaava, consists of a succession of layered dunites intruded by a major sill complex that comprises more than 25 clinopyroxene-hornblende sills, some of which are up to 10 m thick. The sills contain xenoliths of dunite, send apophyses into adjacent dunites and have discordant contacts against layered dunites. This observation means that the early history of the Fiskenæsset complex involved intrusion of a second, hydrous magma batch into earlier crystallised, olivine-rich cumulates.

Meta-gabbros and meta-anorthosites of the Fiskenæsset complex are closely associated with amphibolites of supracrustal origin, and they could be part of the same magmatic system. Escher & Myers (1975) believed that the Fiskenæsset complex was intrusive into the amphibolites. However, the observed contacts are tectonic, and direct evidence for primary intrusive relationships is lacking. Clearly, discordant anorthosite dykes cross-cut strongly deformed metagabbros within the complex (e.g. at 63.1156°N, 50.7155°W). These dykes consist of plagioclase and orthopyroxene and likely post-date all deformation.

Fig. 3. Spinel-bearing plagioclase lherzolite showing the breakdown of olivine and plagioclase to form coronas of clinopyroxene and orthopyroxene. The stability limits of the plagioclase lherzolite are below *c.* 9 kbar and 1200ºC, and the reaction would have occurred between about 700°C, 4 kbar and 870ºC, 7 kbar. Location at 63.932ºN, 51.219ºW.

Tectono-metamorphic development

The Qarliit Nunaat thrust forms the boundary between the Tre Brødre and Tasiusarsuaq terranes (Fig. 1; Friend *et al.* 1996). South of Buksefjorden there is a very high-strain, high-grade shear zone several kilometres wide between the Færingehavn and the Tasiusarsuaq terranes (Stainforth 1977; Crowley 2002). However, on either side of this shear zone, the tectono-metamorphic styles are different; to the north of Buksefjorden we found no evidence for a metamorphic or structural discontinuity. Here, rocks previously considered to be part of the Tre Brødre terrane might therefore be part of the Tasiusarsuaq terrane.

An abrupt change in metamorphic grade, from amphibolite facies just south of Grædefjord to granulite facies a little farther south, within the Tasiusarsuaq terrane, is associated with intensive shearing as predicted in the crustal block model of Windley & Garde (2009). Confirmation of the model comes from the fact that in 2008 we discovered that the boundary is occupied by a north-dipping, over 250-m-wide shear zone with a down-dip lineation, which contains augen gneisses, cataclasites and mylonites. The boundary separates amphibolite facies gneiss with granulite facies relicts to the south from prograde amphibolite facies gneisses to the north, as also predicted by Kalsbeek (1976).

Pressure–temperature (*P–T*) estimates are sparse in the present field area and focused on pyroxene-garnet assemblages (amphibolites) that are restricted to upper amphibolite and granulite facies. Figure 2 shows the locations of estimated geotherms for a 40 km thick crust. The geotherms that bracket the (3.0–2.7 Ga) metamorphism suggest pressures of 5–6 kbar for the conditions of the amphibolite facies to granulite facies transition. These *P–T-t* (*t* = time) conditions are consistent with field observations, e.g. the only aluminosilicate phase found in 2008 was sillimanite, and the observed peak assemblages are consistent with conditions near the amphibolite facies and granulite facies transition at intermediate pressure.

Granulite-facies rocks occur more rarely than suggested on the current 1:100 000 scale maps, although, in the area around the Fiskenæsset complex granulite-facies rocks are

abundant. Some of the area designated as granulite facies contains amphibolite-facies assemblages, but is interpreted to have once attained granulite-facies conditions. However, part of the rocks previously considered retrograde from granulite-facies rocks might better be interpreted as prograde amphibolite-facies rocks that never reached granulite-facies conditions. Full analysis of the *P–T–t* trajectories will require detailed textural and chemical analysis of these rocks.

Garnet-bearing mica schists and amphibolites from Ameralik fjord and Frederikshåb Isblink suggest garnet growth at the expense of plagioclase, which is consistent with a metamorphic event dominated by pressure increase. These observations are best explained by thrust tectonics. Evidence for isobaric or near-isobaric cooling was observed in reaction textures of the plagioclase lherzolite from north of Buksefjorden described in Fig. 3. The lherzolite occurs as a boudin within a refolded zone of amphibolite and ultramafic rocks in grey gneiss. Ultramafic boudins are associated with pegmatite dykes, and this resulted in alteration of the ultramafic rocks. Similar corona textures were noted at Majoqqap Qaava and were interpreted as late igneous or early metamorphic reactions by Myers & Platt (1977).

Cataclastic structures are abundant in the area between Ameralik and Frederikshåb Isblink (e.g. Stainforth 1977). Brittle deformation occurs as an overprint of earlier ductile structures. Pseudotachylytes were observed at a few localities, although cohesive fault rocks (cataclasites) are more common.

References

Andersen, L.S. & Friend, C. 1973: Structure of the Ravns Storø amphibolite belt in the Fiskenæsset region. Rapport Grønlands Geologiske Undersøgelse **51**, 37–40.

Crowley, J.L. 2002: Testing the model of late Archaean terrane accretion in southern West Greenland: a comparison of timing of geological events across the Qarliit nunaat fault, Buksefjorden region. Precambrian Research **116,** 57–79.

Ellitsgaard-Rasmussen, K. & Mouritzen, M. 1954: An anorthosite occurrence from West Greenland. Meddelelser fra Dansk Geologisk Forening **12**, 436–442.

Escher, J.C. & Myers, J.S. 1975: New evidence concerning the original relationships of early Precambrian volcanics and anorthosites in the Fiskenæsset region, southern West Greenland. Rapport Grønlands Geologiske Undersøgelse **75**, 72–76.

Friend, C.R.L., Nutman, A.P., Baadsgaard, H., Kinny, P.D. & McGregor, V.R. 1996: Timing of late Archaean terrane assembly, crustal thickening and granite emplacement in the Nuuk region, southern West Greenland. Earth and Planetary Science Letters **142**, 353–365.

Griffin, W.L., McGregor, V.R., Nutman, A.P., Taylor, P. N. & Bridgwater, D. 1980: Early Archaean granulite-facies metamorphism south of Ameralik, West Greenland. Earth and Planetary Science Letters **50**, 59– 74.

Kalsbeek, F. 1976: Metamorphism in the Fiskenæsset region. Rapport Grønlands Geologiske Undersøgelse **73**, 34–41.

Kalsbeek, F & Myers, J.S. 1973: The geology of the Fiskenæsset region. Rapport Grønlands Geologiske Undersøgelse **51**, 5–18.

Kamber, B.S., Whitehouse, M.J., Bolhar, R. & Moorbath, S. 2005: Volcanic resurfacing and the early terrestrial crust: Zircon U–Pb and REE constraints from the Isua Greenstone Belt, southern West Greenland. Earth and Planetary Science Letters **240**, 276–290.

Myers, J.S. 1985: Stratigraphy and structure of the Fiskenæsset complex, southern West Greenland. Bulletin Grønlands Geologiske Undersøgelse **150**, 72 pp.

Myers, J.S. & Platt, R.G., 1977: Mineral chemistry of layered Archaean anorthosite at Majorqap qâva, near Fiskenæsset, southwest Greenland. Lithos **11**, 59–72.

Næraa, T. & Scherstén, A. 2008: New zircon ages from the Tasiusarsuaq terrane, southern West Greenland. Geological Survey of Denmark and Greenland Bulletin **15**, 73-76.

Nutman, A.P., Friend, C.R.L., Barker, S.L.L. & McGregor, V.R. 2004: Inventory and assessment of Palaeoarchaean gneiss terrains and detrital zircons in southern West Greenland. Precambrian Research **135**, 281–314.

Pidgeon, R.T. & Kalsbeek, F. 1978: Dating of igneous and metamorphic events in the Fiskenaesset region of southern west Greenland. Canadian Journal of Earth Sciences **15**, 2021–2025.

Riciputi, L.R., Valley, J.W. & McGregor, V.R. 1990: Conditions of Archean granulite metamorphism in the Godthab-Fiskenaesset region, southern West Greenland. Journal of Metamorphic Geology **8**, 171–190.

Schiøtte, L., Compston, W. & Bridgwater, D. 1989: U-Pb single-zircon age for the Tinissaq gneiss of southern West Greenland: a controversy resolved. Chemical Geology **79**, 21–30.

Stainforth, J.G. 1977: The structural geology of the area between Ameralik and Buksefjorden, southern West Greenland, 480 pp. Unpublished Ph.D. thesis, Exeter University, UK.

Wells, P.R.A. 1979: Chemical and thermal evolution of Archaean sialic crust, southern West Greenland. Journal of Petrology **20**, 187–226.

Windley, B.F. & Garde, A.A. 2009: Arc-generated blocks with crustal sections in the North Atlantic craton of West Greenland: Crustal growth in the Archean with modern analogues. Earth-Science Reviews **93**, 1–30.

Windley, B.F. & Smith, J.V. 1974: The Fiskenæsset complex, West Greenland, Part II. General mineral chemistry from Qeqertarssuatsiaq. Bulletin Grønlands Geologiske Undersøgelse **108**, 54 pp.

Windley, B.F., Herd, R.K. & Bowden, A.A. 1973: The Fiskenæsset complex, West Greenland, Part I. A preliminary study of the stratigraphy, petrology, and whole rock chemistry from Qeqertarssuatsiaq. Bulletin Grønlands Geologiske Undersøgelse **106**, 80 pp.

Authors' addresses

N.K., A.S.[1] & T.N., *Geological Survey of Denmark and Greenland, Øster Voldgade 10, DK-1350 Copenhagen K, Denmark.* E-mail*: ntk@geus.dk*

J.C.S., *Department of Earth Sciences, University of Bristol, Bristol BS8 1RJ, UK.*

B.F.W., *Department of Geology, University of Leicester, Leicester LE1 7RH, UK.*

[1]Present address: *Department of Geology, Lund University , Sölvegatan 12, S-223 62 Lund, Sweden.*

Shallow core drilling and petroleum geology related field work in East and North-East Greenland 2008

Jørgen A. Bojesen-Koefoed, Morten Bjerager and Stefan Piasecki

In recent years, both the petroleum industry and government research institutions have shown renewed interest in the petroleum potential of the High Arctic. At the same time, a range of activities are taking place, aimed at defining national borders in the Arctic Ocean following ratification of article 76 of the United Nations Convention on the Law of the Sea (UNCLOS). Parallel to the general upsurge in data acquisition activities, the United States Geological Survey has carried out a Circum-Arctic Resource Appraisal (CARA), which for North-East Greenland was published in 2007. This assessment indicated that a significant petroleum exploration potential exists on the North-East Greenland shelf, in particular in the Danmarkshavn Basin and the North Danmarkshavn Salt Province (Fig. 1). The estimated potential amounts to 31 billion barrels of oil equivalents, principally in the form of natural gas. For comparison, this roughly corresponds to one third of the original reserve of the North Sea basins. The geology of the Danmarkshavn Basin and offshore areas farther to the north is only known in broad outline, since no wells have been drilled and only reconnaissance geophysical data are available. Moreover, the extensive ice cover and the overall hostile climate of the region pose significant logistical and technical challenges to data acquisition. Clearly, this emphasises the importance of analogue studies based on the much better known geology of the onshore basins in East and North-East Greenland. In 2007/2008, the Geological Survey of Denmark and Greenland (GEUS) launched a major petroleum industry-sponsored project with the objective of updating and expanding our current understanding of the petroleum geology of East and North-East Greenland. The project is planned to continue for the next four to five years, and includes compilation of relevant existing data in the form of a geographic information system (GIS) product, supplemented by new data obtained from shallow core drilling and new field work. Below we give a brief overview of a range of field activities that took place in East and North-East Greenland in the summer of 2008.

Shallow core drilling in Jameson Land

The objective of the drilling was to recover core material from the Upper Jurassic organic-rich shale of the Katedralen Member (Hareelv Formation) to obtain a reference section of

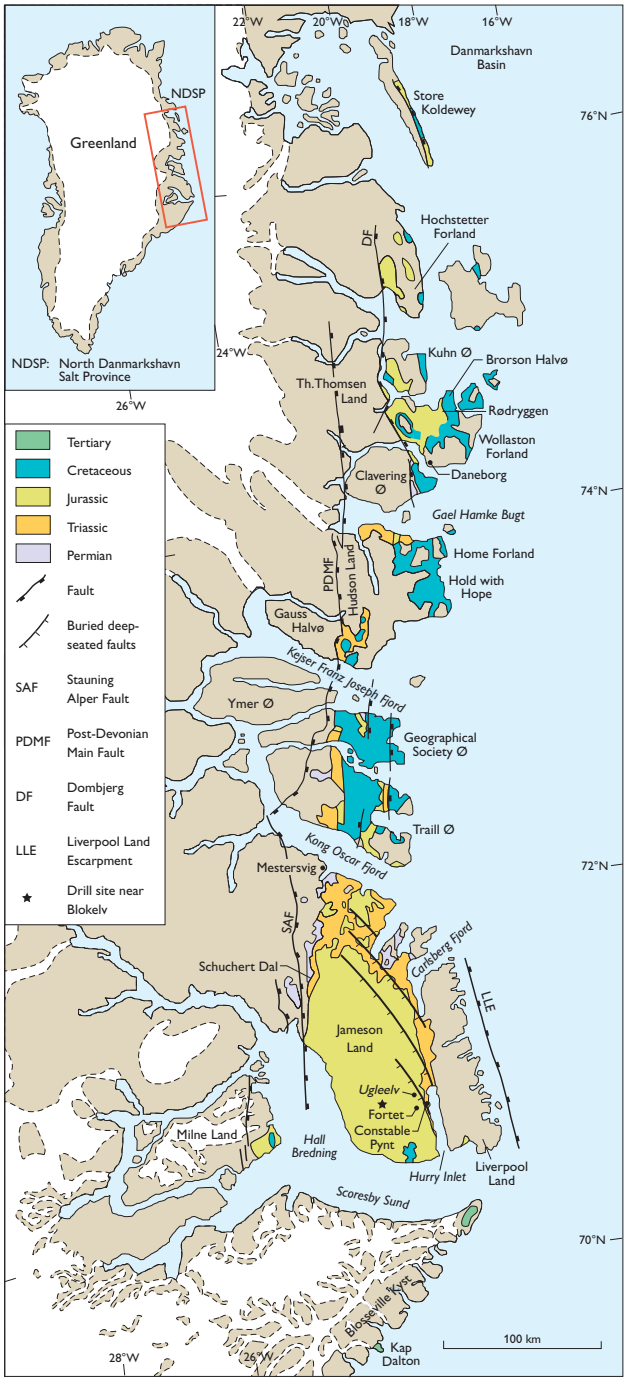

Fig. 1. Map of East and North-East Greenland, showing the distribution of Permian to Neogene sedimentary rocks and the location of place names mentioned in the text. **NDSP**: North Danmarkshavn Salt Basin.

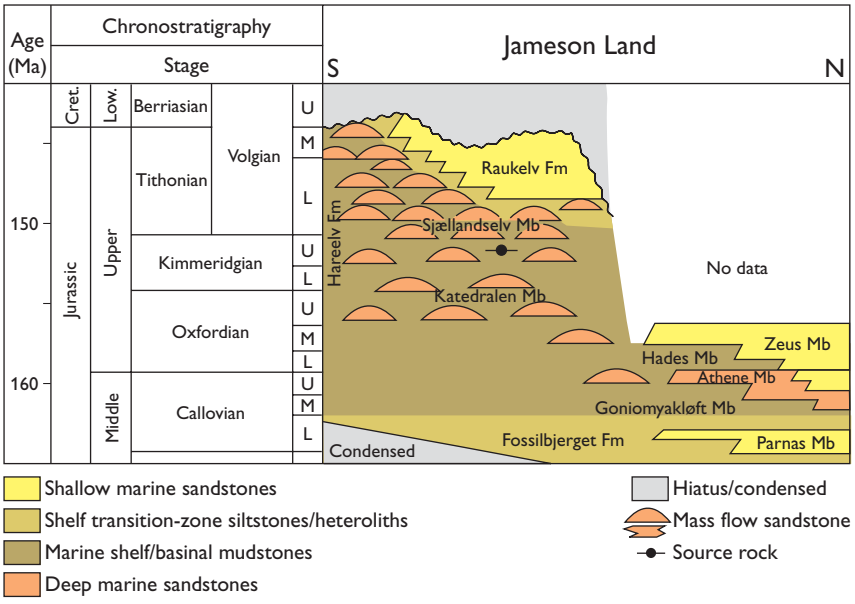

Fig. 2. Chrono- and lithostratigraphy of the Middle and Upper Jurassic in Jameson Land. Modified from Surlyk (2003).

the most prolific source rock in the north Atlantic region (Fig. 2). The deepest and most central part of the Jameson Land Basin at Blokelv approximately 35 km west of Constable Pynt was chosen as the drill site (Fig. 1).

The Blokelv drilling (Fig. 3) produced high quality cores (GGU 511101) with a diameter of 5.6 cm and 99.3% recovery to a depth of 233.8 m (Fig. 4). The top part from 1.72 to 10.08 m recovered homogeneous medium to fine-grained sandstone with two thin shale intervals of the Sjællandselv Member (Hareelv Formation). The Katedralen Member (Hareelv Formation) from 10.08 to 233.8 m consists of alternating sandstone and shale units; the lower boundary of the member was not reached.

Studies of the new cores from the Katedralen Member focus on the stratigraphy and age of the Hareelv Formation and lateral, contemporaneous deposits (Fig. 2). The lower boundary of the Katedralen Member is well known from the Ugleelv region and the west side of Hurry Inlet, where few, condensed beds of mudstone and fine-grained sandstone separate the Fossilbjerget and Hareelv Formations. These beds are age equivalent to the Olympen Formation in central to northern Jameson Land (*P. athleta* to *C. densiplicatum* Chronozones of Late Callovian to Middle Oxfordian age; Larsen & Surlyk 2003).

The deposition of laminated mudstone of the Katedralen Member began in the Late Oxfordian. The continued sedimentation of the Katedralen Member mud reaches into the Kimmeridgian and Volgian especially in eastern and southern Jameson Land (Fig. 2). During the Volgian, the coarse-grained sand of the Sjællandselv Member and Raukelv Formation was deposited in the western and central parts of the Jameson Land Basin at the same time as the Katedralen Member mud was deposited in the easternmost, apparently much deeper basin (Surlyk 2003). The youngest parts of the Katedralen Member are only known from the locality Fortet near Constable Pynt in eastern Jameson Land, where the dinoflagellate assemblage indicates an age not older than latest Middle Volgian (Fig. 2).

The upper boundary of the Katedralen Member is located where laminated mudstone is replaced by homogeneous sandstone of the Sjællandselv Member. The sand slumped into the central basin from shelf-edge deltas prograding from north-west and west. This shift in deposition can be followed from west to east across the basin in a number of shallow core drillings and exposed

Fig 3. Drilling operations near Blokelv in Jameson Land. Three-metre-long cores are drilled at a time, and each time a core is retrieved water is pouring out of the drill hole.

sections. The boundary is strongly diachronous: Kimmeridgian–Volgian in the west to Middle – Upper Volgian in the easternmost part of the basin.

An extensive analytical programme to evaluate source and reservoir rock properties to establish a high-resolution dinoflagellate cyst and macrofossil biostratigraphic zonation, and assess sedimentological, diagenetic and sequence stratigraphic aspects of the penetrated succession is in progress.

Field work

Field work took place by means of helicopter-supported field teams of 2–4 persons, operating primarily out of field camps. The activities covered a wide range of geological disciplines that are briefly described below. Field teams camped at or visited locations from Kap Dalton on the Blosseville Kyst in the south to Kuhn Ø in the north (Fig. 1).

Volcanology

Volcanic rocks in the form of plateau basalts as well as various intrusions abound in East and North-East Greenland, and their histories of emplacement and mutual relationships are important elements in the understanding of the regional geology. A field team sampled and studied the youngest volcanic rocks in the region that are preserved in a small graben at Kap Dalton. Additional studies were undertaken on Hold with Hope and Wollaston Forland and on nearby islands east and north thereof. Samples collected from various outcrops will be subjected to chemical and petrological analyses as well as radiometric dating in order to establish their ages and mutual relationships.

Petroleum source rocks and Cretaceous–Palaeogene stratigraphy

Petroleum source rocks are known to be present in East and North-East Greenland in a number of stratigraphic intervals ranging in age from Middle Devonian to Upper Jurassic, whereas source rocks in younger units still remain to be demonstrated. Among these various units the Upper Jurassic 'Kimmeridge Clay equivalents' referred to as the Hareelv, Kap Leslie and Bernbjerg Formations (Surlyk 2003) must be considered the more important ones with respect to petroleum exploration. The documentation of spatial and temporal variations in petroleum potential within these units is crucial to the prediction of the distribution of the potential in the little-known offshore basins. Upper Jurassic shale of the Bernbjerg Formation was sampled on Hold with Hope and Wollaston Forland, and potential drill sites were found at Rødryggen and Brorson Halvø on Wollaston Forland. In addition, Cretaceous shale was sampled for both stratigraphic and geochemical purposes on Wollaston Forland, whereas sampling of Cretaceous deposits and drill-site identification on Hold with Hope had to be postponed due to the presence of polar bears in the area.

The stratigraphy and sedimentological development of the Cretaceous–Palaeogene succession of North-East Greenland have hitherto received relatively little attention, probably due to a general assumption that it was deposited during a period of tectonic quiescence with little change in overall basin configuration. During the field season in 2008, some effort was devoted to increasing our knowledge of the Cretaceous–Palaeogene development through sedimentological studies and stratigraphic sampling. Among the results was the discovery of a more than 150 m thick, unmapped succession of presumably Palaeogene sand with minor mud-

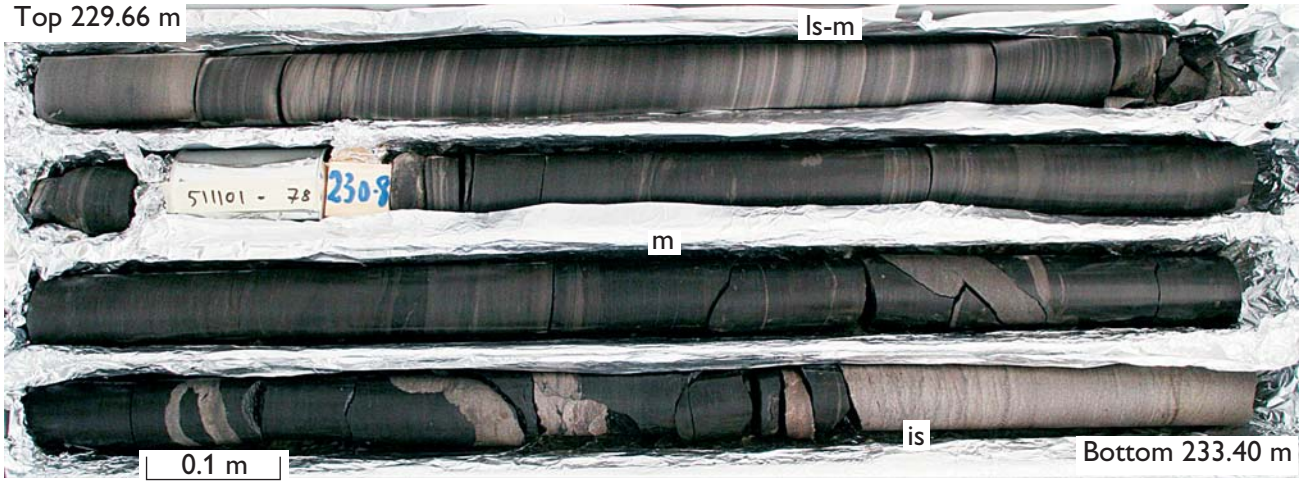

Fig. 4. Core box no. 62 with black organic rich mudstone (**m**), intrusive sandstone dykes (**is**), and laminated heterolithic sandstone-mudstone (**ls-m**) of the Katedralen Member, Hareelv Formation. The diameter of the core is 56 mm.

stones and coal directly underlying the plateau basalts on eastern Wollaston Forland. Sub-basaltic Palaeogene sand is reported from several localities in the region.

Landscape analysis, uplift and sand provenance studies

Burial and uplift are geological processes, the magnitude and timing of which are of utmost importance in petroleum geology. Assessment of these may be undertaken by a combination of methods, including large-scale landform analysis and apatite fission track analysis, which enable us to detect ancient erosion or peneplanisation surfaces as well as quantify palaeogeothermal gradients (Bonow *et al.* 2007). Moreover, identification of the source areas for sandy deposits through geological time is important to understand temporal dispersal patterns of sediment within the basin, and for correlation of sand units. Such provenance studies can be carried out by age determinations and detailed chemical analyses of provenance-sensitive minerals such as zircon and garnet. Since uplift and provenance studies to a large extent make use of the same type of sample material, two field teams collected samples for both purposes. Spot and profile samples were collected at a large number of locations from Milne Land and Jameson Land in the south to Wollaston Forland in the north.

Seepage studies

Experience from central West Greenland shows that when certain requirements are met petroleum seepages may be preserved in the lower parts of the Palaeogene basalt succession and in carbonate veins associated with dykes (Bojesen-Koefoed *et al.* 1999). The utility of the experience gained in West Greenland was tested in North-East Greenland, but with little success, since essentially no traces of petroleum were found in the volcanic rocks exposed in the region. A number of locations on Kuhn Ø and Wollaston Forland were checked, but no hydrocarbons were found. The lavas are indeed very porous, but the level of thermal alteration indicated by the zeolite facies is too low, the volcanic rocks are too thin and healed carbonate-filled veins are nearly absent. Similar studies of the volcanic rocks on Hold with Hope were severely hampered by bad weather and polar bears, but since the geological conditions appear more favourable there and seepages have been recorded previously, further attempts should be made during future field work.

Airborne stereo-photography

Systematic stereo-photography is a valuable tool for large-scale stratigraphy and structural geology (Dueholm & Pedersen 1992). Nearly 2000 stereo-photographs were taken from a Partenavia aircraft during two sessions in (1) Jameson Land, Milne Land, Schuchert Dal, Kong Oscar Fjord, southern Traill Ø region and (2) Kejser Franz Joseph Fjord, Gauss Halvø, Hudson Land, Gael Hamke Bugt, Home Forland and the south-eastern Hold with Hope region.

Future activities in North-East Greenland

The project described here is planned to continue for the next 4–5 years, with both field work and shallow core drilling starting in the south and gradually moving northwards. In addition, an excursion to the region for sponsoring oil companies is planned for 2010. In 2008, the Bureau of Minerals and Petroleum, Greenland, published a 'roadmap' for a future licensing round in North-East Greenland which, pending political approval, will lead to nomination and licensing rounds in 2011–2013. In order to meet the needs of the sponsors, further special studies may be undertaken in the forthcoming years.

Acknowledgements

The staff at the Sirius Sledge Patrol stations at Daneborg and Mestersvig and the staff at Constable Pynt airport are thanked for their practical assistance and hospitality.

References

Bojesen-Koefoed, J.A., Christiansen, F.G., Nytoft, H.P. & Pedersen, A.K 1999: Oil seepage onshore West Greenland: evidence of multiple source rocks and oil mixing. In: Fleet, A.J. & Boldy, S.A.R. (eds): Petroleum Geology of Northwest Europe: proceedings of the 5th conference, 305–314. London: Geological Society.

Bonow, J.M., Japsen, P., Green, P.F., Wilson, R.W., Chalmers, J.A., Klint, K.E.S., van Gool, J.A.M., Lidmar-Bergström, L. & Pedersen, A.K. 2007: A multi-disciplinary study of Phanerozoic landscape development in West Greenland. Geological Survey of Denmark and Greenland Bulletin **13**, 33–36.

Dueholm, K.S. & Pedersen, A.K. (eds) 1992: Geological analysis and mapping using multi-model photogrammetry. Rapport Grønlands Geologiske Undersøgelse **156**, 72 pp.

Larsen, M. & Surlyk, F. 2003: Shelf-edge delta and slope deposition in the Upper Callovian – Middle Oxfordian Olympen Formation, East Greenland. In: Ineson, J.R. & Surlyk, F. (eds): The Jurassic of Denmark and Greenland. Geological Survey of Denmark and Greenland Bulletin **1**, 931–948.

Surlyk, F. 2003: The Jurassic of East Greenland: a sedimentary record of thermal subsidence, onset and culmination of rifting. In: Ineson, J.R. & Surlyk, F. (eds): The Jurassic of Denmark and Greenland. Geological Survey of Denmark and Greenland Bulletin **1**, 659–722.

Authors' address

Geological survey of Denmark and Greenland, Øster Voldgade 10, DK-1350 Copenhagen K, Denmark. E-mail: *jbk@geus.dk*

The bedrock geology under the Inland Ice: the next major challenge for Greenland mapping

Peter R. Dawes

Geological maps are of vital importance for documenting and advancing geological knowledge and they are a prerequisite for any meaningful evaluation of economic resources. In Greenland, mapping is taking place on the mainland – that for two centuries has been the traditional exploration target – and offshore, where only in the last decades has hydrocarbon exploration moved to the continental shelves.

Greenland with its 2 166 000 km^2 is the largest island in the world. However, the land is overwhelmed by ice. A central ice sheet – the Inland Ice – blankets some 81% of the country reducing rock outcrop to a coastal fringe 0 to 300 km wide (Fig. 1). The continental shelves comprise a little more than twice the area of this fringe, *c*. 830 000 km^2.

This preamble serves to emphasise that Greenland's three physiographic units – exposed fringe, offshore and Inland Ice – are of very different size and that mapping has focused on the smallest acreage. Piecing together the composition of the largest, and hitherto unexplored, unit constitutes the next chapter of Greenland mapping.

Historical perspective and aim of this paper

In the last 25 years, great strides have been made in geological understanding as can be seen from two 1:2 500 000 maps (Escher 1970; Escher & Pulvertaft 1995). Apart from the progress recorded in the ice-free fringe, the 1995 map provides a first interpretation of the offshore, and it also includes information of sub-ice bedrock although this is but a single blob of colour at borehole GISP 2 (Fig. 1).

This paper's aim is to provide a first graphic interpretation of the bedrock under the Inland Ice and to review data sources. Its four-page limit does not allow citation of specific sources; these will be covered in a forthcoming paper. This state-of-the-art map is naturally rudimentary in approach with all boundaries arbitrary but it has the prospect of directing attention to future data assembly.

The state of knowledge 2008

Present knowledge of sub-ice geology is based on six main sources, each discussed below with emphasis on its use in compilation of the geological map shown in Fig. 1.

Drill sites

Drilling through the ice is the ultimate way of determining substratum composition. However, the only in *situ rock* sampled is from borehole GISP 2 – an Archaean granitoid rock reactivated during the Palaeoproterozoic (Fig. 1). Other ice cores have revealed information about rock debris, for example, Camp Century (Fountain *et al*. 1981).

Nunataks

Nunataks are restricted to the Inland Ice margin within *c*. 30 km of the nearest land. Most expose locally known rocks and are important for piecing together structural make-up. Of importance for the new map is the 120 km long N–S string of nunataks west of Dronning Louise Land, North-East Greenland. They infer larger sub-ice occurrences of Mesoproterozoic sediments than exist on the neighbouring land.

Coast to coast correlation

Greenland's tapering form enables Precambrian rocks to be correlated across its southern tip and, by extrapolation farther north, under the ice. The presence on both coasts of Archaean rocks flanked north and south by Palaeoproterozoic orogenic belts allows the sub-ice projection of the North Atlantic craton although its southern and northern boundaries are hidden for 250 km and 500 km, respectively. This correlation is strengthened by aeromagnetic data (Fig. 2).

The disappearance of Palaeogene extrusives on both sides of the Inland Ice might suggest a single province. However, both coasts are eruption sites connected to continental breakup but since the role of plumes and hot-spots is still unclear, basalts cannot be excluded from central Greenland.

Glacial erratics

The Inland Ice is a relic of a vast Pleistocene ice cover and the surrounding land is strewn with rocks dropped as the ice retreated. Broadly speaking, erratic suites from southern Greenland represent extensively exposed Precambrian and late Phanerozoic provinces whereas farther north, exotic Precambrian–Palaeozoic suites relate to sub-ice occurrences that are unknown or not exposed locally. Moreover, even the

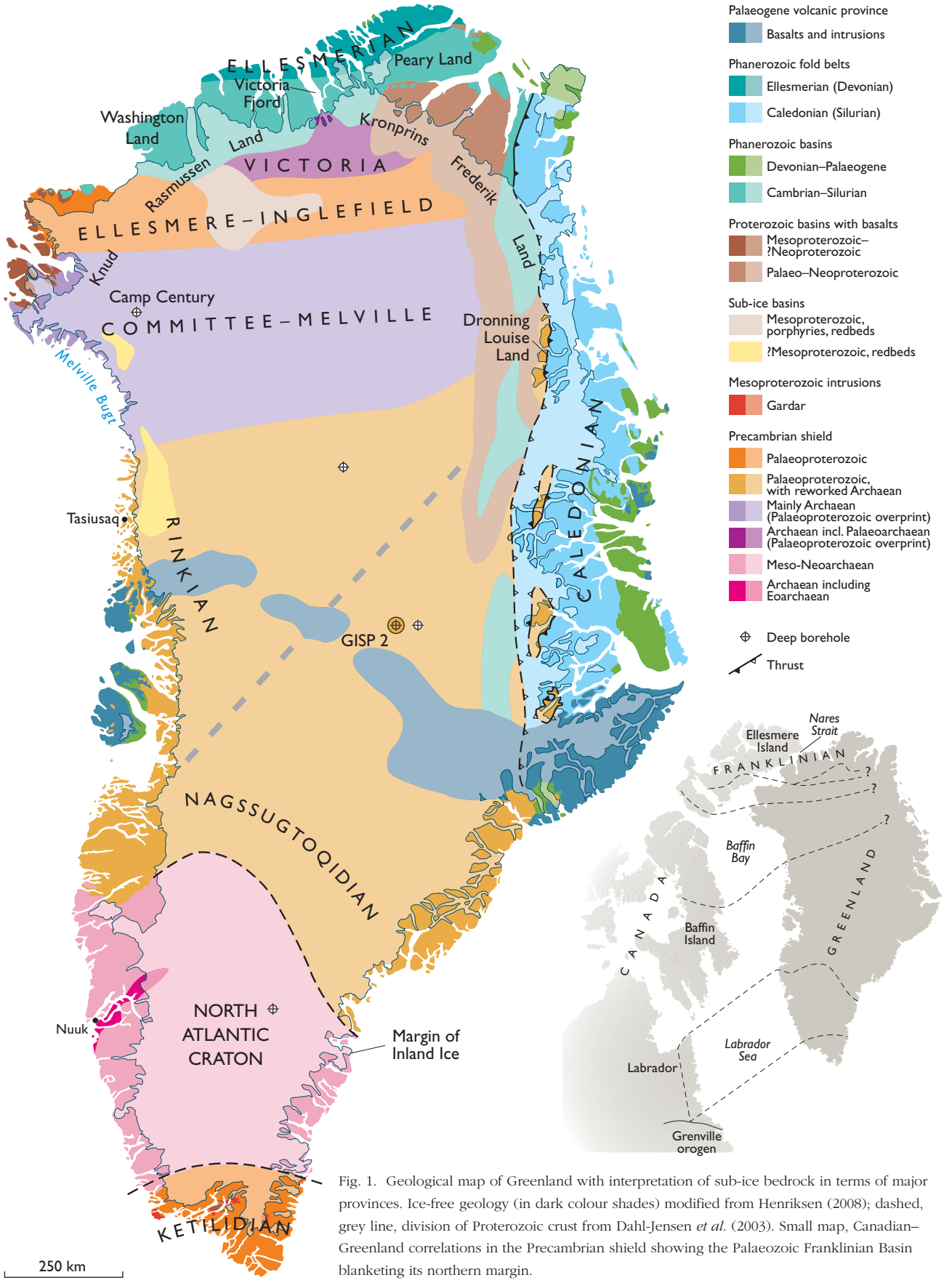

Fig. 1. Geological map of Greenland with interpretation of sub-ice bedrock in terms of major provinces. Ice-free geology (in dark colour shades) modified from Henriksen (2008); dashed, grey line, division of Proterozoic crust from Dahl-Jensen *et al.* (2003). Small map, Canadian–Greenland correlations in the Precambrian shield showing the Palaeozoic Franklinian Basin blanketing its northern margin.

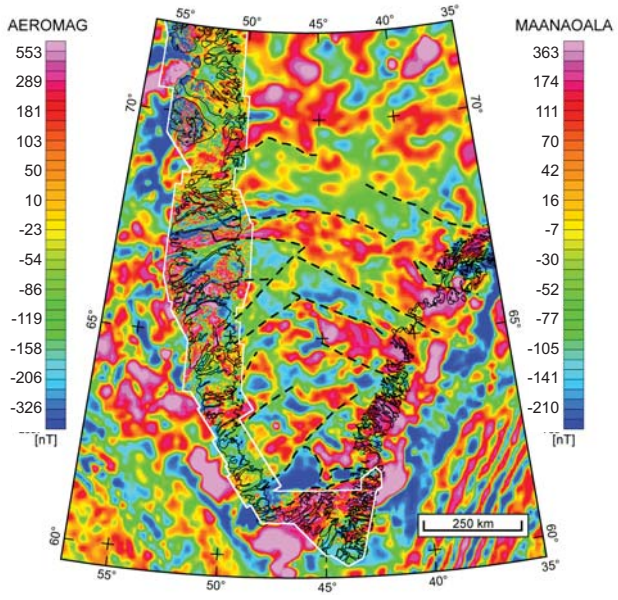

Fig. 2. Grids of total magnetic field over southern Greenland and offshore based on Verhoef *et al.* (1996, low resolution MAANAOALA data, Geological Survey of Canada) and white frame, high resolution AEROMAG data (Geological Survey of Denmark and Greenland). Stippled lines, geological trends by B.M. Stensgaard (personal communication 2009).

absence of particular erratics can be informative, for example, this author has no knowledge of erratics that might indicate a late Palaeozoic – Mesozoic sub-ice source.

Information from five erratic suites is incorporated into Fig. 1. Glacial drift across the Proterozoic–Phanerozoic platform of North Greenland is characterised by shield blocks – granitoid rocks, gneisses and associated rocks. Most of these need laboratory work to cast light on their age and use in reflecting hidden provinces (see 1 below) but some rocks are ready-made indicators (2, 3). Farther south, exotic suites occur on the shield terrain of the west and east coasts (4, 5).

1. The shield erratics isotopically dated are from Peary Land and environs and they suggest sub-ice Archaean crust affected by strong Palaeoproterozoic overprint.
2. Banded iron formation (BIF) characterises the Neoarchaean Committee–Melville orogen of Baffin Island and North-West Greenland. BIF erratics in North Greenland suggest an extension of this terrane far to the east.
3. Erratics of porphyries and basalt, with rare sandstone, in Washington Land indicate a sub-ice volcanic–redbed province (Fig. 3A). Preliminary isotopic work points to a Mesoproterozoic age.
4. Red sandstone and siltstone erratics around Tasiusaq and farther north in North-West Greenland point to extensive sub-ice sources (Fig. 3B).
5. Erratics along the East Greenland ice margin were emphasised by Haller (1971, fig. 48): Proterozoic sandstone and basalt, Cambrian quartzite with *Skolithos* and Ordovician limestone infer extensive sub-ice sources.

Detrital provenance studies

Age and palaeoflow history of detritus within sedimentary rocks – rock clasts and crystals – can be relevant for sub-ice geology. However, minerals like zircon can be transported thousands of kilometres before deposition and identifying sub-ice geology on grains alone is problematical. Thus, the clast–grain couplet of the tilloidal Neoproterozoic Morænesø Formation in southern Peary Land is relevant, particularly so with its south-westerly provenance (Kirkland *et al.* 2009).

Clasts are of local Mesoproterozoic sandstone and dolerite, with less frequent granitoid rocks, BIF and porphyry, suggesting proximal sub-ice sources of Neoarchaean and Mesoproterozoic ages. Age estimates of zircons from granitoid clasts are 2.7 Ga with overprinting at 1.25 Ga. *Zircon crystals* range from Palaeoarchaean to Mesoproterozoic with strong Palaeoproterozoic peaks suggesting large sub-ice areas. A minor 3.3 Ga peak is an obvious link to the substratum (Victoria Fjord complex) that contains the only known rocks of this age in Greenland (Nutman *et al.* 2008). Moreover, the subsidiary status of these grains compared to Neoarchaean also exists in sequential Mesoproterozoic and Cambrian strata implying that Palaeoarchaean rocks form but a minor component of the complex. Kirkland *et al.* (2009) favour two south-western sources for Mesoproterozic detritus: proximal sub-ice Grenville-overprinted rocks and the type Grenvillian of Labrador, more than 2000 km distant. A third source is suggested by Fig. 1: the sub-ice volcanic province that may also source the rare porphyry clasts.

Geophysics

Geophysical methods – satellite, airborne or ice based – undoubtedly have great potential for mapping the sub-ice geology. Preliminary interpretations about structure and

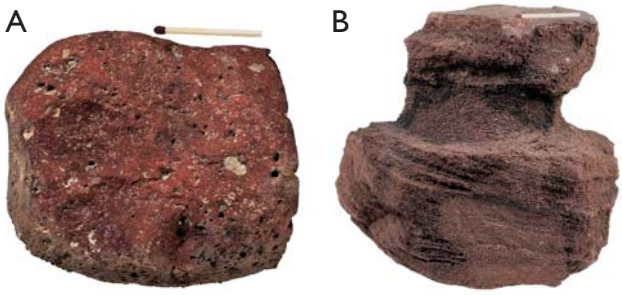

Fig. 3. Glacial erratics from sub-ice provinces unknown in outcrop. **A**: Feldspar porphyry from Washington Land, western North Greenland, GGU 425204. Other porphyry erratics are illustrated in Dawes *et al.* 2000, fig. 3. **B**: Coarse-grained, cross-bedded sandstone from Tasiusaq area, North-West Greenland, GGU 457508. Photos: Jakob Lautrup.

crustal thickness can be made from regional magnetic and gravity surveys. The power of aeromagnetics is illustrated by Verhoef *et al.'s* (1996) compilation of reconnaissance data that shows arcuate coast to coast anomalies coinciding with tectonic segments of the Nagssugtoqidian orogen, while mergence with high-resolution coastal data allows some structural subdivision of the shield (Fig. 2).

Radar and remote-sensing techniques provide physiographic details about the sub-ice landscape, for example, Legarsky *et al.'s* (1998) work used to locate the volcanic province in Knud Rasmussen Land (Fig. 1). Many tectonic provinces display distinct physiographical characteristics and thus 3-D imagery is vital for mapping sub-ice geology. Mountains, plains, plateaux and lowlands are not the only geological indicators, but hills and valleys affect ice dynamics and control water flow, two primary parameters for determining provenances of erratics and detrital material.

Conclusions, future research, ice recession and economic potential

A main conclusion must be that while mapping below the ice is in its infancy, the status of the GEUS databases has promising potential for planning research, whether sampling, drilling or geophysics. One dire need is for low-altitude and ice-based geophysical surveys to facilitate deductions about spatial relationships of sub-ice provinces. The new map leads to eight conclusions, but being conjectural, it raises important questions – too many to discuss in this short paper.

1. Provinces unknown in outcrop occur below the ice.
2. Where it is widest, in the north, the Inland Ice hides the most variable geology: Palaeoarchaean, Neoarchaean, Palaeoproterozoic, Mesoproterozoic and Palaeozoic provinces.
3. Archaean crust underlies Kronprins Frederik Land but its eastern connection is unknown.
4. Whether the Ellesmere–Inglefield juvenile crust links genetically and structurally (or at all) with Palaeoproterozoic rocks within the Caledonian fold belt remains open.
5. The volcanic province of Knud Rasmussen Land reinforces the profusion of Proterozoic rift-related magmatism along the rim of the North American craton.
6. Mesoproterozoic–Ordovician rocks are widespread beyond the Caledonian front linking northern foreland outcrops to sub-ice occurrences in central East Greenland.
7. The potential for sub-ice basins of late Palaeozoic – Mesozoic age is limited.
8. The presence of Palaeogene volcanic rocks in central Greenland cannot be dismissed.

Currently, Greenland plays centre stage in the global climate debate, its recessive ice margin with spectacular, shrinking glaciers being international attractions. With this coveted popularity come startling prophecies, for example, "as its huge ice sheets begin to melt, it [Greenland] could find itself sitting on a fortune in oil and gems" (Barkham 2008). Be this as it may, before the rocks of the hidden 81% have been mapped, assessments of economic potential – often judged poor compared with neighbouring Canada despite common geology (Fig. 1) – remains equivocal.

References

Barkham, P. 2008: Beyond the ice. The Guardian, 11 December 2008, electronic version. London: Guardian News & Media.

Dahl-Jensen, T., Larsen, T.B., Woelbern, I., Bach, T., Hanka, W., Kind, R., Gregersen, S., Mosegaard, K., Voss, P. & Gudmundsson, O. 2003: Depth to Moho in Greenland: receiver-function analysis suggests two Proterozoic blocks in Greenland. Earth and Planetary Science Letters **205**, 379–393.

Dawes, P.R., Thomassen, B. & Andersson, T.I. 2000: A new volcanic province: evidence from glacial erratics in western North Greenland. Geology of Greenland Survey Bulletin **186**, 35–41.

Escher, A. 1970: Geological/tectonic map of Greenland, 1:2 500 000. Copenhagen: Geological Survey of Greenland.

Escher, J.C. & Pulvertaft, T.C.R. 1995: Geological map of Greenland, 1:2 500 000. Copenhagen: Geological Survey of Greenland.

Fountain, J., Usselman, T.M., Wooden, J. & Langway, C.C. 1981: Evidence of the bedrock beneath the Greenland ice sheet, near Camp Century, Greenland. Journal of Glaciology **27**(95), 193–197.

Haller, J. 1971: Geology of the East Greenland Caledonides, 413 pp. New York: Interscience Publishers.

Henriksen, N. 2008: Geological history of Greenland, 272 pp. Copenhagen: Geological Survey of Denmark and Greenland.

Kirkland, C.L., Pease, V., Whitehouse, M.J. & Ineson, J.R. 2009: Provenance record from Mesoproterozoic–Cambrian sediments of Peary Land, North Greenland; implications for the ice-covered shield and Laurentian palaeogeography. Precambrian Research **170,** 43–60.

Legarsky, J., Wong, A., Akins, T. & Gogineni, S.P. 1998: Detection of hills from radar in central-northern Greenland. Journal of Glaciology **44**(146), 182–184.

Nutman, A.P., Dawes, P.R., Kalsbeek, F. & Hamilton, M.A. 2008: Palaeoproterozoic and Archaean gneiss complexes in northern Greenland: Palaeoproterozoic terrane assembly in the High Arctic. Precambrian Research **161**, 419–451.

Verhoef, J., Macnab, R., Roest, W.R. & Arjani-Hamed, J. 1996: Magnetic anomalies of the Arctic and North Atlantic oceans and adjacent land areas. Geological Survey of Canada, Open File Report **3125a**, 225 pp.

Author's address

Geological survey of Denmark and Greenland, Øster Voldgade 10, DK-1350 Copenhagen K, Denmark. E-mail: *prd@geus.dk*

Developing a 3-D model for the Skaergaard intrusion in East Greenland: constraints on structure, mineralisation and petrogenetic models

Troels F.D. Nielsen, Símun D. Olsen and Bo M. Stensgaard

The Skaergaard intrusion (Fig. 1) is probably the most studied layered gabbro intrusion in the world (Wager & Deer 1939; Wager & Brown 1968; McBirney 1996; Nielsen 2004). The intrusion is *c.* 54.5 Ma old and was formed during the Palaeogene opening of the North Atlantic Ocean, intruding into the base of the East Greenland flood basalts. The intrusion is relatively small with a volume of *c.* 300 km^3 (Nielsen 2004). Spectacular magmatic layering and systematic evolution in the compositions of liquidus phases and estimated melt compositions (e.g. Wager & Brown 1968) have made the intrusion the most studied example of the development of the 'Fenner trend' of iron enrichment in basaltic liquids (e.g. Thy *et al.* in press; Veksler in press).

The identification in the late 1980s of significant platinum-group elements (PGE) and gold (Au) occurrences in the intrusion (e.g. Bird *et al.* 1991; Nielsen *et al.* 2005) has led to continued investigation and exploration drilling. The Skaergaard intrusion is suggested to hold *c.* 33 million ounces (1000 tonnes) of PGE and *c.* 13 million ounces (400 tonnes) of Au (Nielsen *et al.* 2005). The mineralised zone is located in a *c.* 100 m thick zone of anomalous PGE and Au enrichment in the upper part of the Middle zone (Bird *et al.* 1991; Nielsen *et al.* 2005) of the Layered series. The mineralised zone consists of a succession of bowl-shaped, stratiform and very tightly controlled levels of palladium (Pd) enrichment referred to as Pd1 to Pd5 (Fig. 2; Nielsen *et al.* 2005). The bottom level, Pd5, is developed from margin to margin of the intrusion, whereas the overlying levels Pd4 to Pd1 are increasingly restricted in width, and the entire succession of Pd levels is only developed in the central part of the intrusion. The structure of the mineralised zone can be compared to a set of bowls with upward-decreasing diameters. Gold is always concentrated in the uppermost palladium levels or in a level above the top palladium level, irrespective of the number of developed Pd levels. More detailed descriptions are provided by Nielsen *et al.* (2005).

The exploration drill cores provide material and structural information from previously inaccessible parts of the intrusion (Nielsen *et al.* 2005). The 3-D image presented in Fig. 4 is based on drill-core information (petrographical, petrophysical, geochemical etc.) and surface information. It allows an unprecedented insight into the internal structure of the upper part of the intrusion and offers a possibility of refinement of volume estimates and quantitative modelling of the

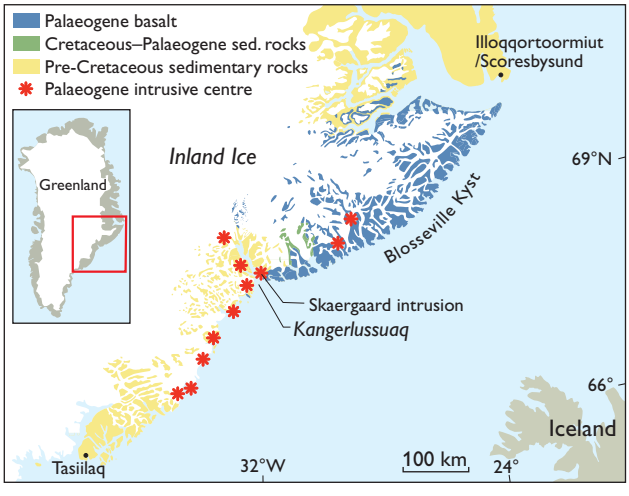

Fig. 1. The Skaergaard intrusion is located in the Kangerlussuaq region in the Palaeogene magmatic province in East Greenland.

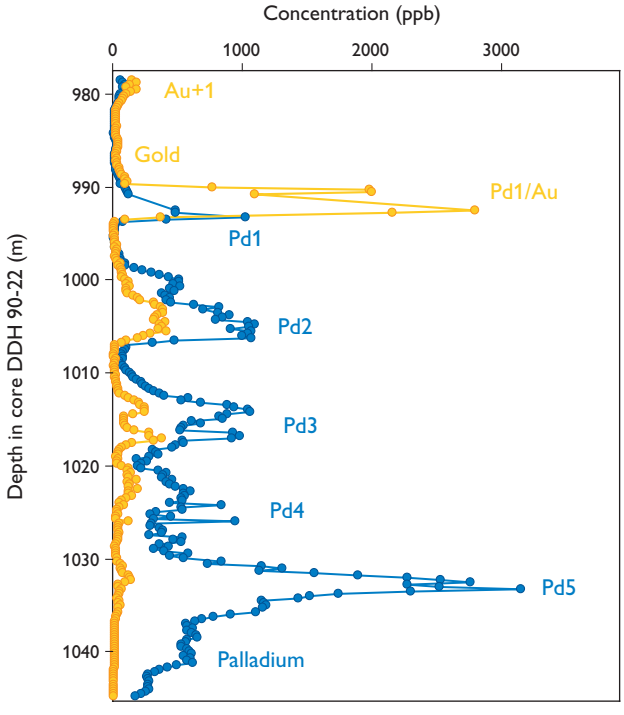

Fig. 2. Characteristic variation in whole-rock Pd concentration in the central parts of the Skaergaard mineralised zone (core DDH 90-22, from Bernstein & Nielsen 2004).

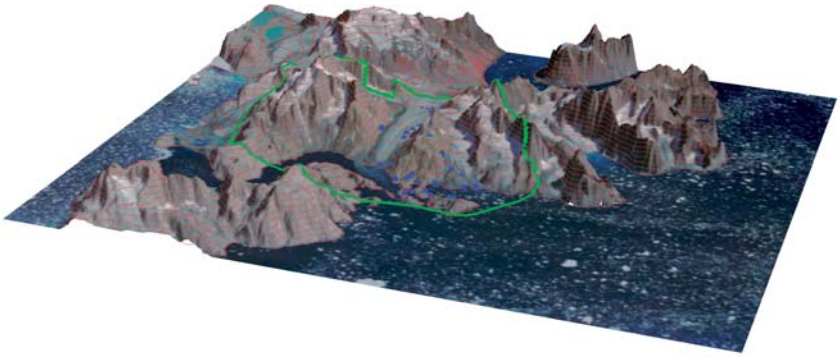

Fig. 3. ASTER satellite image with topography (1.5 × vertical exaggeration; see text for explanation). The green line shows the outer boundary of the Skaergaard intrusion, and the blue dots show the locations of the collars of drill holes.

zones and subzones of the intrusion. A constrained structural model will in turn allow evaluation and revision of crystallisation models for the basaltic liquid in the magma chamber.

3-D modelling of the intrusion and the mineralised zone

The initial aim of the 3-D modelling was a visualisation of the intrusion and the associated PGE and Au mineral occurrences. Geographical information system software was used for the compilation of the surface data used for the model. These data, together with subsurface data, were subsequently imported into modern 3-D mining and resource software (Gemcom GEMS®), which was used for the construction of the 3-D model of the intrusion and its mineralised zone.

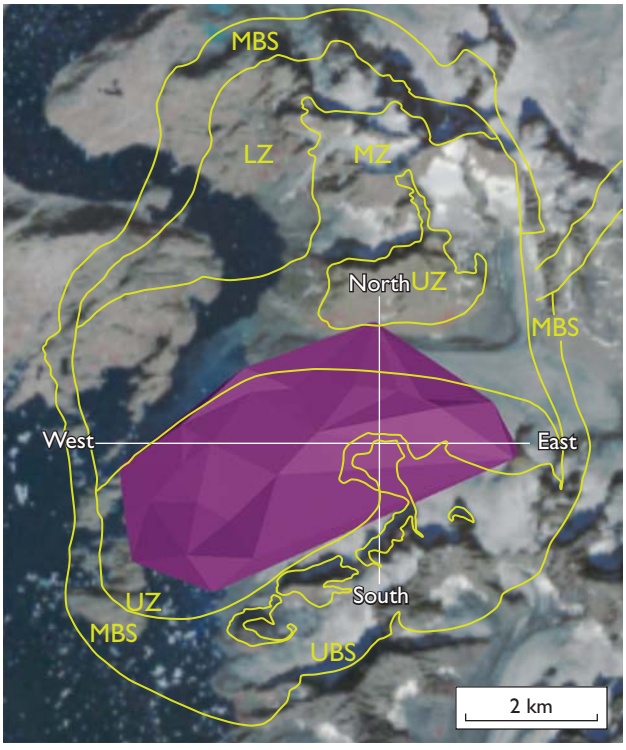

Fig. 4. Satellite image showing the area of the mineralised zone so far covered by the 3-D model (purple area) with the geological boundaries transferred from the geological map of the Skaergaard intrusion (McBirney 1989). **MBS**, Marginal Border Series (wall rocks); **UBS**, Upper Border Series (roof rocks); Layered series (LS; floor rocks) consisting of **LZ**, Lower Zone; **MZ**, Middle Zone; **UZ**, Upper Zone. Islands in UBS: the younger Basistoppen Sill. The two white lines show the location of the 2-D cross-sections (Fig. 5). Abbreviations also apply to Table 1 and Fig. 6.

The detailed topographical model needed for the modelling (Fig. 3) was constructed from satellite Aster data (resolution 30 × 30 m). Aster scenes and the 1:20 000 scale geological map of the intrusion and adjacent area were draped on the terrain model.

Forty-one cores with a total length of 23 425 m have been drilled since 1989. The deepest holes reached levels of *c.* 1200 m below the collars of the drill holes. The petrographic variation in all these cores is described in drill-hole logs in company reports in the archives of the Geological Survey of Denmark and Greenland. These logs were digitalised and compiled. The courses of the drill holes (taking azimuth and dip into account) were visualised in 3-D, and assays for PGE and Au displayed together with the petrographic information. All the information was subsequently assessed for each drill hole, and the delineation of specific lithologies and mineralised sections was interpolated manually by the geologist software operator from one drill hole to another and from drill holes to surface exposures of the mineralised zone. Triangulation surfaces were constructed mathematically by the GEMS software from the delineations and united into wire-frames that represent 3-D solids (geological bodies). The delineation and resulting solids were validated by the software. Dykes in the intrusion were also modelled as solids. Mapped-out fault planes were visualised as 3-D surfaces.

In intrusion-wide images the mineralised zone is a very narrow structure. The 3-D model is best seen 'live', and we have chosen, as examples, to show the initial results of the imaging of the mineralised zone in two vertical 2-D panels through the intrusion (Figs 4, 5). In Fig. 5 the mineralised zone is shown as the zone between the lower boundary of the lowermost Pd-levels (Pd5, cut-off at *c.* 1 gram per tonne Pd) and the top of the Au-rich part of the mineralised zone (Pd1/Au or Au + 1 levels, cut-off at *c.* 0.8 gram per tonne Au).

Results

The west–east section of Fig. 5A shows the mineralised zone to be bowl-shaped with a central depression of *c*. 400 m. The magnitude of the depression is in broad agreement with the margin-to-margin depression of *c*. 700 m modelled by Nielsen (2004) and Nielsen *et al.* (2005). The difference in the magnitude of the depression reflects that the 3-D model does not reach all the way to the margins of the intrusion. As expected, the imaging also shows that the vertical distance between the lower and upper boundaries of the mineralised zone increases towards the centre of the intrusion, in agreement with the structure of the mineralised zone proposed by Nielsen *et al.* (2005). The demonstrated bowl-shape of the mineralised zone, and thus the layered gabbros, corroborates the model suggesting concentric crystallisation of the gabbro on the floor, walls and below the roof of the intrusion (Nielsen 2004). The north–south section (Fig. 5B) shows the general 20° dip of the layered gabbros and the mineralised zone.

Application of 3-D modelling to the evolution of the Skaergaard intrusion

Nielsen (2004) developed a structural model for the intrusion solely on the basis of field observations and analogies. Compared to the classic and traditional accumulation models, the apparent concentric crystallisation in the 300 km^3 magma chamber reduces the volumes of the most evolved zones and subzones in the intrusion and thus the proportions of the products of the crystallisation process.

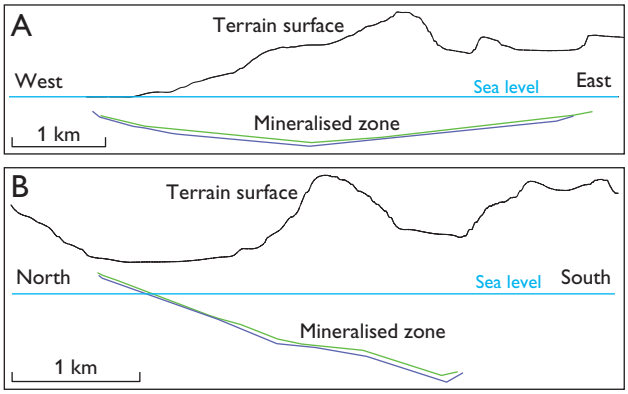

Fig. 5. West–east (**A**) and north–south (**B**) cross-sections through the Skaergaard intrusion. The blue and green lines show the lower and upper boundaries of the Skaergaard mineralised zone (see text for definition). The bowl-shape and the increasing stratigraphic width of the mineralised zone towards the centre of the intrusion are seen (see also Nielsen *et al.* 2005).

The model was used for a mass balance-based estimate of the bulk composition of the intrusion, which turned out to be a composition very similar to that of the contemporaneous flood basalts. The data in Nielsen (2004) can also be used for the calculation of the line of liquid descent (LLD) of the bulk liquid (Fig. 6; Table 1). Toplis & Carroll (1995) modelled the LLD for the Skaergaard intrusion on the basis of experimental investigations. As shown in Fig. 6 the trend of the supposed Skaergaard liquid of Toplis & Carroll (1995) has the same shape as the one calculated using mass balance (Table 1). The data in Fig. 6 are projected from the SiO_2 corner above the plane in the figure, and the difference between the Toplis & Carroll (1995) and the LLD suggested here is a reflection of differences in the starting compositions.

Table 1. Compositions of liquids during the fractionation of the Skaergaard magma

	Bulk SK-TFDN	L1 LZb	L2 LZc	L3 MZ	L4 UZa	L5 UZb	L6 UZc	L7 MG
% solidified	0.00	32.74	55.26	62.56	75.81	85.57	93.43	95.00
SiO_2	47.88	47.03	45.92	46.52	48.19	50.73	58.45	62.08
TiO_2	3.03	3.74	4.86	4.63	3.74	2.65	1.40	1.07
Al_2O_3	13.87	11.93	11.24	11.15	10.75	10.42	11.35	12.39
Fe_2O_3	2.00	2.34	2.70	2.72	2.80	2.78	2.12	1.63
FeO	13.32	15.63	17.97	18.12	18.64	18.53	14.13	10.88
MnO	0.22	0.26	0.29	0.30	0.32	0.34	0.29	0.20
MgO	6.29	6.18	4.62	4.15	3.16	1.83	0.56	0.63
CaO	10.16	9.62	8.78	8.55	7.89	7.37	5.89	4.64
Na_2O	2.56	2.48	2.61	2.71	2.94	3.18	3.78	4.18
K_2O	0.40	0.44	0.55	0.61	0.79	1.07	1.63	1.99
P_2O_5	0.27	0.35	0.47	0.54	0.78	1.10	0.42	0.31
Sum	100.00	100.00	100.01	100.00	100.00	100.00	100.02	100.00
Mg No.	0.457	0.413	0.314	0.290	0.232	0.150	0.066	0.094

Based on bulk liquid SK-TFDN in Nielsen (2004). The composition of the liquid as it evolves is calculated by subtraction of average compositions of correlated LS, MBS and UBS subzones (McBirney 1989) in the mass proportions in Nielsen (2004). The spread sheet with the calculation is available on request. The composition of the liquid of a specific zone refers to the composition of the liquid at the base of the indicated zone. Bulk composition is corrected so that the end-result matches the composition of average melanogranophyre (MG). Fe_2O_3/FeO has been set at 0.15. The abbreviations are explained in Fig. 4.

The LLD of the Skaergaard intrusion is of utmost scientific interest. Well-constrained deviations from the expected can be reflections of processes that have not been taken into account in the modelling of the fractionation process. The lack of balance in the SiO_2 distribution, as reflected in the common quartz-normative compositions of the Upper Border Series of the intrusion (Naslund 1984), was suggested to reflect chemical stratification of the cooling magma (Hoover 1989). But what process would have been responsible for the chemical stratification? SiO_2-enrichment in the upper part of the magma chamber could be due to liquid immiscibility (e.g. Jakobsen *et al.* 2005) or dynamic conditions. Only with well-constrained mass balances and geophysical models for the shape of the magma chamber can numeric models for the evolution of the Skaergaard intrusions be developed and the relative importance of all the suggested processes in the evolution of the melt evaluated.

All well-constrained internal boundaries and the details of the mineralised zone (bulk chemistry, lithologies and mineralogy) in the Skaergaard intrusion will be included in the 3-D model in the coming years. This will allow refinement of the 3-D distributions and volumes of different lithologies, including the mineralised zone, lead to more advanced mass-balance models for the Skaergaard intrusion, and provide more general constraints for modelling of the crystallisation and fractionation processes in basaltic magma chambers.

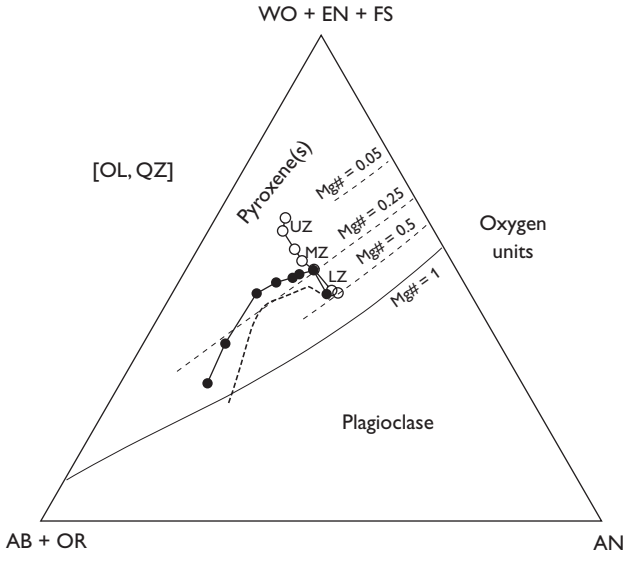

Fig. 6. Skaergaard liquid lines of descent and immiscible liquids in the (Ab + Or)–An–(Wo + En + Fs) projection from Veksler (in press), who used the LLD compositions shown in Table 1. Black dots: model liquids in the same sub-zones of the layered series calculated by mass balance (Table 1). Circles: trapped Skaergaard liquids (McBirney & Naslund 1990). Thick dashed curve: experimental line of liquid descent (Toplis & Caroll 1995). The dashed lines show the boundary between plagioclase and pyroxene crystallisation fields at different Mg numbers (Mg/Mg + Fe; see Veksler in press for details).

References

Bernstein, S. & Nielsen, T.F.D. 2004: Chemical stratigraphy in the Skaergaard intrusion. Danmarks og Grønlands Geologiske Undersøgelse Rapport **2004/123,** 31 pp. + 1 CD.

Bird, D.K., Brooks, C.K., Gannicott, R.A. & Turner, P.A. 1991: A gold-bearing horizon in the Skaergaard Intrusion, East Greenland. Economic Geology **86**, 1083–1092.

Hoover, J.D. 1989: Petrology of the Marginal Border Series of the Skaergaard Intrusion. Journal of Petrology **30**, 399–439.

Jakobsen, J.K., Veksler, I.V., Tegner, C. & Brooks, C.K. 2005: Immiscible iron- and silica-rich melts in basalt petrogenesis documented in the Skaergaard intrusion. Geology **33**, 885–888.

McBirney, A.R. 1989: Geological map of the Skaergaard intrusion, East Greenland. Eugene, USA: University of Oregon.

McBirney, A.R. 1996: The Skaergaard Intrusion. In: Cawthorn, R.G. (ed.): Layered intrusions, 147–180. Amsterdam: Elsevier.

McBirney, A.R. & Naslund, H.R. 1990: The differentiation of the Skaergaard intrusion. A discussion of Hunter and Sparks (Contributions to Mineralogy and Petrology 95, 451–461). Contributions to Mineralogy and Petrology **104**, 235–240.

Naslund, H.R. 1984: Petrology of the Upper Border Series of the Skaergaard Intrusion, East Greenland. Journal of Petrology **25**, 185–212.

Nielsen, T.F.D. 2004: The shape and volume of the Skaergaard intrusion, Greenland: implications for mass balance and bulk composition. Journal of Petrology **45**, 507–530.

Nielsen, T.F.D., Andersen, J.C.Ø & Brooks, C.K. 2005: The Platinova Reef of the Skaergaard intrusion. In: Mungal, J.E. (ed.): Exploration for platinum group element deposits. Mineralogical Association of Canada Short Course Series **35**, 431–455.

Thy, P., Lesher, C.E. & Tegner, C. in press: The Skaergaard liquid line of descent revisited. Contributions to Mineralogy and Petrology.

Toplis, M.J. & Carroll, M.R. 1995: An experimental study of the influence of oxygen fugacity on Fe-Ti oxide stability, phase relations, and mineral–melt equilibria in ferro-basaltic systems. Journal of Petrology **36**, 1137–1170.

Veksler, I.V. in press: Extreme iron enrichment and liquid immiscibility in mafic intrusions: experimental evidence revisited. Lithos.

Wager, L.R. & Brown, G.M. 1968: Layered igneous rocks, 588 pp. Edinburgh: Oliver & Boyd.

Wager, L.R. & Deer, W.A. 1939: Geological investigations in East Greenland, part III. The petrology of the Skaergaard Intrusion, Kangerdlugssuaq, East Greenland. Meddelelser om Grønland **105**(4), 352 pp.

Authors' address

Geological Survey of Denmark and Greenland, Øster Voldgade 10, DK-1350 Copenhagen K, Denmark. E-mail: *tfn@geus.dk*

Diamonds and lithospheric mantle properties in the Neoproterozoic igneous province of southern West Greenland

Agnete Steenfelt, Sven Monrad Jensen, Troels F.D. Nielsen, Karina K. Sand and Karsten Secher

The search for diamonds in Greenland has resulted in the discovery of many new dykes of kimberlite and ultramafic lamprophyre and, most importantly, in the acquisition of a wealth of chemical data on rocks and minerals representing mantle material entrained by the dyke magmas. The discovery of a diamondiferous sheet at Garnet Lake in southern West Greenland stimulated the research (Hutchison 2005). Over the past five to ten years, the Geological Survey of Denmark and Greenland together with the Bureau of Minerals and Petroleum in Greenland and international research groups have acquired, processed and interpreted data with the objective of identifying diamond-favourable regimes within the lithospheric mantle below the Archaean craton in West Greenland. Here we present mineral data from drift samples that allow us to identify where mantle conditions in terms of lithology and depth may be favourable for the occurrence of diamonds.

Neoproterozoic igneous province

The province comprises the Sarfartoq carbonatite complex and abundant dykes and sills of carbonate-rich ultramafic silicate rocks (ultramafic lamprophyre and kimberlite) that have been emplaced in late Neoproterozoic time into Archaean rocks of southern West Greenland between 65°N and 67°30´N (Larsen & Rex 1992; Nielsen *et al.* in press; Steenfelt *et al.* in press). Magma emplacement was concentrated in the Sarfartoq and Maniitsoq regions (Fig. 1), and took place from *c.* 600 Ma to *c.* 555 Ma (Secher *et al.* in press). The first period of magmatism appears to be confined to the Sarfartoq region while later magma pulses affected the entire region (Fig. 1). A 568 ± 11 Ma age of the Garnet Lake sheet (Hutchison & Heaman 2008) places this intrusion in the younger part of the period. Ultramafic dykes (some of which are diamondiferous) of the same age in Labrador, Canada (Tappe *et al.* 2006) show that the magmatism extended into the western part of Laurentia, the then contiguous continent comprising North America and Greenland. The magmatism is thought to have been triggered by incipient continental rifting. At about the same time, more pro-

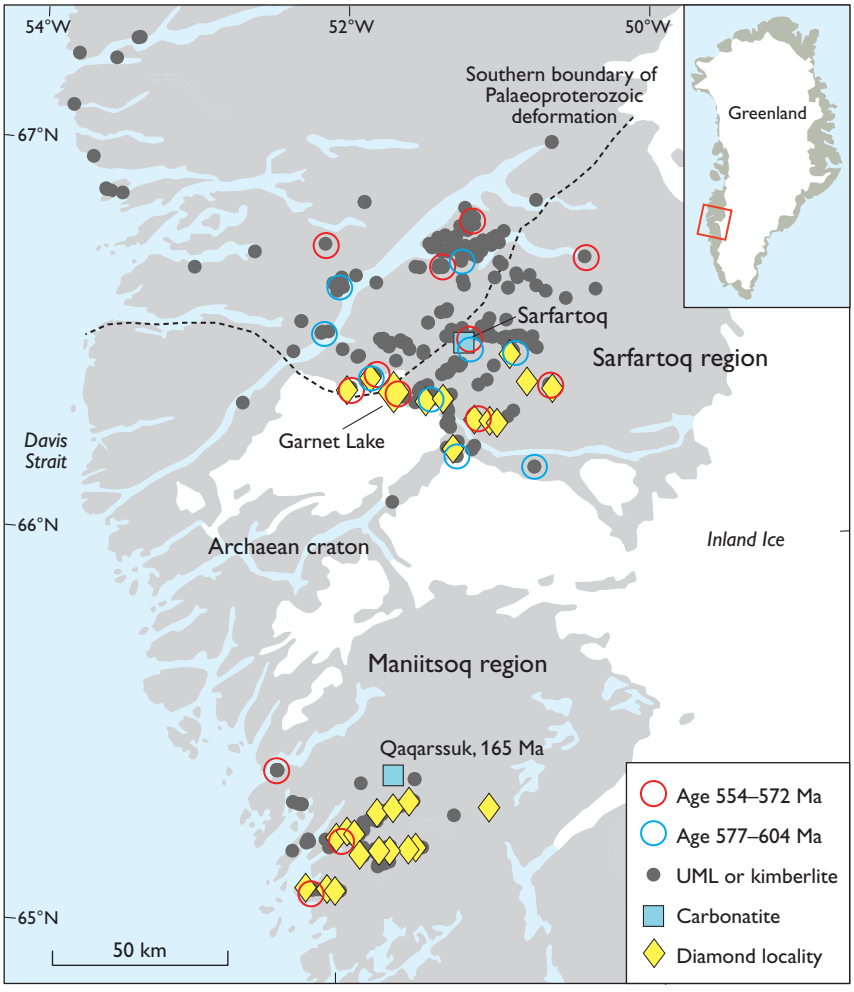

Fig. 1. Neoproterozoic igneous province and localities for rocks tested positive for diamonds (Jensen *et al.* 2004, with later updates from Intex Resources ASA, www.intex-resources.com). The large diamond symbol marks the Garnet Lake commercial diamond operation. The Sarfartoq carbonatite complex and dykes of kimberlite and ultramafic lamprophyre (**UML**) are emplaced into the Archaean craton, which suffered deformation in the northern part during a Palaeoproterozoic collision.

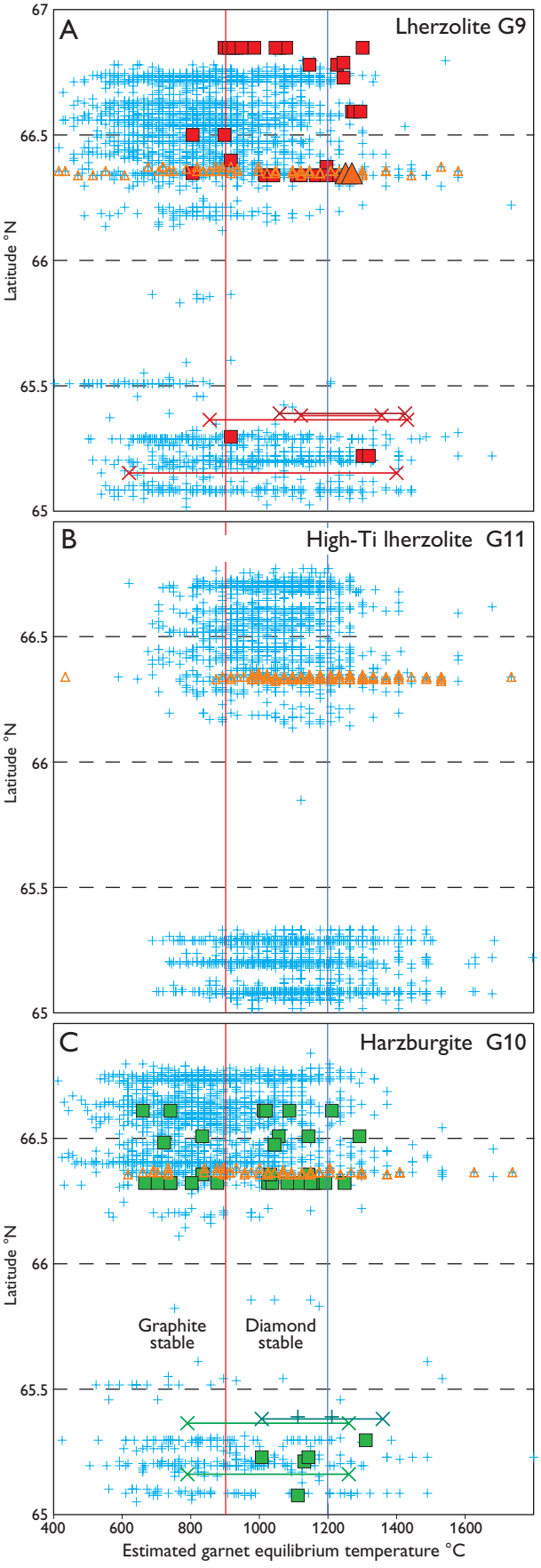

Fig. 2. Estimated temperatures of three classes (**A**: G9, **B**: G11 and **C**: G10) of mantle-derived garnet grains picked from the non-magnetic, heavy mineral fraction of drift samples (mainly till). Northern latitudes on vertical scale: upper group Sarfartoq region (north of 66°N), lower group Maniitsoq region. Orange, open triangles are grains from the Garnet Lake area. Red, vertical line marks the temperature of graphite-diamond phase transition (900°C). Blue line (1200°C, *c.* 180 km depth) marks the cut-off value for deeply derived grains plotted in Fig. 3. Squares represent lithologically sorted temperature estimates based on mantle xenoliths (Larsen & Rønsbo 1993; Garrit 2000; Bizzarro & Stevenson 2003; Jensen *et al.* 2004; Sand *et al.* in press); lines between ×-symbols are ranges in Ni-in-garnet temperatures of grains in garnet concentrates (data from Garrit 2000). Large, filled, red triangles are temperatures determined on xenoliths from Garnet Lake (Hutchison & Heaman 2008).

nounced rifting took place at the northern margin of Laurentia and resulted in the intrusion of a prominent basaltic dyke swarm in North-West Greenland and northern Baffin Land (Dawes 2006).

Exploration and diamond discoveries

Exploration companies have used the so-called kimberlite indicator minerals in their search for host rocks for diamonds. Samples of overburden or drift (mainly till) have been collected systematically over the entire Archaean craton of southern West Greenland and processed to obtain the non-magnetic heavy mineral fraction, from which grains of mantle-derived minerals including peridotitic garnet (pyrope), eclogitic garnet, chromite (chrome-spinel), picroilmenite and chrome-diopside have been picked under a microscope. Many grains were subsequently chemically analysed to verify the visual identification and allow chemical classification. Numerous samples with diamond-indicative, high-pressure mineral compositions indicate that the Neoproterozoic province has a high prospective potential, and subsequent diamond tests have confirmed that the carbonate-rich ultramafic magmas brought up diamondiferous mantle at several localities within the province (Fig. 1). The huge amount of mineral analyses were compiled and quality controlled by Jensen *et al.* (2004).

In 2004 Hudson Resources Inc., guided by drift samples with an abundance of garnets derived from the diamond-stable mantle, discovered a significant amount of diamonds hosted in carbonatite-rich ultramafic rocks at Garnet Lake (Fig. 1) in the Sarfartoq region (Hutchison 2005). Continued exploration has established the presence of a 4 m wide, shallow-dipping sheet of kimberlitic rock with a promising diamond grade and diamond crystals up to 4 carats (0.8 g; Hutchison & Heaman 2008; www. hudsonresources.ca).

The Neoproterozoic lithospheric mantle

Many mineralogical and chemical investigations of mantle xenoliths hosted by the kimberlites and ultramafic lamprophyres have demonstrated that the lithospheric mantle comprises an upper section of peridotitic rock types (lherzolite, harzburgite, dunite) depleted in elements such as Ca, Fe and Ti relative to asthenospheric mantle because of extraction of large portions of basalt. The section of depleted mantle is underlain by a section with a predominance of Fe-Ti-rich, so-called fertile garnet lherzolite (references in Fig. 2). It has also been demonstrated that some xenoliths from both regions have been derived from depths clearly within the high-pressure regime where diamond is stable (references in Fig. 2). The constraints for the Neoproterozoic geotherm have recently been improved to 38–41 mW/m^2, and the thickness of the Neoproterozoic lithosphere has been estimated to be at least 215 km over the entire province (Sand *et al.* in press).

Studies by Hutchison & Heaman (2008) indicate that the diamonds at Garnet Lake probably formed at great depths within the fertile lherzolite, i.e. at temperatures above 1200°C, and within a period of 50 million years before the transporting magma brought them to the surface. The deep lithospheric mantle provenance of the xenoliths is also stressed by Grütter & Tuer (in press), who found an unusually high proportion of high-*T* peridotitic garnets in drift samples from the immediate surroundings of Garnet Lake.

Garnets from deep lithospheric mantle

Garnet is the mineral that has been used most extensively in lithosphere studies and diamond exploration to reflect the temperature and pressure conditions as well as the lithology at the site where it equilibrated. The 15 000 available analyses of garnet grains from the Neoproterozoic province therefore provide excellent material with which to locate dykes that have incorporated material with deep mantle provenance similar to that recorded at Garnet Lake.

Using a chemical discrimination system devised by Grütter *et al.* (2004) we have selected garnets derived from depleted lherzolite (G9; Fig. 2A), fertile lherzolite (G11, Fig. 2B) and harzburgite (G10, Fig. 2C), and determined their equilibration temperatures using MnO concentrations (Grütter *et al.* 1999). The results shown in Fig. 2 are plotted against the latitude of the sample sites in order to reveal any regional differences. Temperatures of Garnet Lake grains and published temperature estimates based on other minerals are shown for comparison.

The diagrams show that a majority of the garnet grains derive from depths where diamond is the stable carbon phase, i.e. where the temperature is above 900°C. It appears that G11 garnets (from fertile lherzolite) mainly come from greater depths and have large populations over the entire latitude interval. This enforces the validity of current models invoking the ubiquitous presence of fertile lherzolite in the

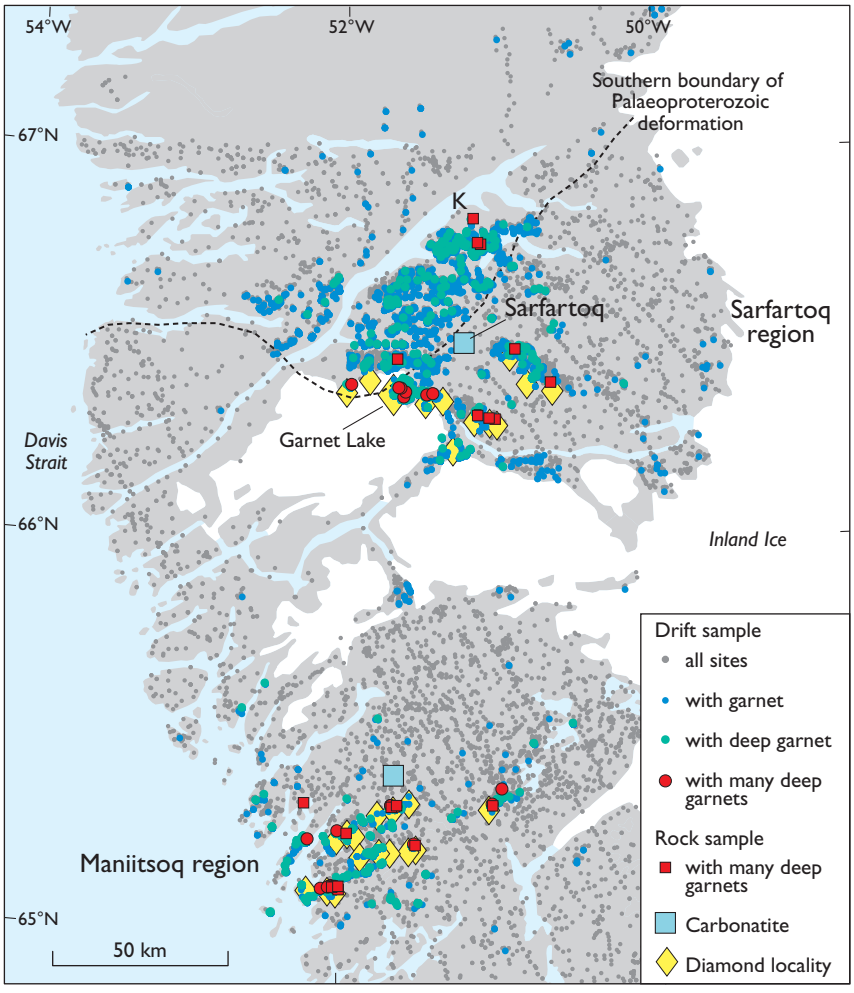

Fig. 3. Neoproterozoic igneous province with localities of drift samples and results of screening garnet grain analyses belonging to classes G9, G10 and G11. Deep garnets (green dots) have *T*-Mn above 1200°C. The red symbols marking samples (drift or rock) with more than 10 deep garnets in the picked populations of peridotitic garnet grains show spatial correlation with diamond occurrences.

lower lithospheric mantle section. A tendency for relatively more G11 grains above 1200°C in the Maniitsoq region is observed. Lherzolitic (G9) and harzburgitic garnets (G10) display origins in wider depth intervals, and very deep grains occur in both regions. The Garnet Lake garnets do stand out in reaching higher temperatures than many grains in the Sarfartoq region. However, grains from several localities in the Maniitsoq region have also yielded temperatures above 1400°C. It should be mentioned that the temperature is inversely correlated with MnO concentrations, so that temperature data above 1600°C are uncertain owing to low analytical precision at low concentrations.

The range in garnet *T*–Mn temperature estimates is in good agreement with estimates using other methods, and the advantage of having the many additional data to establish a more statistically reliable, regional picture of mantle provenance is obvious. In addition, the drift-derived garnets provide information from areas where dykes have not been located or sampled.

Distribution of sites with high diamond potential

Figure 3 shows the extensive coverage of drift sample sites and the clusters of garnet-bearing samples (any mantle-derived kind) where dykes are common (compare Fig. 1). The deep (high-*T*) garnets have a narrower distribution, yet they are abundant in both regions. In order to highlight localities with a high proportion of deep garnets, an arbitrary lower limit of ten grains has been applied. Rock-sample localities with a high proportion (more than ten grains) of deep garnets have been identified and are added as supplementary information. They outline additional localities with diamond potential in the Sarfartoq region.

The distribution of localities rich in deep garnet exhibits spatial correlation with that of diamond-bearing rocks and thus supports the observation made at Garnet Lake that an abundance of deep, lower lithospheric mantle material is characteristic of diamond-bearing dykes. However, the data also demonstrate that Garnet Lake is not unique in the province in this respect and the potential for making equally promising diamond discoveries elsewhere appears to remain. One small area near Kangerlussuaq (K in Fig. 3) has not yet proved positive for diamonds, but is considered a target for further exploration. Subsurface exploration methods would be needed in that area, though, because poor exposure impedes surface recognition of significant dykes.

References

Bizzarro, M. & Stevenson, R.K. 2003: Major element composition of the lithospheric mantle under the North Atlantic Craton: evidence from peridotite xenoliths of the Sarfartoq area, southwestern Greenland. Contributions to Mineralogy and Petrology **146**, 223–240.

Dawes, P.R. 2006: Explanatory notes to the geological map of Greenland, 1:500 000, Thule, Sheet 5. Geological Survey of Denmark and Greenland Map Series **2,** 97 pp. + map.

Garrit, D. 2000: The nature of the Archaean and Proterozoic lithospheric mantle and lower crust in West Greenland illustrated by the geochemistry and petrography of xenoliths from kimberlites, 289 pp. Unpublished Ph.D. thesis, University of Copenhagen, Denmark.

Grütter, H. & Tuer, J. in press: Constraints on deep mantle tenor of Sarfartoq-area kimberlites (Greenland), based on modern thermobarometry of mantle-derived xenocrysts. Lithos.

Grütter, H.S., Apter, D.B. & Kong, J. 1999: Crust-mantle coupling: evidence from mantle-derived xenocrystic garnets. In: Gurney, J.J. *et al*. (eds): Proceedings of the VIIth International Kimberlite Conference **1**, 307–313. Cape Town: Red Roof Design.

Grütter, H.S., Gurney, J.J., Menzies, A.H. & Winter, F. 2004: An updated classification scheme for mantle-derived garnet, for use by diamond explorers. Lithos **77**, 841–857.

Hutchison, M.T. 2005: Diamondiferous kimberlites from the Garnet Lake area, West Greenland: exploration methodologies and petrochemistry. Danmarks og Grønlands Geologiske Undersøgelse Rapport **2005/68**, 33–42.

Hutchison, M.T. & Heaman, L.M. 2008: Chemical and physical characteristics of diamond crystals from Garnet Lake, Sarfartoq, West Greenland: an association with carbonatitic magmatism. The Canadian Mineralogist **46**, 1063–1078.

Jensen, S.M., Secher, K., Rasmussen, T.M. & Schjøth, F. 2004: Diamond exploration data from West Greenland: 2004 update and revision. Danmarks og Grønlands Geologiske Undersøgelse Rapport **2004/117**, 90 pp. + 1 DVD.

Larsen, L.M. & Rex, D.C. 1992: A review of the 2500 Ma span of alkaline-ultramafic, potassic and carbonatitic magmatism in West Greenland. Lithos **28**, 367–402.

Larsen, L.M. & Rønsbo, J. 1993: Conditions of origin of kimberlites in West Greenland: new evidence from the Sarfartoq and Sukkertoppen regions. Rapport Grønlands Geologiske Undersøgelse **159**, 115–120.

Nielsen, T.F.D., Jensen, S.M., Secher, K. & Sand, K.K. in press: Regional and temporal variations in the magmatism of the diamond province of southern West Greenland. Lithos.

Sand, K.K., Waight, T., Pearson, D.G., Nielsen, T.F.D., Makovicky, E. & Hutchison, M.T. in press: The lithospheric mantle below southern West Greenland: a geothermobarometric approach to diamond potential and mantle stratigraphy. Lithos.

Secher, K., Heaman, L.M., Nielsen, T.F.D., Jensen, S.M., Schjøth, F. & Creaser, R. in press: Timing of kimberlite, carbonatite and ultramafic lamprophyre emplacement in the alkaline province located 64°– 67°N in southern West Greenland. Lithos.

Steenfelt, A., Jensen, S.M., Nielsen, T.F.D. & Sand, K.K. in press: Provinces of ultramafic lamprophyre dykes, kimberlite dykes and carbonatite in West Greenland characterised by minerals and chemical components in surface media. Lithos.

Tappe, S., Foley, S.F., Jenner, G.A., Heaman, L.M., Kjarsgaard, B.A., Romer, R.L., Stracke, A., Joyce, N. & Hoefs, J. 2006: Genesis of ultramafic lamprophyres and carbonatites at Aillik Bay, Labrador: a consequence of incipient lithospheric thinning beneath the North Atlantic Craton. Journal of Petrology **47**, 1261–1315.

Authors' addresses

A.S, T.F.D.N. & K.S., *Geological Survey of Denmark and Greenland, Øster Voldgade 10, DK-1350 Copenhagen K, Denmark*. E-mail*: ast@geus.dk*

S.M.J.*, Intex Resources ASA, Munkedamsveien 45A, N-0250 Oslo, Norway.*

K.K.S., *Nano-Science Center, University of Copenhagen, Universitetsparken 5, DK-2100 Copenhagen Ø, Denmark.*

Using spectral mixture analysis of hyperspectral remote sensing data to map lithology of the Sarfartoq carbonatite complex, southern West Greenland

Enton Bedini and Tapani Tukiainen

Remote sensing is the science of acquiring, processing, and interpreting images and related data acquired from aircraft and satellites that record the interaction between matter and electromagnetic energy (Sabins 1997). The 450–2500 nm wavelength region provides mineralogical information based on analysis of electronic absorption features in transitional metals, especially iron, and of molecular absorption features in carbonate, hydrate and hydroxide minerals (Hunt 1977). Landsat Thematic Mapper satellite images are widely used to interpret structure and geology, but due to their broad spectral bandpasses Landsat images cannot identify specific minerals. However, such details can be achieved by processing and analysing data from hyperspectral sensors. These sensors provide a unique combination of high spatial resolution and high spectral resolution imagery of the Earth's surface unavailable from other sources (Goetz *et al.* 1985).

An extensive and complex suite of alkaline igneous rocks of carbonatitic and kimberlitic affinity occurs in the base-

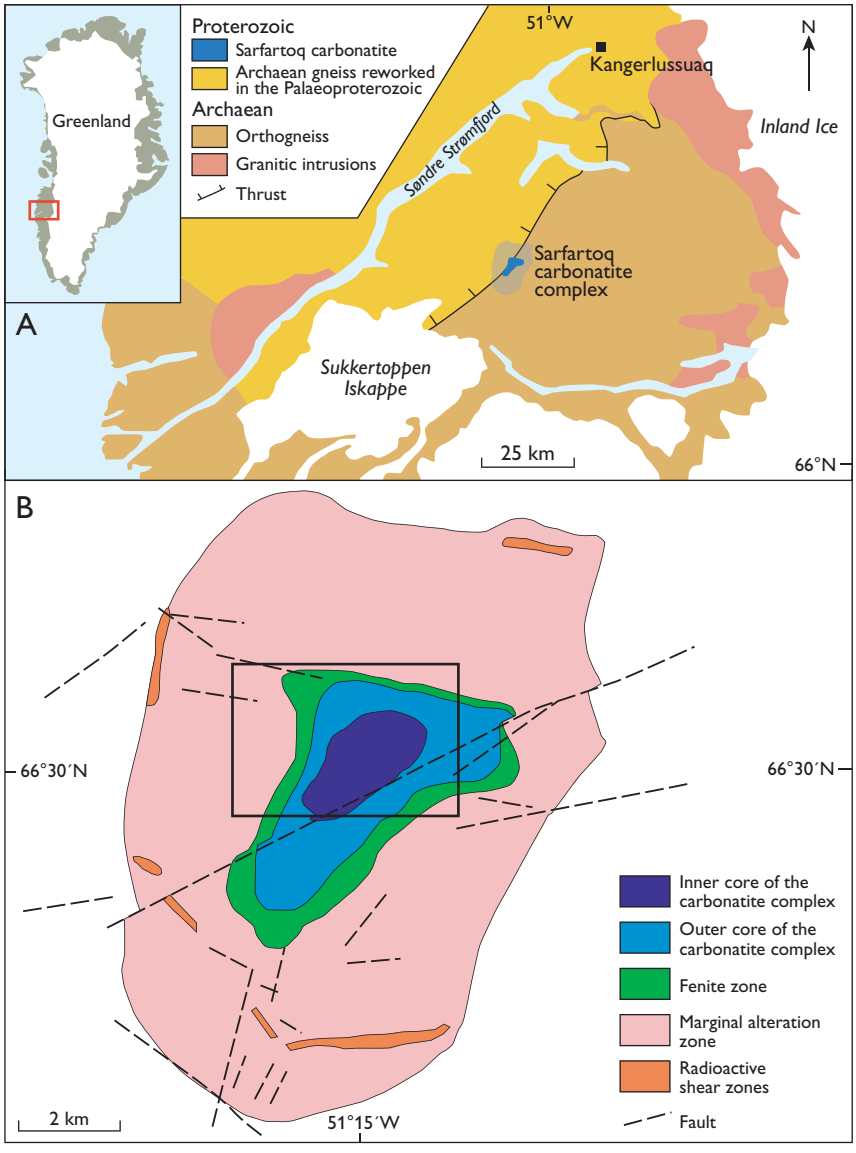

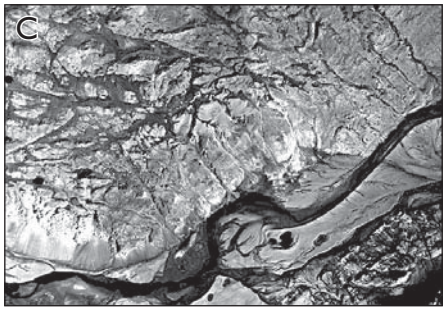

Fig. 1. **A**: Geographical and geological position of the Sarfartoq carbonatite complex in southern West Greenland (modified from Allaart 1982). **B**: Geological map of the Sarfartoq carbonatite complex (modified from Secher 1986). The rectangle indicates the spatial extent of the hyperspectral data analysed in this study. **C**: Band 6 (510 nm) of the hyperspectral image. **D**: Photograph of the outcropping core zone of the Sarfartoq carbonatite within the study area seen from the south-southwest. Height of slope is *c.* 400 m.

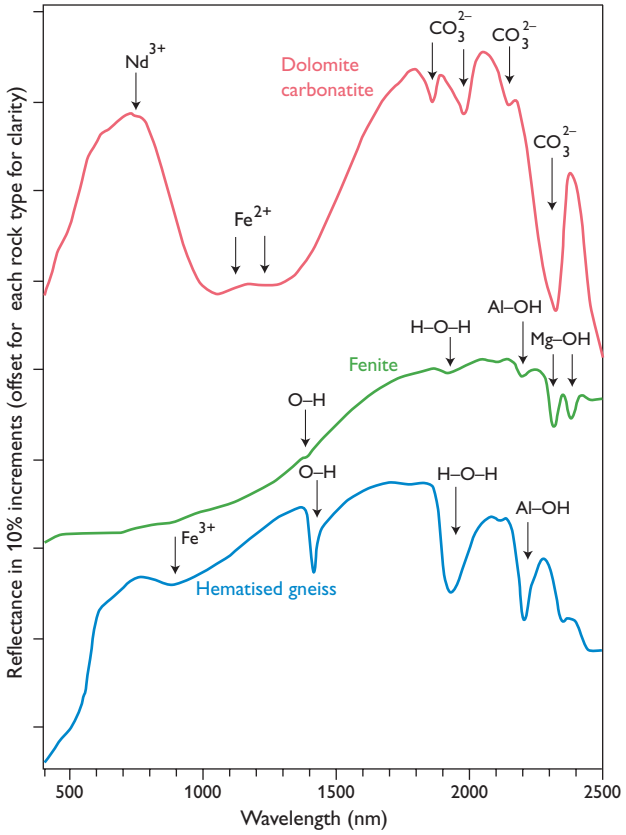

Fig. 2. Characteristic reflectance spectra of dolomite carbonatite, fenite and hematised gneiss.

ment of southern West Greenland (Larsen *et al.* 1983). One of the most important and major carbonatite intrusions is the Sarfartoq carbonatite complex (Fig. 1). This complex consists of an inner and an outer carbonatite core zone, a fenite zone and a marginal alteration zone (Secher & Larsen 1980; Secher 1986). The objective of an on-going research project of the Geological Survey of Denmark and Greenland is to evaluate the use of spectral reflectance techniques and hyperspectral remote sensing data for lithologic mapping and mineral exploration of carbonatites over a known occurrence before applying it to unknown terrains. This short communication reports on the mapping results of spectral mixture analysis of HyMap® airborne hyperspectral data covering an important central part of the Sarfartoq carbonatite complex (Fig. 1). A fuller discussion is presented in Bedini (2009).

Spectral reflectance properties

Reflectance spectra were acquired using an Analytical Spectral Device (ASD Inc., USA) field-portable spectrometer, which records 2151 channels within the 350–2500 nm wavelength range. The reflectance spectra of dolomite carbonatites from the Sarfartoq carbonatite display characteristic carbonate absorption features with the main CO_3^{2-} absorption feature centred around 2320 nm and exhibit a broad ferrous iron absorption feature in the 1000–1300 nm wavelength region (Fig. 2). The depth of this broad ferrous absorption feature is positively correlated with the Fe^{2+} content of the dolomite (Gaffey 1986). However, in reflectance spectra of ferroan carbonatites with limonitic coating, the broad ferrous absorption feature is diminished due to overlapping spectral reflectance features of ferric iron in limonite. Reflectance spectra of carbonatite rocks often display narrow, sharp absorption features at 580 nm, 740 nm, 800 nm and 870 nm, which are attributed to electronic transitions in Nd^{3+} characteristic of rare-earth element-bearing minerals (e.g. Rowan *et al.* 1986).

An almost universal characteristic of carbonatite complexes is the presence of a distinctive metasomatic aureole in which the wall rocks have been converted to aegirine-rich and alkali amphibole-rich rocks (Secher & Larsen 1980). These metasomatic rocks are commonly called fenites and the process fenitisation. Reflectance spectra of the fenitic rocks analysed here display an Mg–OH doublet absorption feature attributed to the alkali amphibole phase present in fenite. In some cases this is associated with a shallow Al–OH absorption feature at around 2200 nm, due to sericite (Fig. 2).

The marginal alteration zone is distinguished by the hematisation/limonitisation of the country rocks. Reflectance spectra of samples from the marginal alteration zone display intense ferric iron spectral features in the visible and near infrared (VNIR) wavelength region (Fig. 2; hematised gneiss). This reflectance spectrum in the short-wave infrared wavelength region exhibits an intense Al–OH absorption feature at 2200 nm associated with two less intense Al–OH absorption features at 2350 and 2450 nm, typical for sericite (Fig. 2).

Sarfartoq HyMap data

The HyMap is an airborne imaging system developed by Integrated Spectronics, Australia, and operated by HyVista Corporation. It consists of sensors located on a fixed-wing aircraft typically flown at an altitude of 2.5 km. The sensors collect reflected solar radiation in 126 bands covering the 450–2500 nm wavelength range, including the visible to near-infrared (VNIR) and short-wave infrared regions of the electromagnetic spectrum (Cocks *et al.* 1998). The Sarfartoq HyMap scenes are part of the HyperGreen-2002 project of the Geological Survey of Denmark and Greenland (Tukiainen & Thorning 2005). They were recorded on 9 August 2002 with 4 m nominal pixel size. The HyMap data were atmospherically corrected using the ATCOR4 model (Richter & Schläpfer 2002).

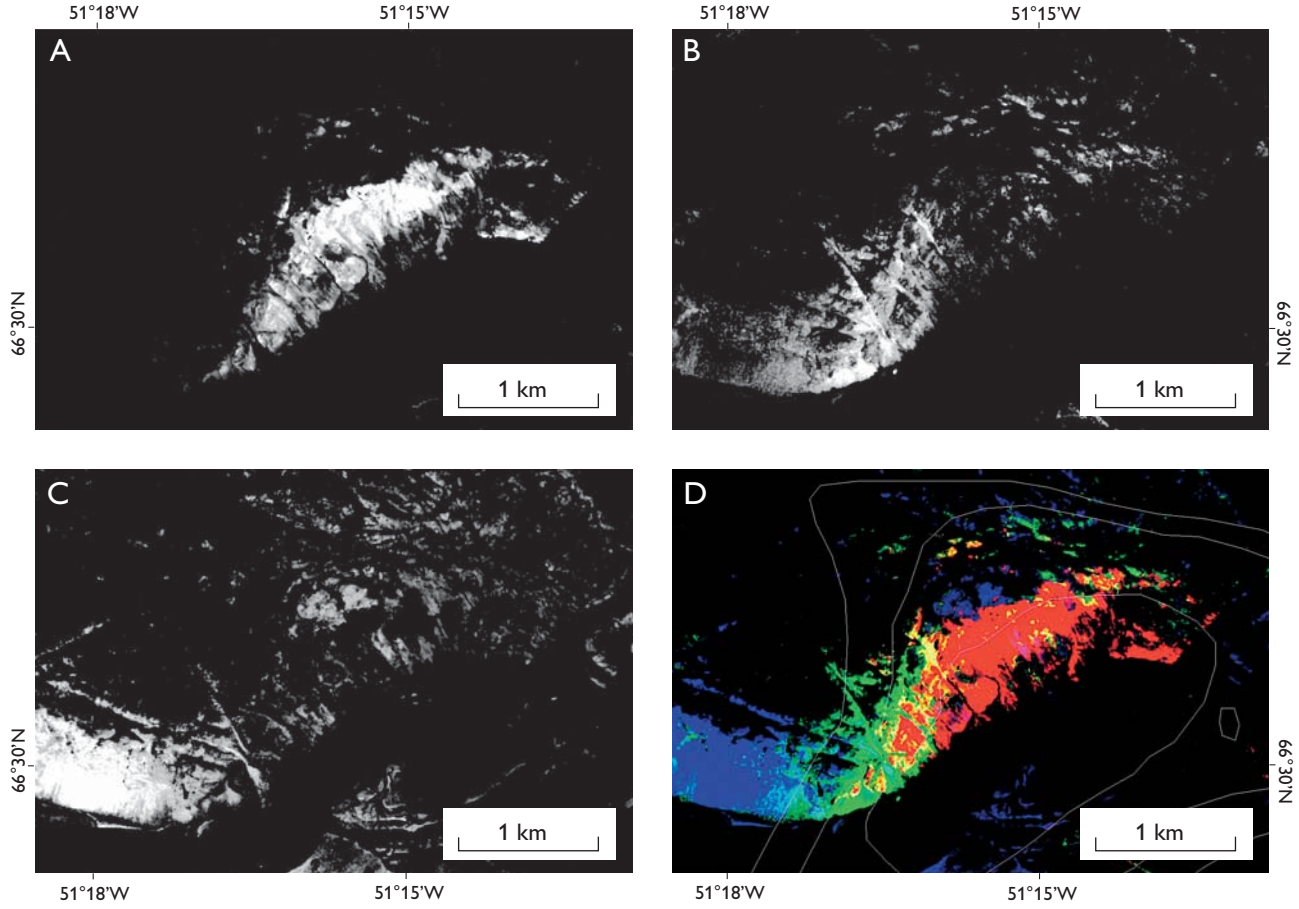

Fig. 3. Fraction abundances produced from the spectral mixture analysis for **A**: Carbonatite. **B**: Fenite. **C**: Hematised gneiss. **D**: Colour composite of the fractions for carbonatite = red, fenite = green and hematised gneiss = blue. Yellow is a mixture of fenite and carbonatite.

Data analysis and results

Dark pixels (using a threshold of 5% mean reflectance) and green vegetation (using a threshold based on the normalised difference vegetation index, NDVI) were filtered out. The hyperspectral data were mean normalised (i.e. each spectrum was divided by its mean). This form of normalisation eliminates effects of different albedo in the spectral unmixing results (e.g. Berman *et al.* 2004). The minimum noise fraction (MNF) transformation (Green *et al.* 1988) was applied to the normalised data. The MNF is a form of principal components analysis but instead of ordering the data in terms of variance, the data are ordered based on the signal-to-noise ratio. In our case the first 20 MNF bands contained most of the information. Image-derived spectral endmembers representing carbonatite, fenite and hematised gneiss were used as input to the spectral mixture analysis (Settle & Drake 1993), which was applied in the MNF space. The application of the spectral mixture analysis in a subset of MNF bands is advantageous, as noise isolated in the excluded MNF bands does not influence the spectral unmixing (e.g. Nielsen 2001). The sum of the fractions was not constrained. The fractions produced from the spectral unmixing analysis were filtered using a 3 × 3 median filter. The spectral unmixing results for the three targets of interest, carbonatite, fenite, and hematised gneiss are shown in Fig. 3A–C. A colour composite of the fractions is shown in Fig. 3D.

The unmixing analysis produced good results for the carbonatite class. The fenite zone and the marginal alteration zone are well mapped within the exposed part of the carbonatite complex along the valley. An important result of the spectral unmixing analysis is the mapping of the outer core zone of the carbonatite consisting of fenitised country rock and carbonatite dykes, distinguished by image analysis as a mixture of fenite and carbonatite (yellow in the colour composite). Other parts of the scene are spectrally dominated by the vegetation cover (grass and lichen), although a mixture of gneiss and lichen is also detectable in some parts of the area. Field validation of the remote sensing mapping results showed accurate mapping of the carbonatite outcrop. The fenite class shows some confusion with the country rocks. Numerous altered spots representing the marginal alteration zone have been detected on the plateau. However, it should

be mentioned that the vegetation cover (lichen and grass) reduces its detection. In the Arctic environment of southern West Greenland green tundra vegetation and lichen constitute a major challenge for remote sensing applied to map surface mineralogy and lithology (e.g. Rivard & Arvidson 1992).

Concluding remarks

Spectral mixture analysis of HyMap hyperspectral data was used to map the outcropping rock types (carbonatite, fenite, hematised country rock) of the Sarfartoq carbonatite complex. The spectral unmixing produced good results for the carbonatite class, distinguishing the inner and outer core zones (the latter as a mixture of fenite and carbonatite) of the carbonatite complex within the study area. To our knowledge, this is the first study that reports the mapping of fenites using hyperspectral reflectance data. In a hyperspectral remote sensing study by Rowan *et al.* (1995) of the Iron Hill carbonatite-alkalic igneous rock complex, Colorado, USA, using data from the airborne visible/infrared imaging spectrometer (AVIRIS), fenite could not be distinguished due to low degree of rock outcrop and lower spatial resolution of the hyperspectral data.

Analysis of high spatial and spectral resolution remote sensing data provides spatially contiguous mineralogical and lithological information for outcropping carbonatite complexes. In inaccessible areas it cannot easily be obtained in any other way. Such information is valuable in multi-disciplinary geological studies of carbonatites and, if combined with other types of data obtained by geophysical, geochemical and petrological techniques, it can assist in mapping and mineral exploration of carbonatite complexes. With future high quality hyperspectral data acquired from sensors mounted on satellites (Staenz 2009), the availability and areal coverage of such datasets will increase, opening new possibilities for the use of hyperspectral remote sensing in geology.

References

Allaart J.H. 1982: Geological map of Greenland 1:500 000. Sheet 2 Frederikshåb Isblink – Søndre Strømfjord. Copenhagen: Geological Survey of Greenland.

Bedini, E. 2009: Mapping lithology of the Sarfartoq carbonatite complex, southern West Greenland, using HyMap imaging spectrometer data. Remote Sensing of Environment **113**, 1208–1219.

Berman, M., Kiiveri, H., Lagerstrom, R., Ernst, A., Dunne, R. & Huntington J. 2004: ICE: a statistical approach to identifying endmembers in hyperspectral images. IEEE Transactions on Geoscience and Remote Sensing **42**, 2085–2095.

Cocks, T., Jenssen, R., Stewart, A., Wilson, I. & Shields, T. 1998: The HyMap airborne hyperspectral sensor: the system, calibration and performance. In: Schaepman, M., Schläpfer, D. & Itten, K.I. (eds): Proceedings 1st EARSeL workshop on imaging spectroscopy, Zürich, 6–8 October, 1998, 37–43. Paris: EARSeL.

Gaffey, S. J. 1986: Spectral reflectance of carbonate minerals in the visible and near infrared (0.35–2.55 microns): calcite, aragonite, and dolomite. American Mineralogist **71**, 151–162.

Goetz, A.F.H., Vane, G., Solomon, J.E & Rock, B.N. 1985: Imaging spectrometry for Earth remote sensing. Science **228**, 1147–1153.

Green, A.A., Berman, M., Switzer, P. & Craig, M.D. 1988: A transformation for ordering multispectral data in terms of image quality with implications for noise removal. IEEE Transactions on Geoscience and Remote Sensing **26**, 65–74.

Hunt, G.R. 1977: Spectral signatures of particulate minerals in the visible and near infrared. Geophysics **42**, 501–513.

Larsen, L.M., Rex, D.C. & Secher, K. 1983: The age of carbonatites, kimberlites and lamprophyres from southern West Greenland: recurrent alkaline magmatism during 2500 million years. Lithos **16**, 215–221.

Nielsen, A.A. 2001: Spectral mixture analysis: linear and semi-parametric full and iterated partial unmixing in multi- and hyperspectral image data. International Journal of Computer Vision **42**, 17–37.

Richter, R. & Schläpfer, D. 2002: Geo-atmospheric processing of airborne imaging spectrometry data. Part 2: atmospheric/topographic correction. International Journal of Remote Sensing **23**, 2631–2649.

Rivard, B. & Arvidson, R.E. 1992: Utility of imaging spectrometry for lithologic mapping in Greenland. Photogrammetric Engineering & Remote Sensing **58**, 945–949.

Rowan, L., Kingston, M.J. & Crowley, J.K. 1986: Spectral reflectance of carbonatites and related alkalic igneous rocks: selected samples from four North American localities. Economic Geology **81**, 857–871.

Rowan, L.C., Bowers, T.L., Crowley, J.K., Anton-Pacheco, C., Gumiel, P. & Kingston, M.J. 1995: Analysis of airborne visible-infrared imaging spectrometer (AVIRIS) data of the Iron Hill, Colorado, carbonatite-alkalic igneous complex. Economic Geology **90**, 1966–1982.

Sabins, F.F. 1997: Remote sensing: principles and interpretation, 432 pp. New York: W.H. Freeman and Company.

Secher, K. 1986: Exploration of the Sarfartôq carbonatite complex, southern West Greenland. In: Kalsbeek, F. & Watt, W.S. (eds): Developments in Greenland geology. Rapport Grønlands Geologiske Undersøgelse **128**, 89–101.

Secher, K. & Larsen, L.M. 1980: Geology and mineralogy of Sarfartôq carbonatite complex, southern West Greenland. Lithos **13**, 199–212.

Settle, J.J. & Drake, N.A. 1993: Linear mixing and the estimation of ground cover proportions. International Journal of Remote Sensing **14**, 1159–1177.

Staenz, K. 2009: Terrestrial imaging spectroscopy – some future perspectives. 6th EARSeL SIG IS Workshop, Tel Aviv, Israel, 16–18 March, 2009.

Tukiainen, T. & Thorning, L. 2005: Detection of kimberlitic rocks in West Greenland using airborne hyperspectral data: the HyperGreen 2002 project. Geological Survey of Denmark and Greenland Bulletin **7**, 69–72.

Authors' address

Geological Survey of Denmark and Greenland, Øster Voldgade 10, DK-1350 Copenhagen K, Denmark. E-mail*: ebe@geus.dk*

Glaciological investigations at the Malmbjerg mining prospect, central East Greenland

Michele Citterio, Ruth Mottram, Signe Hillerup Larsen and Andreas Ahlstrøm

Meeting the technical challenges posed by the Arctic environment is a key issue in the development of Greenland's economy, particularly in the light of increasing interest in developing Greenland's mineral resources both on- and offshore. This paper describes some results of the glaciological investigations carried out at Malmbjerg.

The world-class Malmbjerg molybdenum prospect (71°50′N, 24°16′W) is located in the Stauning Alper, at the confluence of Arcturus Gletscher and the larger Schuchert Gletscher (Fig. 1). The mineral occurrence was discovered in the 1950s and industrial development of the site was attempted in the following decades (Henriksen 2008), but the venture remained economically unviable, largely due to its geographical situation. However, recent technological advances and high demand on the international metal market have led to revived interest in the development of the site as an open-pit mine.

The two glaciers surrounding Malmbjerg are pivotal in the planning of the mine. In particular, surface access to the mine across Arcturus Gletscher is a prerequisite, and the effects of accumulating coarse-grained mine waste on the glacier along the eastern slope of Malmbjerg need to be investigated. Loading of the glacier by the weight of waste rock will modify the ice flow, and darkening of the glacier surface by rock dust will affect meltwater production and, through differential ablation, the elevation and morphology of the glacier surface. Clean glaciers that become covered by debris from naturally occurring rock falls exhibit a much thinner and more homogeneously distributed debris cover, but may nevertheless provide data for comparison. Finally, surge-type glaciers are known to exist in Stauning Alper (Fig. 1), and the likelihood of a surge of Arcturus and Schuchert Gletschers during the anticipated lifetime of the mine needs to be assessed.

The results discussed below are based on data from an automatic weather station (AWS) set up on Schuchert Gletscher in April 2008 by the Geological Survey of Denmark and Greenland (GEUS), and on field observations and ground-penetrating radar surveys carried out in September 2008.

Meteorological observations and melt modelling

An estimate of the magnitude and regime of surface meltwater production and of ablation over the glacier surface is required to properly dimension the mine's infrastructure, to model future differential ablation under a thickening cover of dust and debris and to assess the likelihood of surges of the two glaciers. Observations from the AWS on the glacier surface allow modelling of the surface energy balance and quantifying ablation. Meltwater from the winter snow cover is important since it contributes to the total surface runoff from Arcturus Gletscher. A snow pit showed 576 mm water equivalent of accumulation (corresponding to winter balance) in early April 2008 at the AWS site, where the snow cover had completely melted by mid-June.

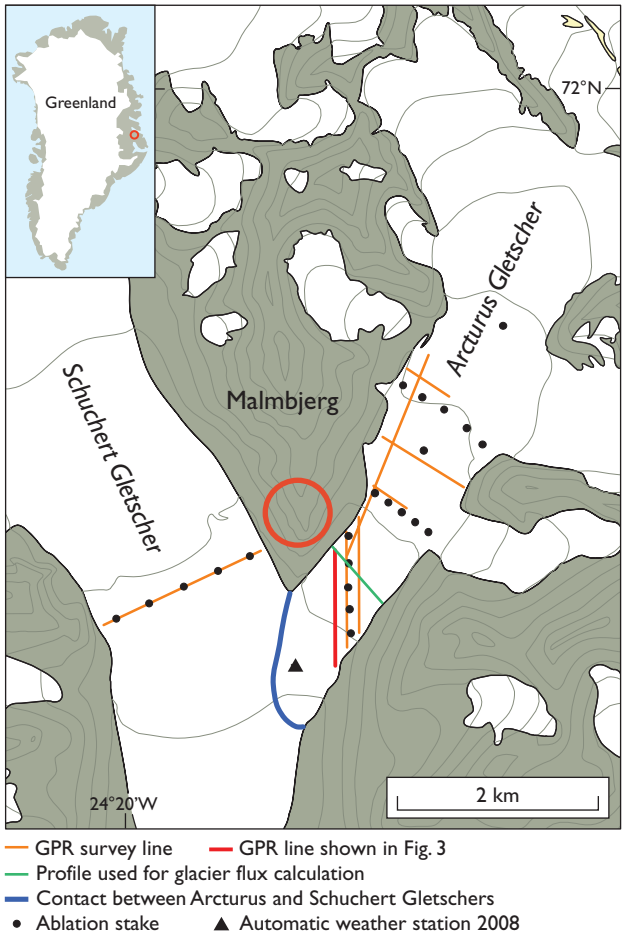

Fig. 1. Topographic map of the Malmbjerg area. Contour interval 100 m. The red circle shows the location of the planned mine. Inset map shows the location of Malmbjerg in East Greenland. Stauning Alper is located immediately to the south-west of Malmbjerg.

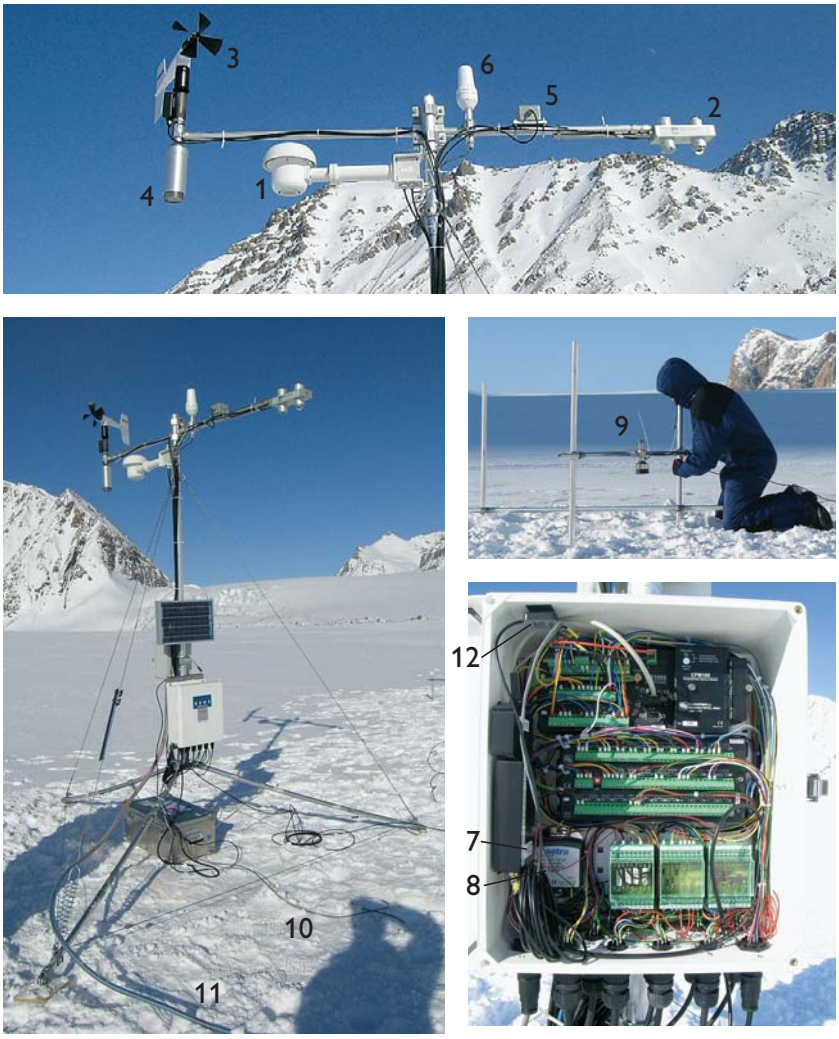

Fig. 2. The automatic weather station: **1**: aspirated radiation shield for air temperature and humidity probes. **2**: radiometers for shortwave and longwave incoming and outgoing radiation. **3**: sensor for wind speed and direction. **4**: sensor to measure snow surface level. **5**: two-axes tilt sensor of the instruments boom. **6**: Iridium satellite antenna. **7**: Iridium satellite radio. **8**: atmospheric pressure. **9**: sensor to measure ice-surface level. **10**: thermistor string for ice temperature (drilled into the ice). **11**: ablation sensor. **12**: GPS antenna.

The AWS records air temperature and humidity in an aspirated radiation shield, as well as wind speed and wind direction, incoming and outgoing shortwave and longwave radiation, barometric pressure, snow depth, ice ablation and the ice-temperature profile at eight levels down to 10 m below the glacier surface (Fig. 2). The measured data are stored locally in the data-logger memory and are transmitted to GEUS in Copenhagen via a satellite link. The system is mounted on an aluminium tripod standing freely on the ice surface, so that the sensor height above the ice surface remains constant throughout the ablation season.

AWS data from May to August 2008 and topographic grids were used as input to the surface energy balance model of Hock & Holmgren (2005) with hourly time-steps over a grid of 50 × 50 m cells. Figure 3A shows a good match between modelled and measured ablation at the AWS site on Arcturus Gletscher, where the surface roughness length for wind speed over ice was set to 1 cm in order to best simulate the on-site ablation measured from the snow pit. Since no field measurements of air temperature lapse rate or accumulation gradient were available from the area, the model was run for a range of values in order to assess the sensitivity of the model to these parameters (values of –3.5, –0.50 and –0.65°C/km and 0.0, 0.5 and 1.0 kg/m^2/m of elevation/year were used). Figure 3B shows the modelled cumulative ablation from May to August 2008 over the entire modelled area with a lapse rate of –5.0°C/km and an accumulation gradient of 0.5 kg/m^2/m of elevation/year. Abundant snowfall at the end of August effectively ended any further significant ablation in 2008. The amount of meltwater produced in 2008 can then be deduced by integrating the model output over the glacier area of interest.

Effects of future glacier surface darkening

Deposition of rock dust derived from blasting and handling of ore and rock waste will result in darkening of the glacier surface around Malmbjerg, with local consequences for mobility across Arcturus Gletscher.

Dust accumulation reduces albedo and initially results in significantly higher ablation rates. Ablation reaches a maximum when the effective thickness of the debris layer is attained, and then gradually decreases until the same ablation rate as clean, bare ice is observed at the critical thickness. Any further thickening of the debris layer results in lower ablation rates, which become negligible under several tens of centimetres or a few metres. Østrem (1959) first established an empirical relationship between ablation rate and thickness of the debris cover (the 'Østrem curve'). Observed values for the effective and critical thicknesses range within 0.25–10 mm and 1.33–30 mm, respectively (Kirkbride & Dugmore 2003), with debris lithology and local climate playing significant roles. For simplicity we assumed in our model that dust

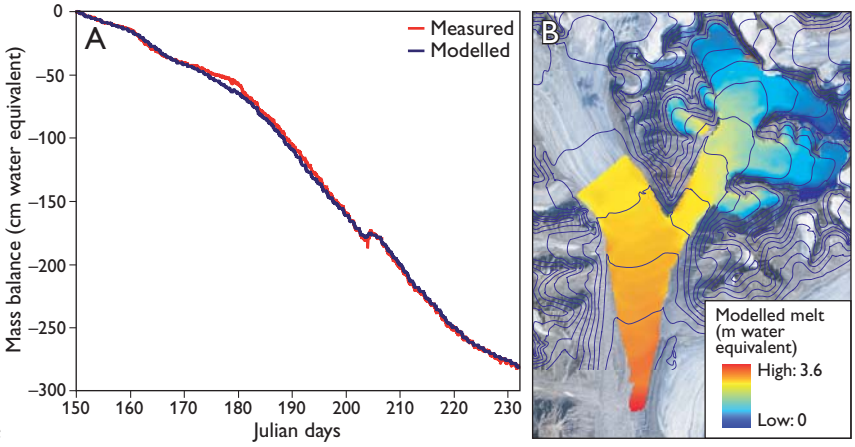

Fig. 3. **A**: Measured versus modelled mass balance from April to August 2008 at the site of the automatic weather station. The last winter snow melted around day 178.
B: Modelled ablation of Arcturus Gletscher and the lower part of Schuchert Gletscher. Contour interval 100 m.

deposition will decrease exponentially with distance from the source. Ice ablation is scaled depending on local debris thickness using an assumed Østrem curve, converted into ice-thickness change and subtracted from the digital elevation model of the preceding time step. Ice dynamics are neglected on the assumption that the glacier is in steady state during the entire modelled time, i.e. emergence and submergence velocity fields remain constant. This is a significant simplification, especially since glacier dynamics will respond to the modified ablation rates on the darkened surface. However, errors due to non-steady state were assumed to vary slowly with distance on the glacier surface, and to be of tolerable magnitude given the semi-quantitative character of this analysis. Modelled results from various dust dispersal patterns show that areas with thick debris cover will become progressively raised over surrounding cleaner ice, and that the total surface meltwater production will peak after a variable number of years; from then on it will fall towards present values.

Ice-radar survey and surge potential

A glacier surge is a strong and comparatively short-lived acceleration of ice flow lasting from a few months to a few years. It is typical of some glaciers with ice dynamics that oscillate without converging to a steady state in which accumulation in the higher parts is balanced by ice flow and ablation in the lower tongue. In the lower parts of a glacier a surge may result in the ice velocity increasing by one or even two orders of magnitude, with the surface becoming heavily crevassed and the glacier terminus possibly advancing by several kilometres. During the much longer quiescent phase following a surge, the ice at lower elevations will stagnate and waste down, while new mass builds up in the accumulation zone until the next surge event. A surge of either Arcturus Gletscher or Schuchert Gletscher would cause considerable difficulties to the mining operations.

Surge-type glaciers are known from Stauning Alper (Olesen & Reeh 1969; Jiskoot *et al.* 2003), and hummocky morphology with extensive ice-cored moraines suggest that both the Arcturus Gletscher and Schuchert Gletscher may be of surge type. To assess the surge potential of Arcturus Gletscher, we estimated how the present mean-ice velocity through a given cross-section of the glacier compares to the balance velocity required in a steady state.

Profiles of Arcturus Gletscher were obtained using ground-penetrating radar (Fig. 4). Processing included migration to produce a geometrically correct representation of the subsurface. Two other features could also be mapped: the cold to temperate transition surface separating cold ice from the underlying temperate ice at the pressure melting point and an englacial meltwater channel.

Analyses based on the balance velocity have commonly compared the ice flow through a cross-section to the net balance up-flow of the cross-section, but no accumulation data are yet available for the two glaciers. We therefore compared the ice flux with the net balance down-flow of the selected cross-section. Although conceptually analogous, this method is not optimal for our purposes, since it cannot detect any mass build-up in the higher reaches of the glacier which are not balanced by the present glacier flow. However, Melvold & Hagen (1998) observed the imbalance between mass supply by ice flow and surface net balance to be strong along the entire length of a surge-type glacier in its quiescent phase, and this adds confidence to our approach. The balance velocity calculated for Arcturus Gletscher through the section

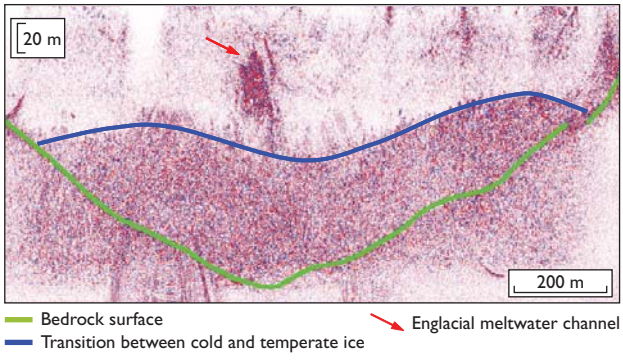

Fig. 4. Migrated ground-penetrating radar profile of Arcturus Gletscher along the path shown in Fig. 1.

marked in Fig. 1 is 18 m per year. This can be compared with the present-day average velocity of 22 m per year obtained from feature tracking on two orthophotographs from 2005 and 2007, and using theoretical results relating surface velocity with mean velocity over a cross-section of parabolic shape (Paterson 1994). Considering the uncertainties involved, we conclude that no imbalance has been detected to suggest that a surge of Arcturus Gletscher will occur in the near future. However, instead of a single year of observations, multi-year average net mass-balance data are needed to provide a more solid assessment.

Accumulation of waste rock and ice deformation

Waste-rock accumulation on the surface of Arcturus Gletscher close to the Malmbjerg slope will affect the dynamics of the glacier, but prediction of such changes and their role is a difficult task, which requires sophisticated three-dimensional numerical models. As a preliminary approach we used simple one- and two-dimensional models to calculate the rate of ice deformation under a specific load, and how this impact could be minimised. A possible similar case may be found at the Kumtor mine in the Tien Shan Mountains in Kyrgyzstan. Gold-mine waste deposited on the Davidov Glacier over a period of 15 years caused a narrowing of the effective flow area, leading to an acceleration of the confined flow unit and increased crevassing extending to the adjacent flow unit of the glacier (Bruce *et al*. 2008).

In the first of our simplified conceptual models we assume the glacier to be a very viscous liquid, and that the rock waste, being thicker than naturally occurring supraglacial debris, will slowly sink into the glacier at a rate controlled by the viscosity of this liquid and the dimensions and shape of the rock particles. This model is analogous to the classical high-school experiment of dropping a ball into syrup and measuring how quickly it settles in order to determine the viscosity of the fluid. The second model assumes that all ice is displaced by the rock, and that the rate of deformation depends on the applied stress, employing a non-linear flow law commonly used in numerical models of glaciers. The two simplified models have been run using the expected timing and pattern of waste-rock accumulation, the profile of the glacier bedrock, and the depth to the temperature transition surface. Several assumptions are involved, for instance concerning the applied stresses and the ice viscosity. Nevertheless, the two models can provide rough upper and lower limits to what is likely to happen and how quickly. Both models predict the highest settling velocities at the lower end of the deposit where the ice is thickest, and the fastest times to the bed (from less than a decade to a few decades) close to the Malmbjerg slope where the ice is thinner.

Final remarks

Planning mining operations at Malmbjerg must include an evaluation of the challenges posed by the glaciers that surround it. Glaciological investigations can provide useful insight into how such challenges can be dealt with as the site is being developed. At the same time, mining sites such as Malmbjerg can become case studies of great scientific interest. However, a single year of observations may not be representative of the local climate; therefore continued operation of the AWS and further surveys are required to provide a better basis for validation of the results.

Acknowledgements

This research has been funded by Quadra Mining Ltd. Jesper Kofoed from Quadra Mining and the team from MT Højgaard A/S at Malmbjerg base camp helped with all aspects of our field work.

References

Bruce, I., Redmond, D. & Thalenhorst, H. 2008: Technical report on the 2007 year-end mineral reserves and resources, Kumtor gold mine, Kyrgyz Republic, for Centerra Gold Inc and Cameco Corporation, 162 pp. Toronto: Strathcona Mineral Services Limited.

Henriksen, N. 2008: Geological history of Greenland, 270 pp. Copenhagen: Geological Survey of Denmark and Greenland.

Hock, R. & Holmgren, B. 2005: A distributed surface energy-balance model for complex topography and its application to Storglaciären, Sweden. Journal of Glaciology **51**(172), 25–36.

Jiskoot, H., Murray, T. & Luckman, A. 2003: Surge potential and drainage-basin characteristics in East Greenland. Annals of Glaciology **36**, 142–148.

Kirkbride, M.P. & Dugmore, A.J. 2003: Glaciological response to distal tephra fallout from the 1947 eruption of Hekla, south Iceland. Journal of Glaciology **49**(166), 420–428.

Melvold, K. & Hagen, J.O. 1998: Evolution of a surge-type glacier in its quiescent phase: Kongsvegen, Spitzbergen 1964–95. Journal of Glaciology **44(**147), 394–404.

Olesen, O.B. & Reeh, N. 1969: Preliminary report on glacier observations in Nordvestfjord, East Greenland. Rapport Grønlands Geologiske Undersøgelse **21**, 41–53.

Østrem, G. 1959: Ice melting under a thin layer of moraine and the existence of ice cores in moraine ridges. Geografiska Annaler **41**, 228–230.

Paterson, W.S.B. 1994: The physics of glaciers, 480 pp. Oxford: Elsevier.

Authors' address

Geological Survey of Denmark and Greenland, Øster Voldgade 10, DK-1350 Copenhagen K, Denmark. E-mail: *mcit@geus.dk*

Holocene climate variability in southern Greenland: results from the Galathea 3 expedition

Niels Nørgaard-Pedersen, Naja Mikkelsen, Majken Djurhuus Poulsen and Aaju S. Simonsen

The third Galathea expedition (Galathea 3) left Copenhagen in August 2006 for a circumnavigation of the globe with the aim of conducting more than 70 scientific programmes en route. The first geological programme took place in South Greenland and included sampling of sediment cores and seismic profiling. The aim of the study is to obtain detailed knowledge about Holocene climate changes and the glaciomarine history.

A number of cores with high sedimentation rates were collected near Narsaq in South Greenland (Fig. 1). Analyses of the cores elucidate the mid- to late Holocene climatic and environmental evolution of the area, which is highly influenced by the dynamic nature of the Greenland ice sheet and changes of the North Atlantic climate. Two major ocean currents, the cold East Greenland Current and the warmer (Atlantic Water) Irminger Current influence the deep fjords of the region, and the two currents are in turn influenced by both polar and lower latitude climate changes.

Evidence from ice cores and marine and lacustrine records in the North Atlantic region show a general climatic cooling from the mid- to late Holocene as a response to decreasing summer insolation. About 5000 years ago, a transition occurred from the Holocene thermal maximum to the Neoglacial (Dahl-Jensen *et al.* 1998). The cooling trend shows different timing and amplitudes in different parts of the North Atlantic region (Kaufman *et al.* 2004), and an apparent counterphase between the climatic conditions of western Greenland and north-western Europe during certain time periods has recently been suggested (Seidenkrantz *et al.* 2008).

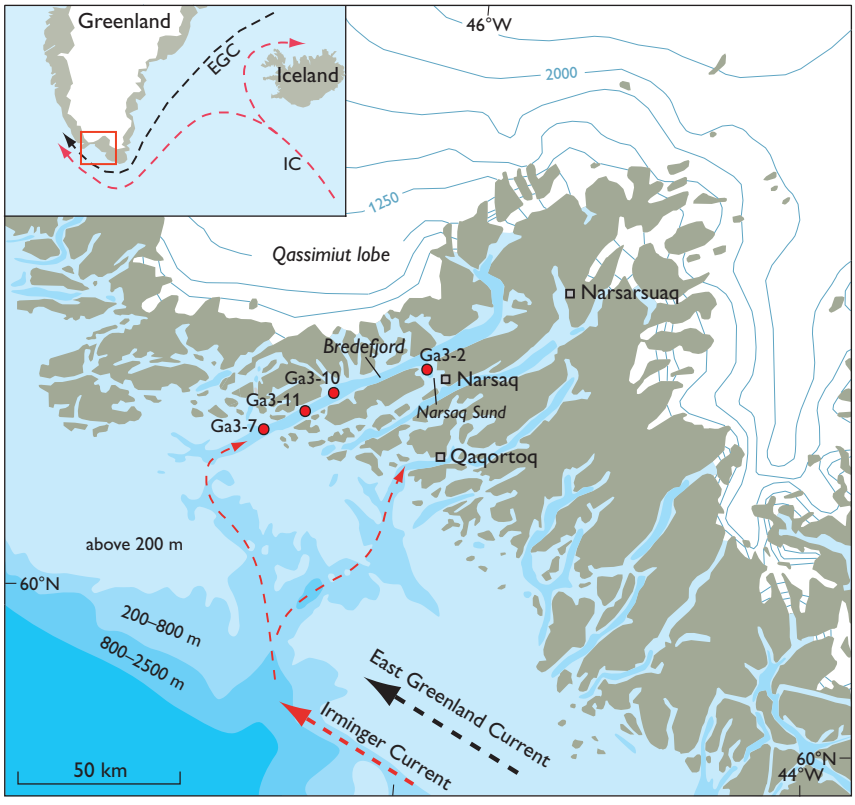

Fig. 1. Map of South Greenland showing the main current systems and locations of investigated cores. The waters of the East Greenland Current and the warmer and more saline Irminger Current (deeper than 200 m) form a stratified water column along the coast of southern Greenland.

The present study investigates climate changes in South Greenland in relation to the previously established pattern of Holocene palaeoceanographic and atmospheric changes as known from other North Atlantic palaeoclimatic studies.

Study area and methods

Glacially eroded and over-deepened fjords reaching depths of 600–700 m dissect South Greenland around Qaqortoq and Narsaq (Fig. 1). Sediment cores were collected in Bredefjord and Narsaq Sund (Fig. 1) using a gravity corer and a box corer at water depths of 270–670 m. A gravity corer with a 750 kg lead weight was used to collect sediment cores up to 6 m long with a diameter of 12 cm. Surface sediments were sampled with a cylindrical 30 cm diameter box corer. All cores were subsampled for analyses of microfossils and age determination using accelerator mass spectrometry ^{14}C dating. The cores were split lengthwise, and magnetic susceptibility was

measured in high resolution using a Bartington MS2E1 probe. Nine samples of benthic foraminifera were used for ^{14}C dating at the Leibniz Laboratory for Radiometric Dating and Isotope Research in Kiel, Germany, and the box cores were analysed for ^{210}Pb and ^{137}Cs content at the Gamma Dating Center, Department of Geography and Geology, University of Copenhagen. A number of basic sediment parameters were determined including sediment wet-bulk density, water content, dry-bulk density and grain-size distribution. Magnetic susceptibility measured at high resolution in general parallels the records of coarse-fraction content, and can therefore be used for correlation and as a high-resolution measure of coarse-fraction influx. In order to estimate the variation in bottom-current velocity, detailed grain-size measurements (range 0.01–1000 µm) were carried out on bulk-sediment samples using a Malvern Mastersizer 2000 laser particle-size analyser at the Department of Geography and Geology, University of Copenhagen. The weighted grain-size means of the sortable silt fraction (10–63 µm) were calculated and used as a proxy for bottom current. The number of lithogenic grains >1 mm (coarse ice-rafted debris, IRD) was counted using a dissecting microscope. The rationale for using grains >1 mm is a compromise between having an adequate number of grains and using grains so large that aeolian transport can be considered negligible. The IRD content is thus used as a proxy for rock fragments from melting of icebergs or sea ice deposited at the site.

The sediment-size fraction 125–1000 µm was separated by dry sieving, and from this fraction 300–400 calcareous benthic foraminifera were picked for analyses. In sediment cores with a fairly uniform sedimentation rate and limited calciumcarbonate dissolution, the abundance of calcareous benthic foraminifera mainly reflects productivity related to food supply.

Fjord environment and sedimentation records

The records from the three gravity cores from Bredefjord are dominated by episodic turbidite sedimentation with very high sedimentation rates of up to 1 cm/year (based on a calibrated ^{14}C age from Ga3-7 (435 cm depth) of *c.* 465 years BP) and is under influence from meltwater supply and glacier calving from the adjacent margin of the Greenland ice sheet (Fig. 1). For this study, we selected core Ga3-2 from the adjacent Narsaq Sund (Fig. 1), which represents a continuous and more slowly accumulating (*c.* 70 cm/1000 years) sedimentation record covering the last *c.* 8000 years. The chronology is based on eight ^{14}C ages (Fig. 2). The record is characterised by a grain-size spectrum of dominantly suspension-settled mud modulated by variable bottom-current influence and IRD rain (Fig. 3). The sedimentation in this turbidite-sheltered part of the fjord system has been controlled by a number of related processes including influx of sediment-laden meltwater plumes with fine-grained sediment, iceberg calving and coarse-sediment IRD transport and strength and changes of fjord circulation/water-mass stratification by Irminger Current and East Greenland Current water masses

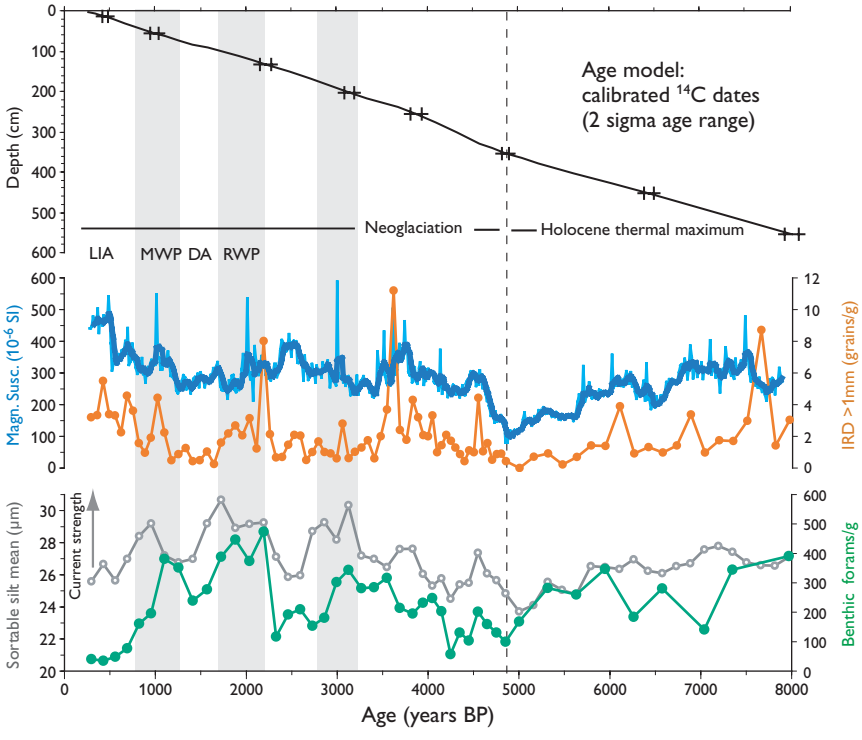

Fig. 2. The Narsaq Sund record (core Ga3-2). The chronology is based on ^{14}C age determinations of eight benthic foraminifera samples. Sediment parameters shown: magnetic susceptibility with five-point running mean, ice-rafted debris content (IRD >1 mm), weighted mean grain size of sortable silt (bottom current proxy), and abundance of calcareous benthic foraminifera/g dry sediment. The grey columns indicate periods of increased bottom currents during the Neoglaciation. European historical climate periods (cf. Lamb 1995) are indicated: **LIA**, Little Ice Age; **MWP**, Medieval Warm Period; **DA**, 'Dark Ages'; **RWP**, Roman Warm Period.

penetrating into the fjord system (Ribergaard 2007). Modified Irminger water is found below *c.* 200 m water depths and East Greenland waters above. During the summer a local brackish meltwater-rich layer characterises the uppermost 10–15 m of the water column.

The Narsaq Sund record

The lower part of the Narsaq Sund record, deposited from about 8.0 to 4.8 ka (ka = thousand years before present), represents the Holocene thermal maximum and shows a progressive reduction in the supply of coarse-grained material, punctuated by increased influx of IRD at about 7.5–6.8 and 6.5–5.7 ka (Fig. 2). The interval 5.7–4.8 ka appears to have been characterised by markedly lower amounts of IRD, and it is suggested that this could reflect a situation in which several of the present tidewater glaciers terminated on land. The Neoglaciation appears to have started at about 4.8 ka, with peak values of IRD at about 4.6, 3.6, 2.2, 1.0, 0.7, and 0.5 ka and onward (Fig. 2). Several of these IRD events appear to be associated with enhanced melting and glacier instability during warming episodes. On the other hand, a marked increase in IRD is noted at the transition to the Little Ice Age at about 0.55 ka. This appears to correlate with the maximum ice advance of the Qassimiut lobe (Weidick *et al.* 2004). A threshold may have been reached during this period, with a marked advance of tidewater glaciers to a new equilibrium state leading to increased IRD deposition in the fjords.

Assemblages of calcareous benthic foraminifera show that the bottom of Narsaq Sund has been dominated by modified Irminger water during most of the Holocene. Bottom-current flow seems to have been quite sluggish before 3.2 ka, whereas the late Holocene was characterised by pronounced episodes of increased bottom-current velocity and increased productivity of calcareous benthic foraminifera (Figs 2, 3). The first episode at 3.2–2.8 ka shows no relation to IRD/-meltwater proxies and the timing at 3.2 ka indicates that the episode may be related to a concurrent major reorganisation of the North Atlantic current systems (cf. Koç *et al.* 1993). During two following periods, at *c.* 2.3–1.7 ka and *c.* 1.3–0.8 ka, marked increases in bottom-water flow also occurred, and it is suggested that the fjord circulation during these time intervals was enhanced by an increased outflow of meltwater. The timing of the latter two events may imply a link to climate changes during the European Roman Warm Period and the Medieval Warm Period (cf. Lamb 1995).

Radiocarbon dating and palaeoecological studies show that the fjord system became ice-free at 13 to 9 ka and the East Greenland Current and the Irminger Current entered the deep and glacially eroded fjords (Weidick *et al.* 2004). During the recession of the Greenland ice-sheet margin from the region, large amounts of icebergs characterised the fjords, but with the onset of the Holocene thermal maximum at 8–5 ka, the temperature increased and became a few degrees higher than today. During the Holocene thermal maximum the Greenland ice sheet reached a minimum size. It became increasingly colder in southern Greenland after the thermal maximum, and with the onset of colder conditions during the Neoglacial period at 4–3 ka the glaciers re-advanced. During the Little Ice Age that culminated around AD 1600–1850, the ice margin expanded several kilometres and the Greenland ice sheet reached its maximum size after the Holocene thermal maximum (Weidick *et al.* 2004). During the late Holocene southern Greenland subsided 6–8 m, probably partly due to the re-advance of the Greenland ice sheet (Sparrenbom *et al.* 2006). At the present time most glaciers in Greenland display marked recession.

The see-saw puzzle of Holocene North Atlantic climate

Recently, Seidenkrantz *et al.* (2008) studied late Holocene marine records from West Greenland and found a complex relationship between the palaeoclimate of West Greenland and that of other parts of the North Atlantic region. Their study indicated that in West Greenland, the European Medieval Warm Period (*c.* 1.3–0.8 ka in the Greenland record) was characterised by a decreased influence of the warm

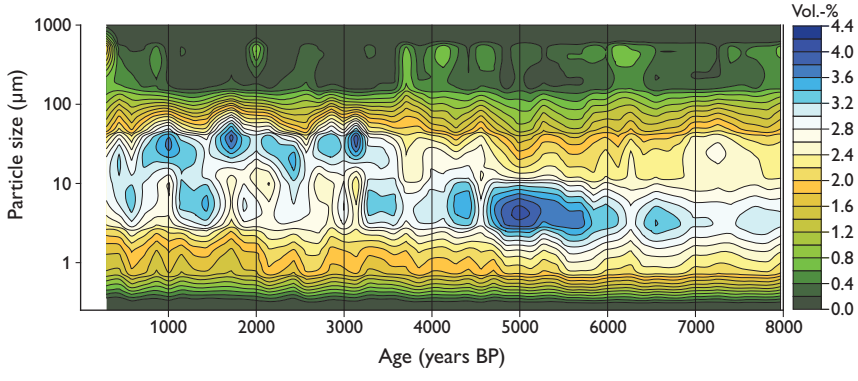

Fig. 3. Particle-size variation plotted against age for the Narsaq Sund Ga3-2 core. A distinct increase in the modal peak of the grain-size distribution occurred at about 3.2 ka. This suggests an increased bottom-water circulation in Narsaq Sund, which may be related to changes of the North Atlantic current systems or increased meltwater discharge.

Irminger Current and thus a relatively cool climate, whereas the colder European 'Dark Ages' (*c.* 1.5–1.3 ka in the Greenland record) appear to have been characterised by a higher meltwater runoff and consequently a warmer climate (Seidenkrantz *et al.* 2008). In contrast, marine, lacustrine and ice-core studies from southern Greenland (e.g. Dahl-Jensen *et al.* 1998; Andresen *et al.* 2004) do not reveal a convincing climate see-saw trend between southern Greenland and northern Europe.

Southern Greenland is located on the main track of cyclones crossing the North Atlantic region on their way towards Iceland. Therefore the area has potential to provide crucial information on major shifts in the North Atlantic atmospheric circulation and general climate regime. The long-term pattern appears to follow climate changes consistent with patterns of East Greenland Current variability (Bond *et al.* 2001), which are partly related to the dominant North Atlantic oscillation (Buch 2002). This long-term see-saw pattern of the influence of the Irminger Current reported by Seidenkrantz *et al.* (2008) is evident in the recent North Atlantic record. Related changes in air temperature, sea-surface temperature, storm patterns, and sea-ice distribution offer a likely explanation for long-term changes and different regional climate trends in the North Atlantic region. There are, however, many unsolved questions in this puzzle, and more high-resolution records are needed from selected sites in order to investigate causes and links between regional climate variations in the North Atlantic region.

Climate change and the demise of the Norse

Norse immigrants settled around AD 985 in South Greenland where farming communities were established in the Eastern Settlement during the Medieval Warm Period. The Norse society no doubt had to cope with a number of socio-economic and environmental problems that eventually caused their disappearance after almost 500 years of existence in Greenland. One of their problems was the general temperature decrease at the transition from the Medieval Warm Period to the Little Ice Age, discussed by Mikkelsen *et al.* (2008). This transition may have brought their living conditions to a critical point although the manner of the demise of the Norse people is still an unsolved question. Temperature decrease, increasing storminess and sea-ice increase threatened the existence of the Norse people and presumably led them to gradually leave Greenland – perhaps for Iceland from where their pioneer ancestors originally set out.

Acknowledgements

We thank captain and crew of the Danish naval ship *Vædderen* for their help and support during the cruise. We gratefully acknowledge financial support from the BG Fund, Det Kongelige Grønlandsfond and the Commission for Scientific Research in Greenland. This is publication no. P29 on the scientific outcome of the Galathea 3 expedition in 2006–2007.

References

Andresen, C.S., Björck, S., Bennike, O. & Bond, G. 2004: Holocene climate changes in southern Greenland: evidence from lake sediments. Journal of Quaternary Science **19**, 783–795.

Bond, G., Kromer, B., Beer, J., Muscheler, R., Evans, M.N., Showers, W., Hoffmann, S., Lottibond, R., Hajdas, I. & Bonani, G. 2001: Persistent solar influence on North Atlantic climate during the Holocene. Science **294**, 2130–2136.

Buch, E. 2002: Present oceanographic conditions in Greenland waters. Danish Meteorological Institute, Scientific Report **02-02**, 39 pp.

Dahl-Jensen, D., Mosegaard, K., Gundestrup, N., Clow, G.D., Johnsen, S.J., Hansen, A.W. & Balling, N. 1998: Past temperatures directly from the Greenland ice sheet. Science **282**, 268–271.

Kaufman, D.S. *et al.* 2004: Holocene thermal maximum in the western Arctic (0–180°W). Quaternary Science Reviews **23**, 529–560.

Koç, N., Jansen, E. & Haflidason, H. 1993: Palaeoceanographic reconstructions of surface ocean conditions in the Greenland, Iceland and Norwegian Seas through the last 14 ka based on diatoms. Quaternary Science Reviews **12,** 115–140.

Lamb, H.H. 1995: Climate history and the modern world, 433 pp. London: Routledge.

Mikkelsen, N., Kuijpers, A. & Arneborg, J. 2008: The Norse in Greenland and late Holocene sea-level change. Polar Record **44**, 45–50.

Ribergaard, M.H. 2007: Oceanographic investigations off West Greenland 2006. Northwest Atlantic Fisheries Organization, Scientific Council Documents **07/1**(N5339), 48 pp.

Seidenkrantz, M.-S., Roncaglia, L., Fischel, A., Heilmann-Clausen, C., Kuijpers, A. & Moros, M. 2008: Variable North Atlantic climate seesaw patterns documented by a late Holocene marine record from Disko Bugt, West Greenland. Marine Micropaleontology **68**, 66–83.

Sparrenbom, C.J., Bennike, O., Björck, S. & Lambeck, K. 2006: Holocene relative sea-level changes in the Qaqortoq area, southern Greenland. Boreas **35**, 171–187.

Weidick, A., Kelly, M. & Bennike, O. 2004: Late Quaternary development of the southern sector of the Greenland Ice Sheet, with particular reference to the Qassimiut lobe. Boreas **33**, 284–299.

Authors' addresses

N.N.P. & N.M., *Geological Survey of Denmark and Greenland, Øster Voldgade 10, DK-1350 Copenhagen, Denmark.* Email: *nnp@geus.dk*

M.D.P., *Department of Geography and Geology, University of Copenhagen, Øster Voldgade 10, DK-1350 Copenhagen K, Denmark.*

A.S.S., *Department of Geology, University of Tromsø, N-9037 Tromsø, Norway.*

Post-rift landscape development of north-east Brazil

Johan M. Bonow, Peter Japsen, Paul F. Green, Peter R. Cobbold, Augusto J. Pedreira, Ragnhild Lilletveit and Dario Chiossi

The evolution of the landscape of north-east Brazil in relation to the burial and exhumation history of both onshore and offshore areas is the focus of a research project carried out for StatoilHydro do Brasil and Petrobras from 2007 to 2009 by the Geological Survey of Denmark and Greenland in collaboration with Geotrack International. In hydrocarbon exploration it is important to understand the regional tectonic framework and thus also to consider the volumes of rocks that may have been present and then removed during the geological past. For example, the timing of hydrocarbon generation and changes in migration routes can be assessed when the timing and magnitude of uplift and erosion is known. Studies in West Greenland have demonstrated the usefulness of large-scale, low-relief, high-level landscapes as markers of uplift events, and in particular the strength of combining the denudation history from landscape analysis with the cooling history from apatite fission-track analysis (AFTA) data and the stratigraphic record (Bonow *et al.* 2006, 2007; Japsen *et al.* 2006, 2009). In the study area, there are two plateaux with elevations up to *c.* 1300 m above sea level (a.s.l.). The plateaux are currently being dissected by deeply incised fluvial valleys, and escarpments separate the two plateaux. The lowlands cut across Early Cretaceous rift systems along the Atlantic margin, including the intracontinental Recôncavo–Tucano–Jatobá (RTJ) Rift and also the Camamu Basin, of which the western margin is exposed onshore (Fig. 1). The RTJ Rift is a mature hydrocarbon province, whereas the deep-water parts of the Camamu Basin are the target of frontier exploration (e.g. Magnavita *et al.* 1994; Davison 1999; Cobbold *et al.* 2008). The post-rift sequence in the RTJ Rift and the inshore Camamu Basin is thin or absent. However, it has been estimated that up to 2000 m of sedimentary cover once was present, but has now been removed (Magnavita *et al.* 1994).

The Atlantic margin of Brazil is characterised by elevated plateaux cut by deeply incised valleys, but this landscape has a pattern common with many other passive continental margins with elevations from 1000 to 2000 m a.s.l. or more around the world, for example in Norway, East and West Greenland and south-east Australia. Mesozoic–Cenozoic rift systems parallel to the coast are generally present offshore

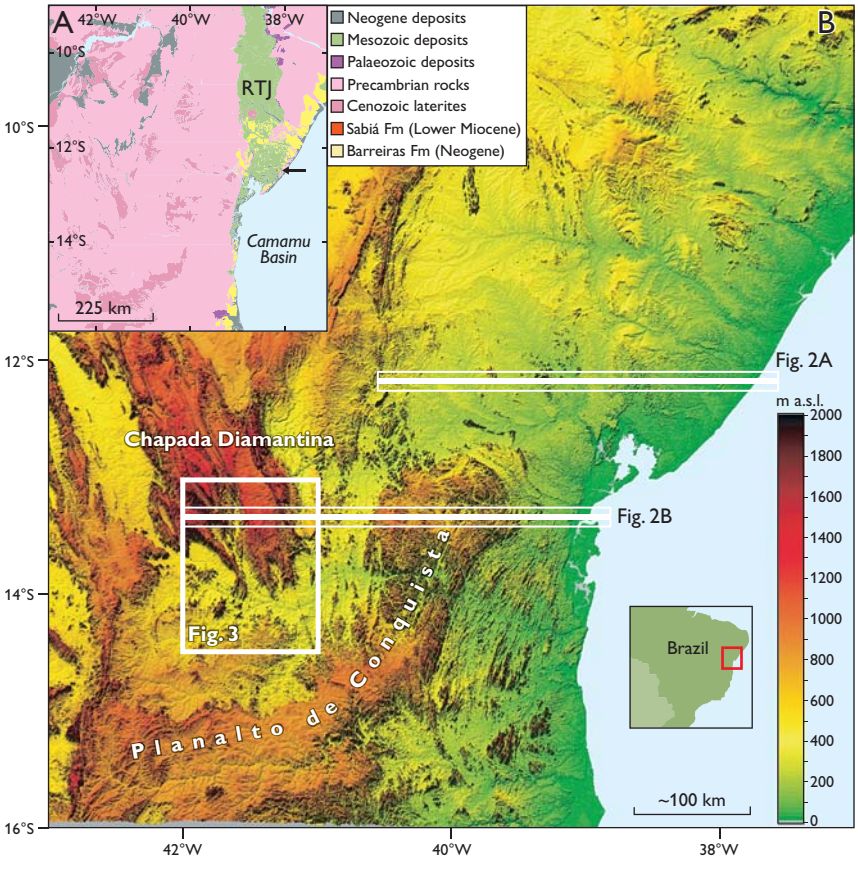

Fig. 1. **A**: Geological map of the study area (based on CPRM 2001, 2003). Precambrian basement is covered by younger sedimentary sequences, which are important age constraints for the different peneplains. **RTJ,** Recôncavo – Tucano–Jatobá Basin. The arrow points at the small Sabiá Formation outcrop. **B**: Topography of the study area. Two topographical features dominate the landscape: a lower surface, which is a plain mainly at 200–500 m a.s.l. (greenish and light yellow) and the higher surface which is a plain mainly at 900–1200 m a.s.l. (orange and reddish). Pronounced escarpments separate the two features. Elevation data source: Jarvis *et al.* (2008).

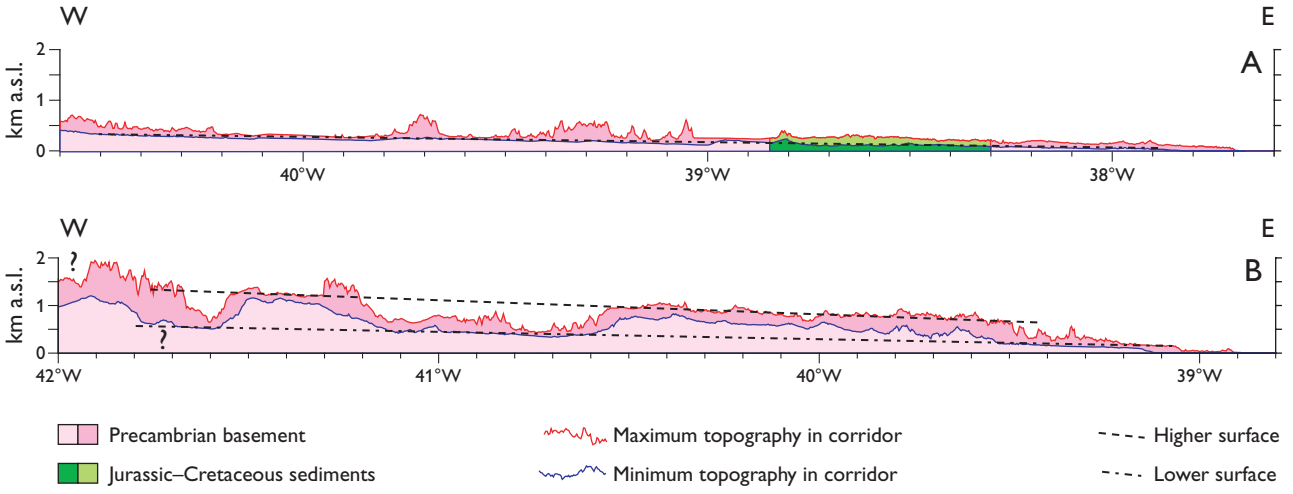

Fig. 2. Two profiles to illustrate the surface mapping. The dotted lines show the interpreted peneplains. The surfaces cut across both the basement, consisting of rocks that have different resistance to erosion, as well as the sedimentary sequence of the RTJ Basin. This shows that the peneplains are erosional features. See Fig. 1B for profile location and corridor width.

with a transition from continental to oceanic crust farther offshore. Several aspects related to elevated, passive continental margins are controversial: the origin of the plateaux, the timing of their uplift to their present elevation and their relation to the adjacent rift systems (Japsen *et al.* 2009). For example, Gallagher *et al*. (1994) found that the almost 3 km high mountain chain Serra do Mar, near Rio de Janeiro, is the remnant of a rift shoulder from the Early Cretaceous break-up in the South Atlantic, whereas Cobbold *et al.* (2001) argued that these mountains were formed during Neogene block-fault tilting.

King (1967) mapped stepped surfaces (i.e. erosion surfaces at distinct levels in the landscape) through the elevated terrains along many passive continental margins, e.g. in eastern Australia, southern Africa and north-east Brazil. King used remnants of sedimentary rocks to constrain the ages of these surfaces and concluded that the main surfaces were formed during the Cenozoic, and consequently that the margins had been uplifted in that same time interval. Furthermore, King found that the highest peaks in the interior of the continents represented remnants of a pre-break-up topography. Subsequent geomorphological research into the development of the passive margins of southern Africa and eastern Australia has, however, regarded the elevated terrains along these passive margins as mainly reflecting preserved rift-shoulders (e.g. Ollier 1985), a model that is commonly used as input to thermochronological studies (e.g. Gallagher *et al.* 1994).

The burial and exhumation history of the study area is currently investigated by combining the cooling history from apatite fission-track analysis from both outcrop and borehole samples with the denudation history from landform analysis and the stratigraphic record. Based on field work carried out during four weeks in July and August 2007, we here report results focused on the rift systems near the Atlantic margin and on the interior highlands in north-east Brazil.

Large-scale landforms

A geomorphological analysis based on the method described by Bonow *et al.* (2006) has led to the identification of two major erosion surfaces (peneplains) of low, relative relief and of regional extent within the study area: a lower surface extending from near-coast areas and far into the interior (up to 500 m a.s.l., greenish colours in Fig. 1B) and a higher surface that includes the plateaux ('planaltos') of Chapada Diamantina (*c.* 1200 m a.s.l., reddish colours in Fig. 1B) and Planalto de Conquista (Fig. 1B; *c.* 900 m a.s.l.). Both surfaces cut across rocks of different ages and resistances and must therefore be erosional features (Fig. 2). These observations show that the surfaces were originally formed by denudation to a near-horizontal plain because even slightly tilted surfaces will be incised by fluvial valleys and the relief rejuvenated, until a new and younger peneplain is formed. The location of these surfaces near the present coast indicates that sea level was the most likely baselevel to which the surfaces graded. After uplift of what is now the higher surface, the lower surface was developed by incision along the main rivers in the area (Figs 1, 3, 4).

The higher surface can be correlated from Chapada Diamantina to Planalto de Conquista at a slightly lower elevation (Fig. 2). It is characterised by an undulating plain with shallow and wide valleys, and it is preserved on high ground with resistant rocks. The higher surface must have developed across a larger area than that presently preserved, as the lower surface has developed at the expense of it. Escarpments often

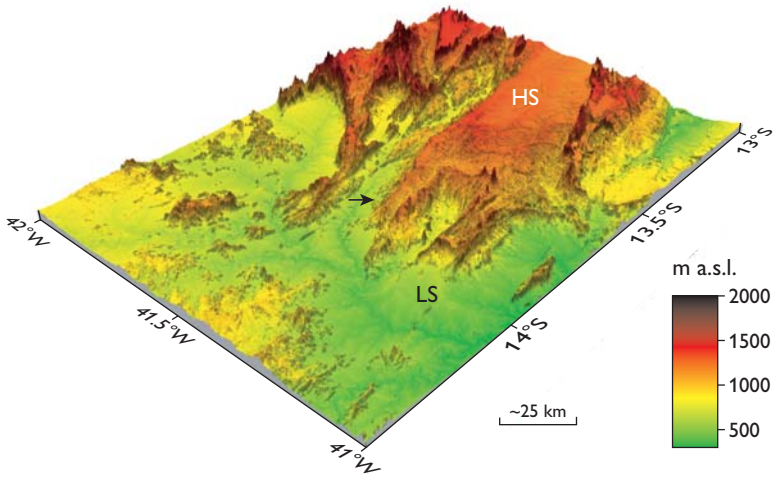

Fig. 3. Digital terrain model with a higher surface (**HS**) and a lower surface (**LS**) that are separated by escarpments in the Chapada Diamantina area. The higher surface forms a coherent plateau at 1200–1400 m a.s.l. (reddish) with only minor valley incisions. This plateau is presently being dissected by rivers along the escarpment, eroding down to the lower surface, here at 500–400 m a.s.l. (greenish). Escarpments are also found above the higher surface, maybe representing steps towards older surfaces at higher elevations. The arrow indicates the location and direction of the photograph in Fig 4. Elevation data source: Jarvis *et al.* (2008).

separate the lower surface from the higher surface (Figs 3, 4). In detail, these escarpments usually coincide with bedrock boundaries, thus reflecting bedrock resistance. The valley patterns and the incision of rivers in the Recôncavo and Tucano basins also show that the lower surface is rapidly being dissected by incising rivers, due to a change in baselevel after formation of the lower surface.

Geological constraints

The lower surface cuts across post-rift strata within the rift and Precambrian basement outside the rift (Figs 1, 2). The formation of the surface thus post-dates the Aptian Marizal Formation (e.g. Magnavita *et al.* 1994). The age of the surface may, however, be further constrained by an outlier of the early Miocene, marine Sabiá Formation within the Recôncavo Basin (Fig. 1A) where this sedimentary unit has been found in deep trenches (Viana *et al.* 1971). This outlier testifies to a marine transgression that occurred before the formation of the lower surface because the outlier is truncated by that surface, and thus the lower surface is younger than early Miocene.

The areas where the higher surface is defined are characterised by laterites (deep weathering profiles) of Cenozoic age (Fig. 1; CPRM 2001, 2003). Both the higher surface and the laterites are currently being destroyed by erosion along the escarpments that outline the plateaux. Consequently, the laterites must have formed at the end of the erosional process that shaped the higher surface. Based on the age of the laterites we can deduce that the higher surface formed during the Cenozoic.

This time interval can be further narrowed if we take into account that the younger, lower surface was formed subsequent to the deposition of the Sabiá Formation. The age of the higher surface may thus tentatively be estimated to be Palaeogene, which implies that the landscape at that time was a peneplain close to sea level. This suggestion is in agreement with observations from similar plateaux north and south of the study area where the plateau surfaces were exposed during the Palaeogene according to stratigraphic data (Sant'Anna *et al.* 1997; Morais Neto *et al.* in press) and geochronological constraints on deep weathering (Spier *et al.* 2006; Lima 2008). Alternatively, both the higher and the lower surface in the study area may have formed during the Neogene, which also agrees with the Cenozoic age of the laterites. Geomorphological analysis alone cannot definitely conclude which alternative is correct, but we prefer the first alternative because it is consistent with independent constraints from outside the study area.

Fig. 4. The lower surface with the escarpment and the higher surface in the background. See Fig. 3 for location.

Conclusions

The landscape in the study area is dominated by two main peneplains, a higher surface and a lower surface that were both formed as low-relief erosion surfaces. The higher surface developed during the Cenozoic, probably during the Palaeogene as other similar plateaux in Brazil. The lower surface formed during the Neogene after the deposition of the Sabiá Formation and an uplift event that raised the higher surface to its present elevation around 1000 m a.s.l.

The uplift resulted in rejuvenation of the relief and subsequent formation of the lower surface. Progressive backward erosion along the main rivers has resulted in escarpments that separate the two surfaces. The escarpments are pronounced at geological boundaries with large differences of erosional resistance. Even the lower surface is presently under destruction due to minor subsequent uplift. In summary, we find that the passive margin topography in the study area was shaped many millions of years after the Early Cretaceous break-up of the South Atlantic. The conclusion that the landscape is mainly Cenozoic is thus in agreement with that of, e.g. King (1967). A better understanding of the timing of uplift events will be achieved from apatite fission-track data as well as the amount of exhumation involved in the formation of the erosion surfaces.

Acknowledgements

The study was funded by StatoilHydro do Brasil and Petrobras.

References

Bonow, J.M., Lidmar-Bergström, K. & Japsen, P. 2006: Palaeosurfaces in central West Greenland as reference for identification of tectonic movements and estimation of erosion. Global and Planetary Change **50**, 161–183.

Bonow, J.M., Japsen, P., Green, P.F., Wilson, R.W., Chalmers, J.A., Klint, K.E.S., van Gool, J.A.M., Lidmar-Bergström, K. & Pedersen, A.K. 2007: A multi-disciplinary study of Phanerozoic landscape development in West Greenland. Geological Survey of Denmark and Greenland Bulletin **13**, 33–36.

Cobbold, P.R., Meisling, K.E. & Mount, V.S. 2001: Reactivation of an obliquely rifted margin, Campos and Santos basins, southeastern Brazil. American Association of Petroleum Geologists Bulletin **85**, 1925–1944.

Cobbold, P.R., Marais-Gilchrist, G., Chiossi, D., Fonseca Chaves, F., Gomes de Souza, F. & Lilletveit, R. 2008: Large submarine slides on a steep and narrow continental margin (Camamu Basin, NE Brazil). American Association of Petroleum Geologists Annual Convention, San Antonio, Texas, 20–23 April, 1 p.

CPRM-Geological Survey of Brazil 2001: Geological map of Brazil, 1:5 000 000 (CD-ROM).

CPRM-Geological Survey of Brazil 2003: Geologia e Recursos Minerais do estado da Bahia 1:1 000 000 (CD-ROM).

Davison, I. 1999: Tectonics and hydrocarbon distribution along the Brazilian South Atlantic margin. Geological Society, London, Special Publications **153,** 133–151.

Gallagher, K., Hawkesworth, C.J. & Mantovani, M.S.M. 1994: The denudation history of the onshore continental margin of SE Brazil inferred from apatite fission track data. Journal of Geophysical Research **99**, 18117–18145.

Japsen, P., Bonow, J.M., Green, P.F., Chalmers, J.A. & Lidmar-Bergström, K. 2006. Elevated, passive continental margins: long-term highs or Neogene uplifts? New evidence from West Greenland. Earth and Planetary Science Letters **248**, 315–324.

Japsen, P., Bonow, J.M., Green, P.F., Chalmers, J.A., & Lidmar-Bergström, K. 2009: Formation, uplift and dissection of planation surfaces at passive continental margins. Earth Surface Processes and Landforms **34,** 683–699.

Jarvis, A., Reuter, H. I., Nelson, A. & Guevara, E. 2008: Hole-filled seamless SRTM data V4, International Centre for Tropical Agriculture (CIAT). Available from http://srtm.csi.cgiar.org.

King, L.C. 1967: The morphology of the Earth, 2nd edition, 699 pp. Edinburgh: Oliver and Boyd.

Lima, M. da Guia 2008: A história do intemperismo na província Borborema oriental, Nordeste do Brasil: Implicações paleoclimáticas e tectônicas, 251 pp. Unpublished Ph.D. thesis, Universidade Federal do Rio Grande do Norte, Brazil.

Magnavita, L.P., Davison, I. & Kusznir, N.J. 1994: Rifting, erosion, and uplift history of the Recôncavo-Tucano-Jatobá Rift, northeast Brazil. Tectonics **13**, 367–388.

Morais Neto, J.M., Green, P.F., Karner, G.D. & Alkmim, F.F. in press: Age of the Serra do Martins Formation, Borborema Plateau, northeastern Brazil: constraints from apatite and zircon fission track analysis. Boletim de Geociências da Petrobras **16**.

Ollier, C.D. 1985: Morphotectonics of passive continental margins: introduction. Zeitschrift für Geomorphologie N.F., Suppl. **54**, 1–9.

Sant'Anna, L.G., Schorscher, H.D. & Riccomini, C. 1997: Cenozoic tectonics of the Fonseca Basin region, eastern Quadrilátero Ferrífero, MG, Brazil. Journal of South American Earth Sciences **10**, 275–284.

Spier, C.A., Vasconcelos, P.M. & Oliviera, S.M.B. 2006: $^{40}Ar/^{39}Ar$ geochronological constraints on the evolution of lateritic iron deposits in the Quadrilátero Ferrífero, Minas Gerais, Brazil. Chemical Geology **234**, 79–104.

Viana, C.F., Gama Junior, E., Simões, I.A., Moura, J.A., Fonseca, J.R. & Alves, R.J. 1971: Revisão estratigráfica da bacia Recôncavo/Tucano. Boletim Técnico da Petrobras **14**, 157–192.

Authors' addresses

J.M.B & P.J., *Geological Survey of Denmark and Greenland, Øster Voldgade 10, DK-1350 Copenhagen K, Denmark.* E-mail: *jbon@geus.dk*

P.F.G., *Geotrack International Pty Ltd, 37 Melville Road, Brunswick West 3055, Victoria, Australia.*

P.R.C., *Géosciences-Rennes (UMR6118 du CNRS), Université de Rennes, 35042 Rennes Cedex, France. A.J.P., Geological Survey of Brazil (CPRM), Avenida Ulysses Guimaraes, 2862, 41213-000 Salvador, Brazil.*

R.L., *StatoilHydro, Angola team, Stavanger, Norway.*

D.C., *StatoilHydro do Brazil, Rio de Janeiro, Brazil.*

De Nationale Geologiske Undersøgelser for Danmark og Grønland (GEUS)

Geological Survey of Denmark and Greenland
Øster Voldgade 10, DK-1350 Copenhagen K
Denmark

The series *Geological Survey of Denmark and Greenland Bulletin* started in 2003 and replaced the two former bulletin series of the Survey, viz. *Geology of Greenland Survey Bulletin* and *Geology of Denmark Survey Bulletin*. Some of the twenty-one volumes published since 1997 in those two series are listed on the facing page. The present series, together with *Geological Survey of Denmark and Greenland Map Series*, now form the peer-reviewed scientific series of the Survey.

Geological Survey of Denmark and Greenland Bulletin

1	The Jurassic of Denmark and Greenland, 948 pp. (28 articles), 2003. *Edited by* J.R. Ineson & F. Surlyk.	500.00
2	Fish otoliths from the Paleocene of Denmark, 94 pp., 2003. *By* W. Schwarzhans.	100.00
3	Late Quaternary environmental changes recorded in the Danish marine molluscan faunas, 268 pp., 2004. *By* K.S. Pedersen.	200.00
4	Review of Survey activities 2003, 100 pp. (24 articles), 2004. *Edited by* M. Sønderholm & A.K. Higgins.	180.00
5	The Jurassic of North-East Greenland, 112 pp. (7 articles), 2004. *Edited by* L. Stemmerik & S. Stouge.	160.00
6	East Greenland Caledonides: stratigraphy, structure and geochronology, 93 pp. (6 articles), 2004. *Edited by* A.K. Higgins and F. Kalsbeek.	160.00
7	Review of Survey activities 2004, 80 pp. (19 articles), 2005. *Edited by* M. Sønderholm & A.K. Higgins.	180.00
8	Structural analysis of the Rubjerg Knude Glaciotectonic Complex, Vendsyssel, northern Denmark, 192 pp., 2005. *By* S.A.S. Pedersen.	300.00
9	Scientific results from the deepened Lopra-1 borehole, Faroe Islands, 156 pp. (11 articles), 2006. *Edited by* J.A. Chalmers & R. Waagstein.	240.00
10	Review of Survey activities 2005, 68 pp. (15 articles), 2006. *Edited by* M. Sønderholm & A.K. Higgins.	180.00
11	Precambrian crustal evolution and Cretaceous–Palaeogene faulting in West Greenland, 204 pp. (12 articles), 2006. *Edited by* A.A. Garde & F. Kalsbeek.	240.00
12	Lithostratigraphy of the Palaeogene – Lower Neogene succession of the Danish North Sea, 77 pp., 2007. *By* P. Schiøler, J. Andsbjerg, O.R. Clausen, G. Dam, K. Dybkjær, L. Hamberg, C. Heilmann-Clausen, E.P. Johannessen, L.E. Kristensen, I. Prince & J.A. Rasmussen.	240.00
13	Review of Survey activities 2006, 76 pp. (17 articles), 2007. *Edited by* M. Sønderholm & A.K. Higgins.	180.00
14	Quaternary glaciation history and glaciology of Jakobshavn Isbræ and the Disko Bugt region, West Greenland: a review, 78 pp., 2007. *By* A. Weidick & O. Bennike.	200.00
15	Review of Survey activities 2007, 96 pp. (22 articles), 2008. *Edited by* O. Bennike & A.K. Higgins.	200.00
16	Evaluation of the quality, thermal maturity and distribution of potential source rocks in the Danish part of the Norwegian–Danish Basin, 66 pp., 2008. *By* H.I. Petersen, L.H. Nielsen, J.A. Bojesen-Koefoed, A. Mathiesen, L. Kristensen & F. Dalhoff.	200.00
17	Review of Survey activities 2008, 84 pp. (19 articles), 2009. *Edited by* O. Bennike, A.A. Garde & W.S. Watt.	

Geological Survey of Denmark and Greenland Map Series

1	Explanatory notes to the Geological map of Greenland, 1:500 000, Humboldt Gletscher, Sheet 6, 48 pp., 2004. *By* P.R. Dawes	280.00
2	Explanatory notes to the Geological map of Greenland, 1:500 000, Thule, Sheet 5 (1991), 97 pp. + map, 2006. *By* P.R. Dawes.	300.00
3	Explanatory notes to the Geological map of Greenland, 1:100 000, Ussuit 67 V.2 Nord, 40 pp. + map, 2007. *By* J.A.M. van Gool & M. Marker.	280.00

Geology of Greenland Survey Bulletin (discontinued)

175 Stratigraphy of the Neill Klinter Group; a Lower – lower Middle Jurassic tidal embayment succession, Jameson Land, East Greenland, 80 pp., 1998. *By* G. Dam & F. Surlyk. 250.00

176 Review of Greenland activities 1996, 112 pp. (18 articles), 1997. *Edited by* A.K. Higgins & J.R. Ineson. 200.00

177 Accretion and evolution of an Archaean high-grade grey gneiss – amphibolite complex: the Fiskefjord area, southern West Greenland, 115 pp., 1997. *By* A.A. Garde. 200.00

178 Lithostratigraphy, sedimentary evolution and sequence stratigraphy of the Upper Proterozoic Lyell Land Group (Eleonore Bay Supergroup) of East and North-East Greenland, 60 pp., 1997. *By* H. Tirsgaard & M. Sønderholm. 200.00

179 The Citronen Fjord massive sulphide deposit, Peary Land, North Greenland: discovery, stratigraphy, mineralization and structural setting, 40 pp., 1998. *By* F.W. van der Stijl & G.Z. Mosher. 200.00

180 Review of Greenland activities 1997, 176 pp. (26 articles), 1998. *Edited by* A.K. Higgins & W.S. Watt. 200.00

181 Precambrian geology of the Disko Bugt region, West Greenland, 179 pp. (15 articles), 1999. *Edited by* F. Kalsbeek. 240.00

182 Vertebrate remains from Upper Silurian – Lower Devonian beds of Hall Land, North Greenland, 80 pp., 1999. *By* H. Blom. 120.00

183 Review of Greenland activities 1998, 81 pp. (10 articles), 1999. *Edited by* A.K. Higgins & W.S. Watt. 200.00

184 Collected research papers: palaeontology, geochronology, geochemistry, 62 pp. (6 articles), 1999. 150.00

185 Greenland from Archaean to Quaternary. Descriptive text to the Geological map of Greenland, 1:2 500 000, 93 pp., 2000. *By* N. Henriksen, A.K. Higgins, F. Kalsbeek & T.C.R. Pulvertaft. 225.00

186 Review of Greenland activities 1999, 105 pp. (13 articles), 2000. *Edited by* P.R. Dawes & A.K. Higgins. 225.00

187 Palynology and deposition in the Wandel Sea Basin, eastern North Greenland, 101 pp. (6 articles), 2000. *Edited by* L. Stemmerik. 160.00

188 The structure of the Cretaceous–Palaeogene sedimentary-volcanic area of Svartenhuk Halvø, central West Greenland, 40 pp., 2000. *By* J. Gutzon Larsen & T.C.R. Pulvertaft. 130.00

189 Review of Greenland activities 2000, 131 pp. (17 articles), 2001. *Edited by* A.K. Higgins & K. Secher. 160.00

190 The Ilímaussaq alkaline complex, South Greenland: status of mineralogical research with new results, 167 pp. (19 articles), 2001. *Edited by* H. Sørensen. 160.00

191 Review of Greenland activities 2001, 161 pp. (20 articles), 2002. *Edited by* A.K. Higgins, K. Secher & M. Sønderholm. 200.00

Geology of Denmark Survey Bulletin (discontinued)

36 Petroleum potential and depositional environments of Middle Jurassic coals and non-marine deposits, Danish Central Graben, with special reference to the Søgne Basin, 78 pp., 1998. *By* H.I. Petersen, J. Andsbjerg, J.A. Bojesen-Koefoed, H.P. Nytoft & P. Rosenberg. 250.00

37 The Selandian (Paleocene) mollusc fauna from Copenhagen, Denmark: the Poul Harder 1920 collection, 85 pp., 2001. *By* K.I. Schnetler. 150.00

Prices are in Danish kroner exclusive of local taxes, postage and handling

Note that information on the publications of the former Geological Survey of Denmark and the former Geological Survey of Greenland (amalgamated in 1995 to form the present Geological Survey of Denmark and Greenland) can be found on the Survey's website: *www.geus.dk*